

7-3-2012

Concrete microstructure homogenization technique with application to model concrete serviceability

Tai Fan

Follow this and additional works at: https://digitalrepository.unm.edu/ce_etds

Recommended Citation

Fan, Tai. "Concrete microstructure homogenization technique with application to model concrete serviceability." (2012).
https://digitalrepository.unm.edu/ce_etds/6

This Dissertation is brought to you for free and open access by the Engineering ETDs at UNM Digital Repository. It has been accepted for inclusion in Civil Engineering ETDs by an authorized administrator of UNM Digital Repository. For more information, please contact disc@unm.edu.

Tai Fan

Candidate

Department of Civil Engineering


Department

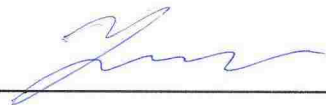
This dissertation is approved, and it is acceptable in quality and form for publication:

Approved by the Dissertation Committee:

Mahmoud Reda Taha  , Chairperson

Walter Gerstle 

Arup K. Maji 

Yu-Lin Shen 

**CONCRETE MICROSTRUCTURE HOMOGENIZATION TECHNIQUE
WITH APPLICATION TO MODEL CONCRETE SERVICEABILITY**

BY

TAI FAN

B.Sc., Civil Engineering, Chang'an University, China, 2000
M.Sc., Civil Engineering, Beijing University of Technology, China, 2004

DISSERTATION

Submitted in Partial Fulfillment of the
Requirements for the Degree of

Doctor of Philosophy

Engineering

The University of New Mexico
Albuquerque, New Mexico

May, 2012

ACKNOWLEDGEMENTS

I would like to gratefully and sincerely thank people and organizations listed below for their help during my Ph.D. study at the University of New Mexico.

To my advisor and committee chair Dr. Mahmoud Reda Taha. I am indebted deeply to him for his patience, supports and mentorship;

To my committee members, Dr. Walter Gerstle, Dr. Arup K. Maji, and Dr. Yu-Lin Shen, for their time and attention during the busy semesters;

To Dr. Timothy Ross, Dr. John Stormont, and Dr. Rafi Tarefder, for their time and attention to be my qualifying examiner;

To Dr. Jung Joong Kim, for his valuable discussions, suggestions, and help in my research and life;

To Aaron Reinhardt and Andrew Garner, for their help in nanoindentation test and other laboratory work;

To Jacob Hayes, for his help in cutting concrete and other laboratory work;

To Eslam Soliman, for his help in the laboratory work and life;

To Michael Sheyka and Bernardo Gonzalo Farfan, for their work as the administrator of the computer server at different periods of time;

To Josie Gibson, Candyce Torres, Yolanda Sanchez and Rebekah Lucero, for their help with the administrative tasks necessary to complete my doctoral program;

To Sigma Xi: The Scientific Research Society-UNM Chapter, for the award of “Excellence in Graduate Research”;

Finally, the financial support for basic research on concrete from the Defence Threat Reduction Agency (DTRA) is greatly acknowledged and appreciated.

**CONCRETE MICROSTRUCTURE HOMOGENIZATION TECHNIQUE WITH
APPLICATION TO MODEL CONCRETE SERVICEABILITY**

by

Tai Fan

B.Sc. & M.Sc., Civil Engineering

Doctor of Philosophy, Engineering

ABSTRACT

Conventionally, mechanical properties of concrete are attained through experiment by leaving microstructural phases interaction in a black box. To fully understand concrete, it is necessary to bridge the gap between microstructure and macro properties. In this dissertation, with several models being given progressively, an innovative homogenization model of concrete is proposed in which concrete is regarded as cement and aggregate particles connected by interfacial transition zone (ITZ). Defined on a representative volume element (RVE), the relationship between microstructure and macro properties is established. The proposed model is validated by experimental results and then applied in the study of concrete serviceability.

The concrete homogenization model includes RVE in two scale levels: cement paste RVE in microscale and concrete RVE in mesoscale. Cement paste RVE is composed by microstructural phases (water, unhydrated cement, calcium hydroxide, calcium silicate hydrate, etc.), which are determined by the validated three-dimensional

(3D) cement hydration and microstructural development model HYMOSTRUC[®] or CEMHYD3D. The developed cement paste RVE at different hydration ages is transferred to a finite element method (FEM) model and upscaled by homogenization as inputs for concrete RVE in the mesoscale. Cement paste homogenization model is validated by the experimental study of nanosilica effects on the mechanical properties of cement paste.

Concrete RVE can be generated by converting realistic or (re)constructed concrete material image into finite element environment. In this dissertation, cell operation method is presented to (re)construct concrete. The similarity between (re)constructed image and target image is verified by low-order correlation functions. In the discrete model of concrete, each cement paste element or each aggregate is treated as a discrete particle; and these particles are bonded together by equivalent ITZ. To simulate cracking and particle interaction, ITZ is represented by cohesive zone model (CZM) and contact mechanism.

This dissertation will demonstrate that the concrete homogenization technique can capture the relationship between structure and material, and enable us to study concrete serviceability in view of microstructure evolution. As the applications of the proposed homogenization model of concrete, following studies on concrete serviceability are carried out: deflection variation in reinforced concrete (RC) beams propagated from concrete microstructural variability, and mechanical consequences of concrete subjected to alkali-silica reaction (ASR).

Due to the inherent uncertainty in concrete microstructure, variation of RC beam deflection is inevitable. For satisfactory use of RC members, it is necessary to incorporate uncertainty of concrete properties in deflection prediction. With the help of

homogenization modeling, microstructural variability in concrete is projected to the deflection variation in RC beams.

Alkali-silica reaction (ASR) is a kind of chemical reaction in concrete. Alkali in cement meets with reactive silica in aggregate and expanding gels are produced if there is enough water. The swelling of gels will induce stress and alter concrete microstructure. In some cases, this alteration includes cracking and expansion in concrete member. The condition becomes more complicated when the expansion caused by swelling gels is confined by reinforcement and prestress in concrete. Using the proposed homogenization technique, the mechanical consequence of ASR on concrete is simulated. ASR gels expansion is achieved by aggregate volume increase, which causes internal stress and deteriorates ITZ in concrete RVE model. The proposed mechanical model of concrete subjected to ASR is demonstrated on plain concrete specimens (prism and cylinder). The simulated cases are validated by experimental work by others. It is proved that the proposed ASR model by using concrete microstructure homogenization can stand with ASR chemical and diffusional models given by other researchers to predict the serviceability of concrete structure subjected to ASR.

TABLE OF CONTENTS

| | |
|--|-----------|
| CHAPTER 1. INTRODUCTION..... | 1 |
| CHAPTER 2. LITERATURE REVIEW | 9 |
| 2.1. HOMOGENIZATION | 9 |
| 2.2. HOMOGENIZATION MODELS OF CONCRETE | 16 |
| 2.3. RECONSTRUCTION OF RVE WITH RANDOM MICROSTRUCTURE..... | 19 |
| 2.3.1. <i>Representativeness</i> | 19 |
| 2.3.2. <i>Similarity</i> | 20 |
| 2.4. INTERFACIAL TRANSITION ZONE (ITZ) | 22 |
| 2.5. ALKALI SILICA REACTION (ASR) | 23 |
| 2.5.1. <i>ASR mechanisms</i> | 24 |
| 2.5.2. <i>Experimental study of ASR</i> | 25 |
| 2.5.3. <i>Models of ASR</i> | 30 |
| CHAPTER 3. METHODS..... | 34 |
| 3.1. HOMOGENIZATION METHODS | 34 |
| 3.1.1. <i>Boundary conditions used in homogenization</i> | 35 |
| 3.1.2. <i>Analytical approach</i> | 37 |
| 3.1.2.1. Direct method..... | 38 |
| 3.1.2.2. Variational method | 39 |
| 3.1.2.3. Approximate method | 39 |
| 3.1.3. <i>Numerical approach</i> | 40 |
| 3.1.3.1. Specimen testing method | 40 |
| 3.1.3.2. Multiscale method | 43 |
| 3.1.3.3. Coupled multiscale method..... | 43 |
| 3.2. RECONSTRUCTION OF CONCRETE RVE | 45 |
| 3.2.1. <i>Non-uniqueness of two-point correlation function in heterogeneous composites</i> | 45 |
| 3.2.2. <i>Reconstruction of concrete RVE</i> | 49 |
| 3.3. RECONSTRUCTION OF CEMENT PASTE..... | 53 |
| 3.3.1. <i>HYMOSTRUC[®]</i> | 53 |
| 3.3.2. <i>CEMHYD3D</i> | 54 |
| CHAPTER 4. APPLICATION OF HOMOGENIZATION METHOD TO MODEL CEMENT PASTE..... | 56 |
| 4.1. MODEL I | 56 |
| 4.1.1. <i>Introduction</i> | 56 |
| 4.1.2. <i>Methods</i> | 59 |
| 4.1.3. <i>Results and Discussion</i> | 70 |
| 4.1.4. <i>Conclusion</i> | 73 |

| | |
|--|------------|
| 4.1. MODEL II..... | 75 |
| 4.2.1. <i>Nanoindentation test and results</i> | 76 |
| 4.2.1.1. Results from nanoindentation using Berkovich indenter..... | 76 |
| 4.2.1.2. Results from nanoindentation using Spherical indenter and discussion... | 79 |
| 4.2.2. <i>Homogenization model of cement paste</i> | 82 |
| 4.2.3. <i>Results and conclusion</i> | 83 |
| CHAPTER 5. APPLICATION OF HOMOGENIZATION METHOD TO MODEL CONCRETE | 85 |
| 5.1. MODEL I: SERVICEABILITY PREDICTION USING CONCRETE HOMOGENIZATION | 85 |
| 5.1.1. <i>Introduction</i> | 85 |
| 5.1.2. <i>Concrete homogenization</i> | 86 |
| 5.1.3. <i>Case study</i> | 87 |
| 5.1.4. <i>Conclusions</i> | 90 |
| 5.2. MODEL II: ESTIMATING UNCERTAINTY IN CONCRETE DEFLECTION USING AN ENHANCED CONCRETE HOMOGENIZATION APPROACH..... | 92 |
| 5.2.1. <i>Introduction</i> | 92 |
| 5.2.2. <i>Methods</i> | 95 |
| 5.2.3. <i>Case study</i> | 102 |
| 5.2.4. <i>Results and discussion</i> | 108 |
| 5.2.5. <i>Conclusions</i> | 113 |
| 5.3. MODEL III: MODELING ASR IN CONCRETE USING CONCRETE HOMOGENIZATION | 115 |
| 5.3.1. <i>Introduction</i> | 115 |
| 5.3.2. <i>Methods</i> | 118 |
| 5.3.3. <i>Case study</i> | 124 |
| 5.3.4. <i>Results and discussion</i> | 126 |
| 5.3.5. <i>Conclusions</i> | 134 |
| CHAPTER 6. CONCLUSIONS AND FUTURE WORKS | 135 |
| 6.1. CONCLUSIONS..... | 135 |
| 6.2. FUTURE WORKS..... | 138 |
| REFERENCES | 141 |

PREFACE

The following publications have been co-authored by Tai Fan during his course of study:

1. **Fan, T.**, Kim, J. J., Reda Taha, M. M., & Shrive, N. G. (2009). A three-dimensional finite element model simulating damage and creep interaction in masonry. Proceedings of 11th Canadian Masonry Symposium (El-Dakhakhny et al. Eds), CD, Toronto, Canada.
2. Kim, J. J., **Fan, T.**, & Reda Taha, M. M. (2009). Examining uncertainty in deflection of reinforced concrete beams using concrete homogenization techniques. Proceedings of International Conference on Computational Design in Engineering (CODE09), Seoul, South Korea.
3. Kim, J. J., **Fan, T.**, & Reda Taha, M. M. (2010). A homogenization model examining the significance of nanoparticles on concrete strength and stiffness. Journal of the Transportation Research Board (TRB), No. 2141, 28-35.
4. **Fan, T.**, Kim, J. J., Reda Taha, M. M., & Shrive, N. G. (2010). Simulating damage and creep interaction in masonry columns considering interface debonding. Proceedings of 8th International Masonry Society Conference, Dresden, Germany, 1791-1799.
5. **Fan, T.**, Kim, J. J., Reda Taha M. M, & Shrive, N. G. (2011). Examining creep buckling in composite masonry columns. 11th North American Masonry Conference, Minneapolis, Minnesota, USA.
6. Kim, J. J. **Fan, T.**, & Reda Taha M. M. (2011). A homogenization approach for uncertainty quantification of deflection in reinforced concrete beams considering microstructural variability. Structural Engineering and Mechanics-An International Journal, Vol. 38, No. 4, 503-516.
7. Kim, J. J. **Fan, T.**, & Reda Taha M. M. (2011). Quantifying deflection variation in RC beams propagated from microstructural variability in concrete using homogenization technique. ACI Special Publication for Andrew Scanlon Symposium, in press.
8. Kim, J. J., **Fan, T.**, Reda Taha M. M., & Shrive, N. G. (2012). The effect of damage and creep interaction on the behaviour of masonry columns including interface debonding and cracking. Materials and Structures, Vol. 45, 15-29.

Chapter 1. Introduction

In current structural analysis of reinforced concrete structures, concrete material heterogeneity is typically neglected. While this approach proved suitable for ultimate strength design it is insufficient for reliable serviceability calculations. The reason is that concrete serviceability (e.g. cracking and deflection) is strongly tied to concrete microstructure and durability. There is a need for developing modeling techniques that are to bridge the gap between concrete material depicted by concrete microstructure and concrete structural behavior represented by serviceability.

An innovative homogenization modeling technique of concrete is proposed in this dissertation. At the microscale, cement paste representative volume element (RVE) incorporates hydrated cement microstructure phases followed by cement hydration; at the mesoscale, concrete RVE is modeled as discrete particles connected by interfacial transition zone (ITZ) with cracking and contact mechanisms. Based on the RVEs, the relationship between microstructure and macro properties is developed. The proposed model is validated by experimental results and its application for serviceability modeling in concrete is demonstrated by two case studies. The first study estimates uncertainty in concrete deflection, and the second discusses simulating the mechanical behavior of concrete subjected to alkali-silica reaction (ASR). The simulated results match well with experimental observations. It is shown that, concrete variability attributed to random microstructure is captured. The proposed modeling technique is proved capable of providing the link to integrate durability in concrete serviceability behavior.

The mechanical properties of concrete are determined by a group of specimens statistically. This fact indicates that common size concrete has no statistical homogeneity in mechanics (Hill 1963, Hashin 1983). Random microstructure and variation of phase properties are the sources for uncertainties in concrete (Ostoja-Starzewski et al. 2001; Kaint 2003; Khisaeva & Ostoja-Starzewskib 2006; Ostoja-Starzewski 2006 & 2007). Rather than a continuum material, it is more reasonable to consider concrete as a cluster of aggregate and cement paste particles linked by interfacial transition zone (ITZ) (Kim et al. 2009; Guo et al. 2009; Kim et al. 2010). Relationship between microstructure and macro properties can be built by homogenization to overcome the limitation of empirical description on concrete properties. In this dissertation, several homogenization models of concrete are proposed and applied. Ultimately, a discrete numerical model of concrete is given, in which particle interaction is achieved by cracking propagation and contact mechanics, and homogenization is used to bridge the scale gaps.

Evolution of particles and ITZ due to cement hydration, damage and loading will accompany concrete whole life. Cement hydration and reconstruction of cement paste are addressed by cement hydration and microstructure development models. Special theories and algorithms have been well developed in the literature such as HYMOSTRUC[®] (van Breugel 1995a & 1995b) or CEMHYD3D (Bentz 1997 & 2005). The developed microstructure of cement paste at different hydration ages can be transferred to a FEM model and homogenized out mechanical properties as inputs for simulation of concrete in large scale. While microstructure of cement paste is established by hydration models, (re)construction of concrete mesostructure is another important issue. It is challenge to (re)construct concrete RVE having same statistical descriptors with target image. First is

the irregular shape of aggregate, which is difficult to be generated by general mathematic equation. For simplicity, circular or overlapping spheres or circles were used in the literature to denote aggregate (Kurukuri 2005; Kim et al. 2009; Le Pape et al. 2009; Kim et al. 2011). Effects of aggregate particle shape were recognized (Häfner et al. 2006; Le Pape et al. 2009). Häfner et al. (2006) proposed an approach to regenerate aggregate by considering aggregate shape, size distribution and separation with significant time consumption. In this dissertation, concrete RVE is first built by converting the realistic concrete image into finite element model after Wu et al. (2010). Then a new method named cell operation is proposed to regenerate concrete image sharing similar statistical descriptors with two dimensional images of original concrete section. The similarity between reconstructed material and original image is verified by low-order correlation functions such as two-point correlation functions (Torquato 2002; Sumanasooriya et al. 2009; Li et al. 2010). The objective of microstructure (re)construction is to introduce randomness to RVE and simultaneously ensure the RVE generated is the same material with target image.

In this discrete model, particles are assumed to follow linear elasticity and the unknown properties of ITZ are found during the modeling process such that simulated results match experimental observations. Damage is realized by softening the ITZ. Moreover, time dependent properties such as creep can be modeled by memorizing position and deformation of particles and then relaxing stresses in each time step due to creep characteristics of the cement and/or the ITZ. The validated mesoscale model is then applied in the study of concrete serviceability.

Due to the limitation of current computational capacity, this modeling strategy cannot be realized on concrete unless introducing homogenization. Homogenization shares the same idea with experiment to get the average properties of composite material based on a representative volume element (RVE) or specimen (Hashin 1983). Strictly speaking, all materials are discrete composites with load-dependent properties and unsolvable boundary conditions (Suquet 1985; Hollister & Kikuchi 1992; Terada & Kikuchi 1995; Michel et al. 1999; Fish & Shek 2000). While scale separation cannot meet the requirement suggested by Hill (1956 & 1963) and Hashin (1983), approximation is inevitable and a balance between accuracy and computation cost has to be found in homogenization. By setting a tolerance to uncertainty from microstructure, RVE size can be determined (Kanit et al. 2003; Khisaeva & Ostoja-Starzewskib 2006); and uncertainty from phase properties will be investigated separately. The apparent properties attained from specimen are mapped on concrete structure to predict its macro performance. In nanoscale level, phases in cement paste RVE like calcium hydroxide (CH), calcium silicate hydroxide (C-S-H), etc., are assumed to be linear elastic and fully bonded (Haecker et al. 2005). Concrete nonlinearity is introduced by considering local damage, cracking propagation and particle contact mechanics.

Cement paste microstructure is developed by existing program package such as HYMOSTRUC[®] (van Breugel 1995a & 1995b) or CEMHYD3D (Bentz 1997 & 2005). Homogenization model of cement paste is validated by experimental study of nanosilica effect on the mechanical properties of cement paste. Nanosilica is a kind of pozzolantic material which can change cement paste microstructure by converting the weak CH crystals into strong C-S-H (Takemoto et al. 1980). This validation also endorses the

application of the proposed homogenization model of cement paste to simulate concrete with other pozzolantic additions like silica fume (microsilica) and fly ash, and gives a way in the direction of material optimizing.

With cement paste mechanical properties generated from cement paste RVE as inputs, homogenization model of concrete is validated by test results found in literature. The validation is focused on the constitutive model of concrete, and the serviceability study of concrete including propagating the microstructural variability of concrete to predict the deflection variation in RC beams. Furthermore, mechanical progression of concrete subjected to durability damage such as alkali-silica reaction (ASR) is also demonstrated.

Concrete is a composite material with significant variation in mechanical properties. Like other composite, the variation is inevitable because it is inherited from phases at lower scale level, such as randomness of microstructure, uncertain properties of each phase, etc. Deflection of RC beam includes wide variation especially when the moment redistribution mechanism due to cracking is considered. To quantify deflection variation in RC beams, we can do test or simulation. However, the probability-based investigation will need significantly large amount of specimens and tests that is cost prohibitive to conduct. On the other hand, the behavior in microstructure cannot be studied by traditional test methods. Numerical method is therefore necessary not only in view of cost but also in understanding of material microstructure. Uncertainties of phase mechanical properties and random microstructure can be treated as parameters to the cement paste RVE and concrete RVE models, while the macro properties corresponding to each case as output, and the variation of deflection can be quantified via Monte Carlo

(MC) simulation (Choi et al. 2004). The variation propagation predicted from numerical method will be validated by experiment results.

ASR was first discovered by Stanton (1940). It is the chemical reaction in concrete between alkali in cement and reactive aggregate. When ASR takes place, it will produce gels that can expand when absorbs water. The swelling of ASR gels will change concrete microstructure by inducing internal stress. Concrete structures affected by ASR are reported worldwide, for example, bridge and viaduct in Netherland (den Uijl et al. 2002), Temple-sur-Lot Dam in France (Sellier et al. 2009) and Ikata Nuclear Power Station in Japan (Takakura et al. 2005a & 2005b). Preventive measures against ASR are available but cannot work on the existing concrete structures. The safety concern of those important concrete structures has been drawing attention of researchers. Many experiments on ASR were launched out. Generally, it is concluded that ASR will degrade concrete, causing decrease in stiffness and strength (Clayton et al. 1988; Narayan Swarny et al. 1989; Fan et al. 1998). However, interaction of ASR expansion with reinforcement and/or prestress in concrete sometimes tells a different story. Ahmed et al. (1998) reported a case in which the shear capacity of RC beams is enhanced by ASR expansion. In other words, the mechanical consequences of ASR on concrete structure shall be studied in structural context. Test on concrete specimens (cylinder, prism or drilled core) cannot predict the performance of a structure subjected to ASR (Clayton et al. 1988). Furthermore, due to the long duration, accelerated speed ASR test is generally adopted. ASR expansion measured from accelerated test is different from ASR expansion in fields (Ideker et al. 2010). These difficulties in ASR study call for the understanding of ASR mechanism and make it necessary to model ASR by using homogenization methods.

The mechanical model of concrete subjected to ASR shall handle two basic challenges (Bažant et al. 2000). First is to simulate the chemical reaction on the basis of temperature, moisture and contents of alkali and silica. The second challenge is to model the mechanical alteration of concrete structure subjected to ASR. This dissertation will focus on the latter. By selecting ASR expansion ratio as the index, the proposed homogenization modeling of concrete simulates ASR-affected concrete via expanding aggregate to get target expansion ratio. Aggregate expansion can damage ITZ and the mechanical evolution due to ASR is achieved. The proposed ASR model is validated by experimental data of plain concrete specimens subjected to ASR.

Using the proposed homogenization technique, macro mechanical performance of concrete gains the opportunity to be connected with its microstructure. This is an important step towards bridging the gap between concrete material and structure that can lead to more accurate modeling and better design.

This dissertation is organized as follows. Chapter 1 is the introduction. Chapter 2 is a review of the literature that provides details on work done on homogenization methods, interfacial transition zone modeling approaches, methods to reconstruct concrete microstructure, and alkali-silica reaction (ASR) in concrete.

Chapter 3 presents the methods used in this dissertation, including homogenization methods, (re)construction of cement paste and concrete representative volume elements (RVEs).

Chapter 4 demonstrates the application of homogenization technique to model cement paste. With the help of cement hydration methods suggested by others, the proposed method for homogenization of cement paste is validated by experiments. In

these experiments, nanosilica was added to the cement paste. The mechanical effects of nanosilica are captured accurately by the homogenization technique.

Chapter 5 is focused on the applications of concrete homogenization methods. Mechanical properties from cement paste RVE are upscaled for concrete simulation. Benefited from the capability to study concrete from microstructure, the proposed model can propagate microstructural uncertainties to quantify the variation of deflection of reinforced concrete beams. The predicted results are validated by experiments reported by others. Another application is to simulate concrete subjected to ASR. By expanding aggregate in concrete RVE, cracking and mechanical evolution due to ASR are attained. The numerical results of ASR simulation are validated by ASR tests reported in the literature.

This dissertation is concluded in Chapter 6, which outlines the works done and gives vista of future works.

Chapter 2. Literature Review

2.1. Homogenization

In engineering, the idea of homogenization is prevalent. Concrete is studied by continuum mechanics in which continuum assumption is applied and mechanical property is determined experimentally based on specimens. Sharing this idea, the average property of composite defined on a representative volume element (RVE) can be attained analytically by understanding the particle interaction mechanism in microstructure (Hill 1963; Hashin 1983). In order to meet the continuum assumption, dimensions of particle size in microstructure, RVE or specimen, and macro structure shall satisfy the scale separation principle as shown in Equation (2.1) (Hill 1956 & 1963; Hashin 1983).

$$L_{micro} \ll L_{RVE} \ll L_{macro} \quad (2.1)$$

where, L_{micro} is the largest phase size in microstructure; L_{RVE} is the smallest specimen or RVE size and L_{macro} is the macrostructure size. Hill (1956) suggested that an effective continuum may be produced if the smallest dimension of specimen is 10^3 times larger than the largest particle size in microstructure. For concrete, the required scale separation is difficult to be satisfied. Part of the challenge is attributed to the fact that the cement paste is another heterogeneous composite. Strictly speaking, rather than a material, concrete shall be looked as a structure whose apparent properties are dependent on the boundary conditions applied. This point is illustrated in Figure 2.1. For concrete domain Ω , keeping its average stress (or average strain) constant, the corresponding boundary conditions and average strain (or average stress) produced are different in different structure or loading conditions. Therefore, different constitutive model (stress-strain

curve) will be produced under different boundary conditions for the domain Ω (Hill 1963, Hashin 1983, Suquet 1985, Hollister & Kikuchi 1992, Terada & Kikuchi 1995, Michel et al. 1999, Fish & Shek 2000).

Moreover, microstructure of concrete is random and hence each RVE or specimen is unique. Concrete material properties can only be defined approximately during the struggle to find the balance of reducing the cost in experiment or simulation by minimizing RVE size and improving the accuracy by increasing scale separation or finding actual boundary conditions. Ironically, aiming to get accurate macro continuum properties of composite, development of homogenization requires solving the actual boundary conditions of RVE in which continuum assumption is abandoned. However, actual boundary conditions are unsolvable (Hill 1963; Hashin 1983; Suquet 1985; Hollister & Kikuchi 1992; Terada & Kikuchi 1995; Michel et al. 1999; Fish & Shek 2000). Approximation is then unavoidable and a balance between accuracy and cost has to be found. For important structure, full scale test is necessary, which is analogous to simulate structure directly from microstructure.

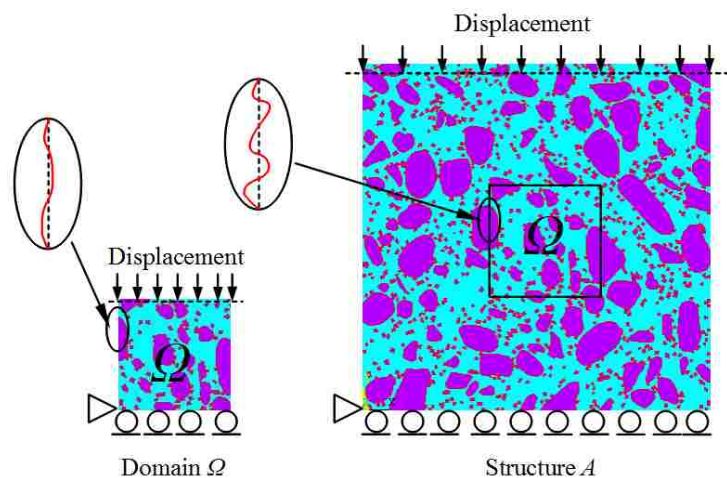


Figure 2.1: Mechanical properties are loading-dependent in concrete

Pioneer works in homogenization tried to find analytical solution of average properties derived from fields of RVE applied by adaptive boundary conditions. For most composite material, the fields are too complicated (Hill 1963; Hashin 1983). Analytical method is only practical for linear elastic composite with very simple microstructure, and satisfactory average properties can even be attained via the coarse solution of field (Hill 1963; Hashin 1983). However, acceptable average value does not mean analytical solution at certain point in microstructure is acceptable. It is common to observe 10 times difference of stress value in realistic microstructure with analytical solution (Hashin 1983).

Development of computer technique makes homogenization possible in numerical approach, which is the practical homogenization technique for nonlinear composite with complicated microstructure (Hollister & Kikuchi 1992). Numerical homogenization can be regarded as an expedient tool. Due to the limitation of computational capability, to model macrostructure directly from microstructure is frustrated (Fish & Shek 2000). In other words, more or less, information will be lost in the process of homogenization; therefore, the best way to model structure is from microstructure directly. But this approach is impossible due to the huge amount of elements and nodes. Homogenization is a bridge. It handles a RVE in microscale, getting and transferring information to models in macroscale. In nonlinear homogenization, this could be an interactive process in which RVE and macrostructure are coupled.

Various boundary conditions can be used in homogenization (Hollister & Kikuchi 1992; Kurukuri 2005). The only criterion is to ensure that, if RVE is statistically homogeneous, the produced fields are homogeneous except along the boundary layers

(Hill 1963; Hashin 1983). If scale separation is satisfied, different boundary conditions will give similar results (Hollister & Kikuchi 1992; Kurukuri 2005). Otherwise, for one RVE, different average properties are generated under different boundary conditions. There are two critical criteria for acceptable boundary conditions that, they have the maximum similarity with realistic boundary conditions in the macrostructure, and they can be implemented conveniently (Hollister & Kikuchi 1992). The former criterion is equivalent to minimum entropy theory (Berdichevsky 2007) recognizing that: under certain average stress, the minimum strain energy will be generated by realistic boundary conditions (Hollister & Kikuchi 1992; Michel et al. 1999; Fish & Shek 2000).

Practically, scale separation is limited to computational capacity and experimental cost (Fish & Shek 2000). The only way to improve homogenization is to solve the realistic boundary conditions on RVE. But the determination of actual boundary conditions of RVE is impossible mathematically. As shown in Figure 2.2, a RVE is an element in macrostructure, and four controlling nodes at RVE corners cannot determine the boundary conditions along RVE edges.

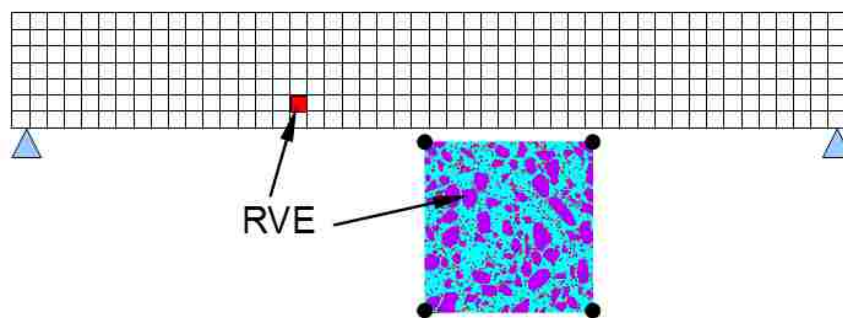


Figure 2.2: RVE and macro structure

For composite material with periodic microstructure, or even if the microstructure is random but scale separation is enough, the problem can be addressed by the asymptotic assumption developed independently by Sanchez-Palencia, Bakhvalov and Babuška

(Berdichevsky 2007): fields in composite material might be depicted approximately by asymptotic expansion. The accurate field in RVE is constituted with global constant and perturbations due to microstructure (Equation 2.2). Conveniently, as shown in Figure 2.3, the macro (for structure) and micro (for RVE) coordinates are denoted by x and y , respectively. The two coordinate systems have relation shown in Equation (2.3).

$$u_i(x, y, \delta) = u_i^0(x, y) + \delta u_i^1(x, y) + \delta^2 u_i^2(x, y) + \dots \quad (2.2)$$

$$\delta = \frac{x_i}{y_i} \quad (2.3)$$

where u_i is the exact field; u_i^0 is the average field; u_i^1 , u_i^2 , etc., are the perturb values of field due to microstructure; “...” denotes the omitted higher order items; δ is the ratio of global structure size to the microstructure size.

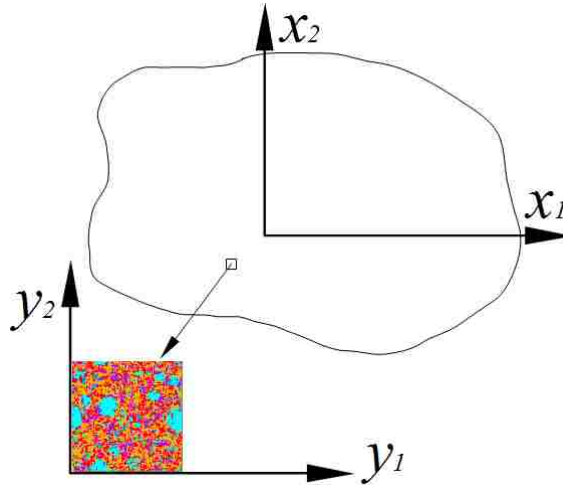


Figure 2.3: Macrostructure and periodic RVE

Assuming microstructure is periodic, periodic fields and periodic boundary conditions are expected in RVE except zones where stress gradient is significant. Knowing average stress or strain, the corresponding strain or strain can be solved iteratively by the introduction of periodic assumption (Suquet 1985; Hollister & Kikuchi

1992; Jasson 1992; Terada & Kikuchi 1995; Fish et al. 1997; Smit et al. 1998; Fish & Shek 2000; Allair 2001; Berdichevsky 2007; Li et al. 2008). Generally, in Equation (2.2), only the first order is considered. In order to improve accuracy, second order can be included with the cost to solve extra equations (Fish & Chen 2001; Kouznetsova et al. 2004; Kaczmarczyk et al. 2008). The method to couple macrostructure and microstructure with the help of periodic assumption is called multiscale homogenization. Obviously, near the boundaries of macrostructure, or, if microstructure is random and scale separation is not enough, periodic assumption cannot be satisfied and incompatibility will happen along RVE edges. The multiscale homogenization was improved as coupled multiscale homogenization analysis by considering the incompatibility along RVE edges (Fish & Shek 2000).

In summary, there are three homogenization methods as shown in Figures 2.4-2.6. The classic specimen testing method is the simplest one. With prescribed boundary conditions, relationship of average stress and strain can be attained easily (Kurukuri 2005; Sacco 2009; Böhlke et al. 2010). In multiscale homogenization, boundary conditions need to be solved by minimizing strain energy based on periodic assumption. The coupled multiscale method proposed by Fish and Shek (2000) can consider the incompatibility by interface elements shown in Figure 2.6 besides solving periodic boundary conditions. The three methods will give similar results if scale separation is large enough. Otherwise, more accurate results can only be obtained with long computation time. It is worth noting that, in Figure 2.5, iteration is still needed to solve the periodic boundary conditions. One of the derivations from periodic assumption is that, on the corresponding edges of RVE, fluctuations of displacement are same, except the

displacement contributing to the average macro strain. Periodic assumption just reduces the number of unknowns. For certain average strain, stress field can be determined by iteration via minimizing the strain energy in RVE. Exception cannot become reality unless another assumption is introduced, that is, fluctuations of displacement are assumed as zeros at the edges of RVE.

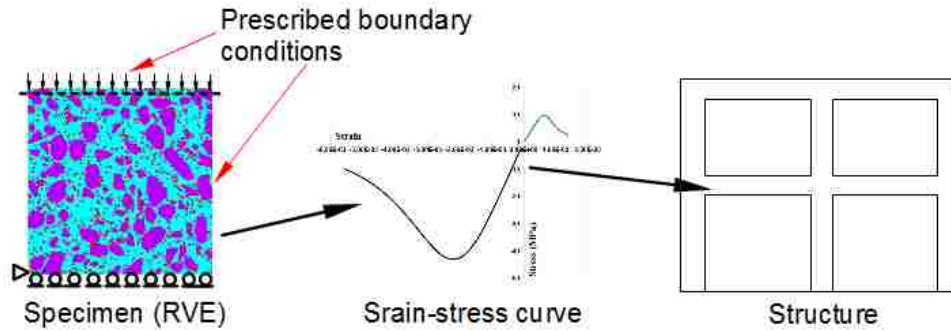


Figure 2.4: Specimen testing method

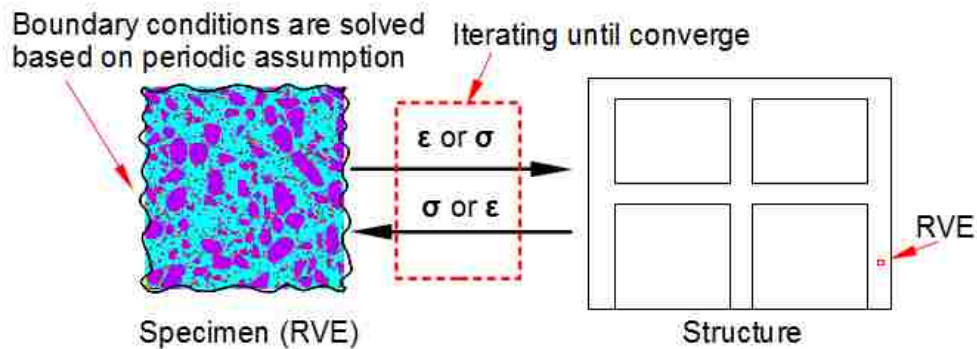


Figure 2.5: Multiscale method

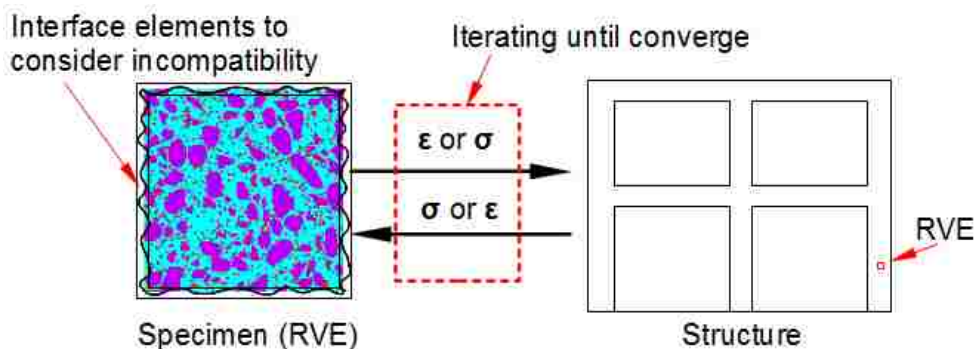


Figure 2.6: Coupled multiscale method (Fish & Shek 2000)

In some circumstances, periodic assumption cannot work, scale separation is not enough while the required accuracy makes it necessary to consider the fluctuations along RVE boundaries, homogenization will turn into a computational technique to couple substructure and global structure in simulation (Fish & Shek 2000), which is called as substructure technique and is presented briefly by Logan (2006). RVE is not necessary to be representative in that case and shall be called substructure and each substructure is unique. This approach is difficult to be implemented for huge structure because of being very computational expensive.

2.2. Homogenization Models of Concrete

Homogenization techniques are still under development. The mature parts of homogenization such as multicontinuum technology for continuous fiber-reinforced composite and variational asymptotical method for unit cell with simple microstructure are commercialized in program packages. However, there is much work to be done in correlating macro performance with microstructure for complex composites like concrete using homogenization analysis. Researchers all over the world are working to improve homogenization technique and to enhance concrete model based on micro-mechanics.

It is worth noting the work done by Schlangen and van Mier (1992), Chang et al. (2002), van Mier et al. (2002) and Guo et al. (2009) to model concrete by using a microstructural mechanics method, in which an assumed lattice network of beams or trusses is generated based on concrete mesostructure; and the properties of lattice elements are determined from concrete constituent properties (Guo et al. 2009). Concrete mesostructure is replaced by the equivalent lattice network to be simulated. The classical lattice model of concrete was improved by Cusatis et al. (2003a & 2003b) as

confinement-shear lattice model, in which the lattice spacing was determined by considering realistic mesostructure. Shear transmission was introduced with the capacity of friction and cohesion. The lattice model was used to study concrete fracture behavior (Cusatis & Cedolin 2007).

Microplane model for quasibrittle material like concrete was proposed by Bazant and Oh (1985) and improved by Cusatis et al. (Bazant et al. 2004; Cusatis et al. 2008a & 2008b). The model is based on the slip theory of plasticity. In microstructure, material is described by stress and strain vectors at any possible direction, and the micro vectors are correlated to macro stress and strain by a variational principle. Although no homogenization is mentioned in aforementioned works, they give ideas to model concrete in microstructural mechanics approach.

Kurukuri (2005) developed a concrete RVE model to study concrete damage, in which aggregate particles were generated by randomly dispersed spheres and damage was simulated via isotropic nonlocal damage model. Prescribed boundary conditions were applied on the RVE to generate load-displacement curve. Wriggers & Moftah (2006) developed a mesoscale model for concrete to consider homogenization and damage behavior. In their model, aggregate particles were also generated by randomly dispersed spheres. High volume ratio of aggregate was achieved by a new algorithm that to move and rotate the intersecting particles until a free position satisfying the placing requirements is found. Isotropic damage model was applied to simulate mechanical behaviour of concrete under uniaxial compressive loading. Häfner et al. (2006) were not satisfied with spheres to denote aggregate particles in concrete, and proposed an approach

to regenerate aggregate particles considering aggregate shape, size distribution and separation.

In 2009, a concrete RVE model including ITZ to connect cement paste and aggregate was proposed by our research group at the University of New Mexico (Kim et al. 2009). In this model, concrete is composed by three phases as cement paste, aggregate and ITZ. The properties of the cement paste are predicted by using cement hydration model enabling time dependent strength growth. Aggregate is denoted by sphere or circle in two-dimensional model and all phases are fully bounded. Specimen testing homogenization is used to get the average properties of RVE. The fluctuation of mechanical properties due to random microstructure is investigated. In the same year, Le Pape et al. (2009) suggested a homogenization model of concrete. Two phases in concrete RVE were considered: aggregate and cement paste. Aggregate is generated by overlapped spheres and cement paste strength is determined by a virtual cement and concrete aging analysis toolbox *Vi(CA)2T*. In order to overcome mesh problem, interphase element was introduced. Concrete RVE first is meshed freely without considering aggregate particles, and then elements including more than one phase will be redefined as interphase elements. The properties of interphase element are determined by homogenization on the basis of property and volume fraction of each phase.

Permeability of pervious concrete was also studied by using concrete RVE (Sumanasooriya et al. 2010). Two-point correlation function was used to verify the similarity between generated concrete RVE and original planar section image. Penetration simulating of concrete shield was carried out by using concrete homogenization (Wu et al. 2010). In this case, concrete RVE was built by converting

actual 3D concrete image into finite element environment and perfect bond is assumed between phases. Multiscale homogenization method is used to predict global structure behavior based on concrete RVE.

2.3. Reconstruction of RVE with Random Microstructure

For material with random microstructure, RVE constructed shall be big enough to demonstrate its representativeness (Kanit et al. 2003, Khisaeva & Ostoja-Starzewskib 2006), and the microstructure shall have the maximum similarity with original material (Torquato 2002, Sumanasooriya et al. 2009, Li et al. 2010). Two critical issues shall be considered here: representativeness and similarity of microstructure. The two issues are discussed below.

2.3.1. Representativeness

The representativeness of RVE for material with random microstructure is discussed thoroughly by Kanit (2003) and Khisaeva & Ostoja-Starzewskib (2006). It was proposed that this RVE would rather be considered a statistical volume element (SVE) due to stochastic aspect of microstructure (Ostoj-Starzewski 2006 & 2007). It might be necessary to construct a RVE according to the purpose of use on the basis of representativeness and cost. For certain size L_I , 100 RVEs are generated and homogenized out mechanical property E , which has the probability distribution function (PDF) as shown in Figure 2.7.. If the PDF variance is within an accepted range, the size of RVE can be considered big enough and the RVE is representative.

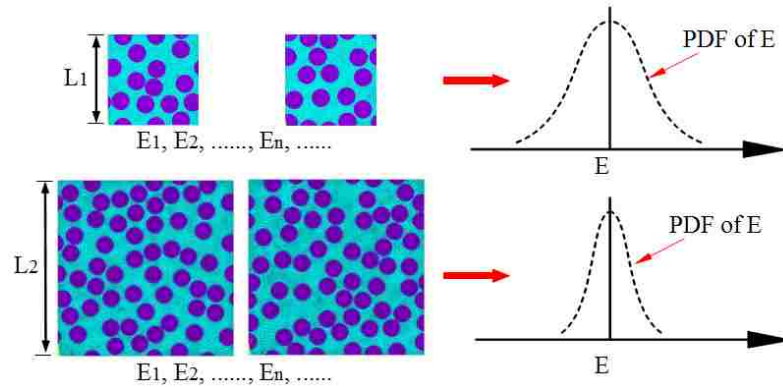


Figure 2.7: PDF of homogenized property from different RVE size showing the significance of RVE size on the uncertainty of concrete material characteristics

However, in some circumstances, it is difficult to attain enough images of microstructure. For this case, a new method is proposed here to check the representativeness. For a RVE with size L , 100 sub-RVEs will be cut from it randomly as size $L/2$. The homogenized property from a RVE is one value. However, the homogenized property from 100 sub-RVEs scatters and its probability distribution function (PDF) is shown in Figure 2.8. If coefficient of variation (COV) is within an accepted range (e.g. $\text{COV} \leq 15\%$), we can say the RVE size is big enough and the condition meets representativeness requirements.

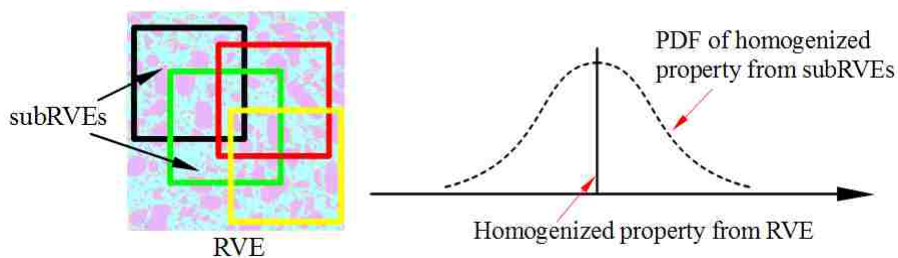


Figure 2.8: Homogenized property from RVE and subRVEs

2.3.2. Similarity

If RVE is constructed by converting material image into finite element environment, similarity can be ensured automatically. But in many cases, it is not easy to

get enough images of original microstructure. RVE has to be generated based on limited information and similarity needs to be checked by statistical descriptors such as two-point correlation function, which is a standard technique for the (re)construction of microstructure (Torquato, 2002). But it worth noting that, two-point correlation function is a necessary but not enough condition to specify an image.

For a point x in a image, if this point is included in i -th phase V_i , the indicator I of x for phase i is 1 and this can be described as (Li et al. 2010)

$$I^{(i)}(x) = \begin{cases} 1, & \text{if } x \in V_i \\ 0, & \text{otherwise} \end{cases} \quad (2.4)$$

For a specific distance r between two points, the indicators of n -points for a series of m -phases are summarized and normalized by the summation of indicators of all possible series of m -phases.

$$P_r^{S_k} = \frac{\sum_{l=1}^N I_l^{S_k}(X)}{\sum_{l=1}^N I_l^{S_1}(X) + \dots + \sum_{l=1}^N I_l^{S_k}(X) + \dots + \sum_{k=1}^N I_k^{S_{m \times m}}(X)} \quad (2.5)$$

where, N is the number of point set X generation. The above equation represents a probability that a random choice of n -points spacing r lies in a series of m -phases. This equation also represents the volume fraction of i -th phase with the series of m -phases as $\{i, i, \dots, i\}$ with spacing r of zero. Two-point correlation function is used for two-phase microstructure. For two phase composite material of phase 0 and phase 1, the possible series of two phases are four cases of $\{0,0\}$, $\{0,1\}$, $\{1,0\}$, $\{1,1\}$, considering randomly selected 4 vectors (length of r) in composite space as shown in Figure 2.9. The values of I are listed in Table 2.1 for different circumstances. By increasing the number of vectors and decreasing r , the calculated $P^{(1,1)}$ converges to the volume fraction of Phase 1.

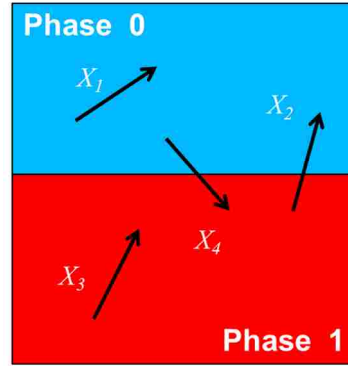


Figure 2.9: Four vectors in composite space

Table 2.1: Vectors value

| N | x_1 | x_2 | $I\{0,0\}$ | $I\{1,0\}$ | $I\{0,1\}$ | $I\{1,1\}$ |
|-----|---------|---------|------------|------------|------------|------------|
| 1 | Phase 0 | Phase 0 | 1 | 0 | 0 | 0 |
| 2 | Phase 1 | Phase 0 | 0 | 1 | 0 | 0 |
| 3 | Phase 1 | Phase 1 | 0 | 0 | 0 | 1 |
| 4 | Phase 0 | Phase 1 | 0 | 0 | 1 | 0 |
| Sum | | | 1 | 1 | 1 | 1 |

2.4. Interfacial Transition Zone (ITZ)

As a prominent construction material, workability and mechanical performance are the two important characteristics for concrete. While the former is achieved via cement paste, concrete mechanical properties are improved by adding aggregate particles or by innovative approaches such as pozzolanic reaction. However, as a multiphase composite, different phases or particles in concrete can only be connected by bondage zone developed from cement paste, which is called as interfacial transition zone (ITZ) in the literature (Scrivener 2004, Paulon et al. 2004). ITZ plays an important role in determining concrete strength, stiffness and durability (Li et al. 1999). Therefore, how to model ITZ is the key challenge in concrete homogenization. Guo et al. (2009) introduced lattice element to model ITZ. Kim et al. (2009) modeled ITZ by plane elements with thickness. The properties of ITZ were typically assumed due to limited knowledge of ITZ.

2.5. Alkali Silica Reaction (ASR)

ASR was first reported by Stanton in 1940. This type of chemical reaction is called “concrete cancer” (Sharp, 2006) and has been attracting attentions from researchers all over the world. While cement hydration will improve concrete stiffness and strength, with ASR this may be not the case. A kind of gel is developed through ASR. The ASR gel can expand when it absorbs water. Swelling of ASR gel first will occupy voids, and then will push other particles in concrete microstructure. If the pressure is high enough, cracking and volume expansion can be observed on macro concrete structure. Now researchers reach the consensus that ASR will damage concrete material if ASR expansion reaches the threshold as experiment results reported in literature: 20% decrease of the modulus of elasticity without reduction of other mechanical properties (Multon et al. 2005), 70% decrease of the uniaxial tensile strength (den Uijl & Kaptijn 2002). However, existence of reinforcement and prestressing strands can make the problem more complex. Ahmed et al. (1998) published a case in which a RC beam subjected to ASR has damaged concrete but improved shear capacity.

With the progressive understanding of ASR, several methods to prevent ASR from concrete were given and adopted in design and construction, such as keeping concrete dry, using nonreactive aggregate or adding fly ash to concrete mix (Heijnen & Larbi 1999). These measures work well for concrete project built now, but they are helpless for existing structure. For example, some structures are designed to serve in water, and reactive aggregate cannot be avoided for concrete structure cast 10 years ago.

ASR is a relative slow process, for a structure, if ASR is a problem, this structure generally is important and was designed to stand safely for a service life of 50 or 100

years. ASR was not considered when those structures were built. The question raised now is, are these structures safe to stand for the next 50 years? To answer this question, appraisal of the existing structures is required. However, for concrete structure subjected to ASR, strength test methods are questionable due to the fact that, ASR's effect on concrete is not only the degradation of material, but also the superposition of concrete expansion and confinement from reinforcement or prestress. For a prestressed bridge girder, the ASR expansion ratio on surface is about 1.5 times of that at the core of the girder, based on drilled cores (Clayton et al. 1990). Moreover, steel is stretched by ASR expansion (Swamy & Al-Asali 1989). Strength test on concrete cores drilled from structure does not necessarily reflect the realistic boundary conditions. Therefore, study from microstructure seems necessary, and several numerical models were recently deployed by researchers. In the following section, we will introduce the current state of knowledge on ASR.

2.5.1. ASR mechanisms

Alkali in cement, reactive silica in aggregate and adequate moisture is the three necessary conditions for ASR (Neville 1996). This chemical reaction is too complicated and its details are difficult to be figured out (Bažant 2000). In some senses, ASR process can be depicted as following. Along the surface of aggregate, transported by water, alkali from cement meets with silica from aggregate, chemical reaction between silica and cement happens and ASR gel is generated. The ASR gel expands when it absorbs water. The swelling gel first occupies voids in concrete. With ASR proceeding and gel expanding, internal stress will be produced. The process is simplified as shown in Figure 2.10. Temperature, moisture, and contents of alkali and silica will affect the chemical

reaction while outer confinement will influence ASR expansion. To study ASR, experiment needs to be launched out to quantify the consequences of circumstances. Then numerical models need to be established in two levels: chemical reaction and mechanical interaction.

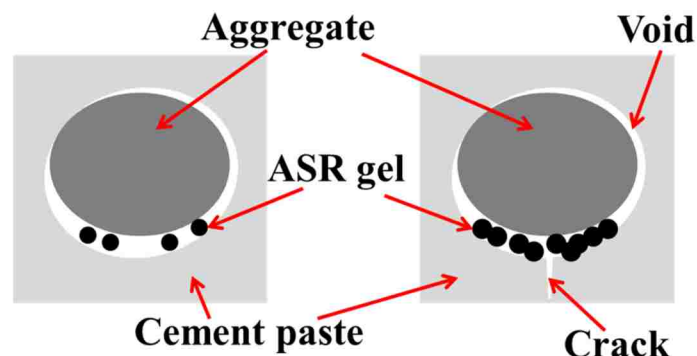


Figure 2.10: Generation and expansion of ASR gel

2.5.2. Experimental study of ASR

In 1989, Swamy and Al-Asali published test results on the deformation and strength of RC beams subjected to ASR. Five beams were cast, one is the control beam without reactive aggregate, and two beams have normal reactive aggregate while the other two include highly reactive aggregate. All beams have identical steel reinforcement and have dimension of 75mm×100mm×800mm. The five beams and their control specimens (75mm×75mm×300mm prism) were kept in temperature of 20°C and relative humidity of 96% for two years. Then the five beams were loaded to failure.

It was observed that, ASR affected whole concrete members. Expansion due to ASR decreases from surface to core and is confined by steel reinforcement. Correspondingly, steel was elongated by ASR expansion. But no debonding was observed between steel and concrete. ASR-induced volume expansion, working together with reinforcement, causes strain gradient along the cross-section of beams, hence

hogging and cracking. Stiffness of the beams is decreased by ASR. Interaction of ASR-induced expansion with reinforcement can be analogous to prestressed concrete structure. Expansion was measured along casting direction.

Clayton et al. (1990) presented test results of prestressed concrete beams. Totally 28 I-beams were cast, with and without shear reinforcement. After demolding, each I-beam was cut into one 5-meter and two 2.5-meter length beams. These beams with their control specimens were cured in 20°C water tanks for 5 months before test. Some specimens were cured for over 2 years. Concrete strength was reduced by ASR. The original relationship between compressive strength and tensile strength in concrete was redefined too. Clayton et al. (1990) did not hypothesize tensile strength loss due to ASR can be evaluated by cylinder splitting test. That is because ASR expansion in casting direction is different from the ASR expansion in lateral direction, and the former is about 1.5 times the latter. Different expansion ratio might mean different deterioration. Besides different expansion in different direction, experiment demonstrated that expansion ratio increases from outer to inner of concrete members. ASR-induced expansion ratio on the surface is about 1.5 times of the expansion at the core, attributing to prestress and reinforcement. This work reported no more strength loss if expansion ratio is bigger than 0.01. Flexural capacity did not see obvious decrease. Shear capacity of concrete beam lost 20% due to ASR, but it can restore by the prestress effect due to ASR expansion, which limits the concrete damage.

The enhanced shear capacity of RC beams was proved by experiment done by Ahmed et al. (1998). Four RC beams were cured in 40°C water to accelerate ASR for five months before test. Reinforcement significantly reduced ASR expansion by 74%

compared to the concrete prisms without reinforcement. It was believed that prestressing due to ASR expansion contributes to the improved shear capacity. Chang and Kesler (1958) also reported the similar results about RC beams.

Fan and Hanson (1998) carried out the experiment on RC beams and concrete cylinders with and without ASR. All specimens were put in a water tank for one year. The water was first heated to 38°C for 5 or 7 days, then cooled down to 24°C for 2 days. This process was repeated until the test finished. Due to ASR, compressive strength, splitting tensile strength and dynamic modulus of concrete cylinders observed significant decrease as 24%, 38% and 31% at age of about 180 days, respectively, compared to those values at age of 28 days. There is nearly no more decrease if expansion ratio is bigger than 0.01, which is comparable to the discovery by Clayton et al (1990). However, experiment demonstrates that reduction in concrete strength and stiffness did not lead to decrease of flexural capacity in RC beams, even if the beams were cracked by ASR.

Ahmed et al. (1999) launched out another batch of tests on RC beams subjected to ASR, focusing on the bond strength between concrete and reinforcement. Twenty-four beams with dimension of 120mm×200mm×1300mm with their control specimens were cast and cured in the hot water tank (38°C) for five months. Experiments revealed that, in the first four weeks, shrinkage was over ASR expansion. Ultrasonic pulse velocity (UPV) decreased with the ASR proceeding. Concrete strength and stiffness observed reductions in concrete prisms and cylinders due to ASR. Bond strength between reinforcement and concrete was also deteriorated. The fatigue life of concrete beam was damaged by ASR.

Bearing capacity of plain and reinforced concrete blocks was studied by Ahmed et al. (1999). Totally, 35 plain and reinforced concrete blocks with dimension of

200mm×200mm×300mm, and 4 plain and reinforced concrete blocks with dimension of 400mm×400mm×600mm were made and put into 38°C water to accelerate ASR for 6 months. The specimens were loaded by different ways. Results showed that ASR can damage concrete. Smaller expansion was expected in bigger concrete block, and smaller expansion lead to less damage.

den Uijl and Kaptijn (2002) studied ASR-affected structures in service, including bridge decks and 35 years old viaducts. Concrete cores were drilled and six beams were sawn from these structures. Uniaxial tensile tests were carried out on cores and shear tests were launched on beams. It was reported the big different reduction in splitting tensile strength and uniaxial tensile strength are different, about 15% and 70% loss, respectively. This indicated that ASR expansion might change concrete as anisotropic material, that is, the orientation-dependent tensile strength.

Aforementioned experiments are all about concrete members without external loading. Monette et al. (2002) carried out systemic tests on concrete beams conditioned in hot water to accelerate ASR without loading, with sustained loading or cyclic flexural loading. Concrete material properties were gotten from control specimens such as cylinders and prisms, which were cured in the same accelerating circumstances without loading. It was demonstrated that reinforcement and sustained load confined ASR expansion. Although the static modulus of elasticity, dynamic modulus of elasticity and modulus of rupture decreased, no reduction in the flexural capacity of RC beams was observed, whether they were under sustained loading, cyclic loading or service loading, even increase in shear capacity was observed due to ASR expansion.

A large integration of ASR experiment was performed by Multon et al. (2005), aiming to understand ASR and give data to validate numerical model. RC beams and their control specimens were cast and conditioned in 38°C temperature for about 2 years. To establish the relation between ASR and humidity, moisture gradient was created by immersing bottom surface of beam into water and leaving top surface of beam in the air with relative humidity (RH) of 30%. Tests indicated that ASR expansion can be reduced by reinforcement. Due to ASR, only the modulus of elasticity decreased. It seems that effect of cement hydration was larger than ASR.

Multon & Toutlemonde (2006) studied the effect of applied stress on concrete members subjected to ASR. They concluded that the total volumetric expansion can be regarded as constant. While ASR expansion is confined in the direction external stress applied, larger expansion ratio is expected in other directions.

The experiment lasting about four years was done by Asai et al. (2009). Five prestressed concrete beam specimens and their control prisms and cylinders were cast and cured in accelerated ASR circumstances. Tests on the cylinders showed that, compressive strength, modulus of elasticity and tensile strength decreased with the development of ASR. The reduction in mechanical properties reached the limit when ASR expansion ratio is beyond 1.1%. ASR-induced cracking developed along the direction prestress applied. It was also found that the mechanical consequences of ASR on concrete were affected by compressive load. In the direction of compressive load applied, no obvious degradation was observed in concrete.

Due to the long duration of ASR, most experiments used accelerated speed test method. Although accelerated test is allowed in codes (CSA, ASTM), Ideker et al. (2010)

observed that ASR expansion ratio in the accelerated test is significantly lower than normal speed test. So is the ASR mechanism in field same with that in lab? More research is necessary to answer the question.

In conclusion, experiments give us the first impression of ASR, which can be affected by temperature, moisture and mechanical boundary conditions. For concrete without ASR, compressive strength is already correlated to tensile strength by experiment to build the design system for concrete structure. But this relationship can be destroyed by ASR and the traditional concrete design is challenged. Researchers tend to select the macro ASR expansion ratio as the index to the mechanical consequences. Maybe there is no better flag available to measure the ASR development. Scattering results are common in ASR experiment.

2.5.3. Models of ASR

To model ASR, two subjects need to be addressed. First is to simulate the chemical process of ASR, which shall predict the amount of gel generated based on circumstances. Second is to model the mechanical behavior of concrete subjected to ASR. The mechanical model can choose an index such as ASR expansion ratio to build the relationship between mechanical performance and ASR development.

Bažant & Steffens (2000) gave a way to simulate the chemical process of ASR. Similar with the cement hydration model HYMOSTRUC[®] presented by van Breugel (1995), the chemical reaction is developed on an idealized spherical reactive particle. From outer to inner, silica is consumed and ASR gel is generated. Swelling of gels causes ASR expansion. Reaction speed is affected by two diffusion processes, reactive silica dispersing into water from aggregate and water immersing into gels to cause expansion.

Bažant & Steffens discussed the effect of aggregate particle size on ASR, and their model succeeded in simulating the phenomenon discovered by Meyer et al. (1998): there is a critical size of aggregate particle which can cause maximum damage to concrete.

Ulm et al. (2000) published a thermo-chemo-mechanics model for ASR expansion. ASR was studied from microscopy and ASR expansion was assumed as imposed strain in concrete. Temperature and moisture were regarded as the two key factors affecting ASR. A coefficient defining relationship between ASR expansion ratio and outer circumstances was adopted. This expansion coefficient is derived through experiment. In this model, prestress or anisotropy of ASR expansion is not considered.

Another ASR model was presented by Bangert et al. (2004). Concrete was treated as composite constituted by three phases as skeleton, liquid and gas. But only one-dimensional parameter as the volume fraction of each phase is studied. ASR expansion is quantified by a chemical model which can correlate temperature and water with ASR development. Experiments were used to determine the parameters needed. Material deterioration was achieved by the imposed expansion strain gradients.

Schlangen & Copuroglu (2008) presented a lattice model for ASR, which only simulates mechanical effects of the ASR expansion. In the finite element model, concrete is composed by three phases as ITZ, aggregate and cement paste. All elements are linked by virtual beam elements which can transfer force and moment. By expanding ITZ or aggregate, the macro ASR expansion can be achieved. Expansion of elements damages the virtual linking elements and concrete. The idea to model concrete subjected to ASR by using lattice model was also proposed by Cusatis et al. (2011).

An ASR model which can consider creep, shrinkage and anisotropic damage was presented by researchers and applied in a dam appraisal (Grimal et al. 2008, Sellier et al. 2009). Based on the experimental results, relationship between macro expansion ratio and temperature, moisture, amount and type of reactants, are established. The calculated ASR expansion strain was imposed on the finite element model of a dam to induce cracking and damage.

Matsushima et al (2009) gave a way to model cracking caused by ASR. In the finite element modeling of concrete, aggregate particle was denoted by rectangular elements randomly dispersed in concrete. Concrete damage was achieved by the expansion of aggregate elements. By correlating ASR expansion ratio to moisture based on experiment results, concrete degradation can be predicted if moisture is known. Similar idea is seen in the models given by Multon et al. (2009), Grimal et al. (2008) and Sellier et al. (2009). In these models, researchers used experimental approach to build the relation between ASR expansion ratio and circumstance parameters. Finally, the relation between circumstances and mechanical consequences of concrete subjected to ASR can be developed.

Comby-Peyrot et al. (2009) developed a 3D mesoscale concrete model. First, concrete finite element model was generated and meshed. Based on the existing mesh, aggregate are created randomly. Although authors mentioned that concrete was composed by aggregate, mortar and ITZ, no mechanical property was considered for ITZ. Damage is realized by killing mortar element whose strain reaches the critical value. The critical strain value is determined inversely by experiment. In this model, ASR expansion is simulated by expanding aggregate elements. The expansion of aggregate elements

follows an expansion-time curve determined by test. Cracking and progressive loss of stiffness in concrete were well simulated.

Dunant & Scrivener (2010) simulated ASR expansion by planting gels in aggregate particles. The growth of ASR gels can cause crack and deteriorate concrete.

In conclusion, ASR simulation is generally divided in two stages. So far the details of ASR are not figured out; therefore experiment is the only way to correlate ASR expansion to temperature, moisture, contents of reactants, and other factors. Once the chemical model to simulate ASR is determined, mechanical simulation of ASR expansion is needed to predict the physical consequences. This is typically done by imposing strain or by expanding certain elements, such as aggregate particles.

Chapter 3. Methods

3.1. Homogenization Methods

Mechanical properties of material are attained by applying adaptive boundary conditions on specimen or RVE. The accuracy of properties generated depends on the boundary conditions applied. Therefore, several boundary conditions generally used in homogenization will be introduced here. Then homogenization methods in analytical and numerical approach are presented. Considering the three factors, required accuracy, computational time and complexity of concrete microstructure, specimen testing method is selected in this dissertation to model cement paste and concrete RVE.

For composite with random microstructure, concept of statistical volume element (SVE) is used to replace RVE by some researchers (Ostoja-Starzewskib 2006 & 2007). The reason is that, the common selected size of RVE is relative small and cannot be exactly representative of microstructure including randomness. Rather by one RVE, the mechanical properties of composite shall be depicted statistically by a group of SVEs, analogous to the number requirement in code for concrete specimen. With the scale separation is difficult to be satisfied, with the randomness in microstructure and unsolvable boundary conditions; approximation is inevitable in homogenization, whether in numerical or experimental approach. A balance between accuracy and cost needs to be determined for a specific problem. The word RVE will be used in this dissertation with recognizing the fact that RVE is only the approximate representative for material with random microstructure.

3.1.1. Boundary conditions used in homogenization

There are two categories of boundary conditions. One category is prescribed boundary conditions, which are known in advance. Homogeneous boundary condition belongs to this category. If both traction and displacement are applied, they are called mixed boundary condition in the literature (Kurukuri 2005, Böhlke et al. 2010). The other category of boundary conditions is characterized by the need to be solved during analysis. Periodic boundary condition proposed by Suquet (1985) is the typical one. It is believed that periodic boundary condition tends to give more accurate results even when periodic assumption cannot be satisfied (Hollister & Kikuchi 1992).

Mixed boundary condition

The mixed boundary condition shown in Figure 3.1 is one type of mixed boundary conditions (Böhlke et al. 2010). Displacement is prescribed on the left and right boundaries for the tensile or compressive direction; on other boundaries, zero traction is applied.

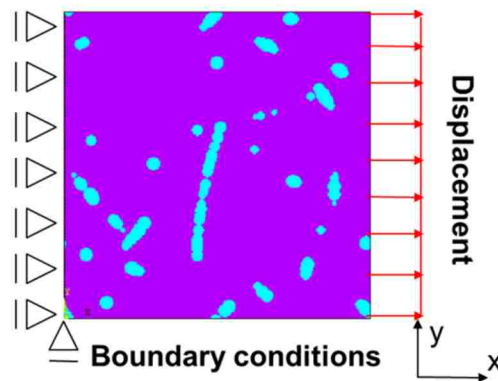


Figure 3.1: Mixed boundary condition on RVE

Homogeneous boundary condition

In analytical approach, homogeneous boundary condition is presented to produce homogeneous fields in a homogeneous RVE (Hashin 1983). It is prescribed as

$$u_i(s) = \varepsilon_{ij}^0 x_j \quad (3.1)$$

$$t_i(s) = \sigma_{ij}^0 n_j \quad (3.2)$$

where u_i is the displacement applied in i -th direction on the boundary s at point x_j ; ε_{ij}^0 is the constant strain in ij -th direction; t_i is the traction applied in i -th direction on the boundary s at point x_j ; n_j is the normal vector to boundary s ; σ_{ij}^0 is the constant stress in ij -th direction.

Periodic boundary condition

To consider the fluctuations along RVE boundaries, periodic boundary condition is proposed by Suquet (1985) as

$$u_i(s^+) = \varepsilon_{ij}^0 x_j^+ + u_i^* \quad (3.3)$$

$$u_i(s^-) = \varepsilon_{ij}^0 x_j^- + u_i^* \quad (3.4)$$

$$u_i(s^+) - u_i(s^-) = \varepsilon_{ij}^0 (x_j^+ - x_j^-) = \varepsilon_{ij}^0 L_{RVE} \quad (3.5)$$

where s^+ and s^- are the two opposite parallel edges of RVE; x_j^+ and x_j^- are a pair of points on the edges s^+ and s^- ; u_i^* is the unknown periodic displacement function; L_{RVE} is the edge size of RVE. In the literature, Equation (3.5) is simplified by setting an arbitrary value for x_j^- (Kurukuri 2005). The average strain and stress in RVE can be obtained from Equations 3.6 and 3.7, respectively (Hollister & Kikuchi 1992; Sun & Vaidya 1996).

$$\bar{\varepsilon}_{ij} = \frac{1}{|V_{RVE}|} \int_{V_{RVE}} \varepsilon_{ij} dV_{RVE} = \frac{1}{|V_{RVE}|} \int_{S_{RVE}} \frac{1}{2} (u_i n_j + u_j n_i) dS_{RVE} \quad (3.6)$$

$$\bar{\sigma}_{ij} = \frac{1}{|V_{RVE}|} \int_{V_{RVE}} \sigma_{ij} dV_{RVE} = \frac{1}{|V_{RVE}|} \int_{S_{RVE}} \frac{1}{2} (t_i y_j + t_j y_i) dS_{RVE} \quad (3.7)$$

where, $\bar{\varepsilon}_{ij}$ and $\bar{\sigma}_{ij}$ are the average stress and strain in ij -th direction. Average stress and strain are related by effective stiffness tensor as (Hollister & Kikuchi 1992, Sun & Vaidya 1996)

$$\bar{\sigma}_{ij} = \bar{C}_{ijkl} \bar{\varepsilon}_{kl} \quad (3.8)$$

where, \bar{C}_{ijkl} is the composite material effective property and called as stiffness tensor. If RVE cannot be representative, \bar{C}_{ijkl} denotes the apparent property of composite material.

Compared to homogeneous boundary condition, periodic boundary condition needs to be solved iteratively. It can be found that homogeneous boundary condition is the special case of periodic boundary condition. When boundary condition is implemented in FEM, the effective property will be affected by the discreteness of FEM. The effect will diminish by increasing the RVE size or using a fine FEM mesh due to Saint-Venant's principle (Hollister & Kikuchi 1992; Sun & Vaidya 1996).

3.1.2. Analytical approach

Analytical approach aims to determine the solution of fields in RVE analytically. Except in special cases, it has to compromise the complexity and stops at the average properties of composite material with simple microstructure (Hill 1963, Hashin 1983). Exact solution of fields does induce exact solution of average properties. In many cases, decent average properties can come from fields with big differences in details from the exact one because it is an average problem (Hashin 1983). Application of analytical approach is strictly limited to two-phase composite material with simple aggregate geometry such as circle or ellipse. In analytical approach, it is convenient to describe material properties via the bulk modulus K and shear modulus G rather than Poisson's

ratio ν and the modulus of elasticity E . The relationships between these parameters are described in Equations (3.9-3.11) (Hill 1963).

$$\nu = \frac{1/2 - G/3K}{1 + G/3K} \quad (3.9)$$

$$\frac{3}{E} = \frac{1}{G} + \frac{1}{3K} \quad (3.10)$$

$$E = 2G(1 + \nu) = 3K(1 - 2\nu) \quad (3.11)$$

The average properties, bulk modulus \bar{K} and shear modulus \bar{G} , will be expressed by each phase's property and volume fraction.

3.1.2.1. Direct method

To find the exact solution of material properties is the target of direct method. For linear two-phase composite material, when homogeneous boundary condition applied, Equations (3.12-3.13) present the relationship between fields and properties (Hashin 1983).

$$\bar{K} = K_M + (K_A - K_M) \frac{\bar{\varepsilon}_A}{\bar{\varepsilon}} V_A \quad (3.12)$$

$$\bar{G} = G_M + (G_A - G_M) \frac{\varepsilon_A^*}{\varepsilon^*} V_A \quad (3.13)$$

where, subscript M denotes phase matrix; subscript A denotes phase aggregate. V_A is the volume fraction of phase aggregate. $\bar{\varepsilon}_A$ is the average strain of phase aggregate; $\bar{\varepsilon}$ is the average strain of composite. ε_A^* and ε^* denote the strain fluctuation in aggregate and composite, respectively. Based on the dilute assumption that field in each particle will not be affected by other particles in the composite material, the relationship for two-phase composite with circular particles is given in Equations (3.14-3.15) (Hashin 1983).

$$\bar{K} = K_M + (K_A - K_M) \frac{3K_M + 4G_M}{3K_A + 4G_A} V_A \quad (3.14)$$

$$\bar{G} = G_M + (G_A - G_M) \frac{5(3K_M + 4G_M)}{9K_M + 8G_M + 6(K_M + 2G_M)G_A/G_M} V_A \quad (3.15)$$

Accurate results can be given when V_A diminishes to zero.

3.1.2.2. Variational method

Variational method gives bounds of average properties. Via variational method, Hashin and Shtrikman (1962 & 1963) derived the upper and lower bounds for the average properties of two-phase composite with irregular aggregate geometry. Equations (3.16-3.20) provide the bounds (Hashin & Shtrikman, 1962 & 1963).

$$\bar{K}_- = K_M + \frac{V_A}{1/(K_A - K_M) + 3V_M/(3K_M + 4G_M)} \quad (3.16)$$

$$\bar{K}_+ = K_A + \frac{V_M}{1/(K_M - K_A) + 3V_A/(3K_A + 4G_A)} \quad (3.17)$$

$$\bar{G}_- = G_M + \frac{V_A}{1/(G_A - G_M) + 6V_M(K_M + 2G_M)/5G_M(3K_M + 4G_M)} \quad (3.18)$$

$$\bar{G}_+ = G_A + \frac{V_M}{1/(G_M - G_A) + 6V_A(K_A + 2G_A)/5G_A(3K_A + 4G_A)} \quad (3.19)$$

$$K_M < K_A \text{ and } G_M < G_A \quad (3.20)$$

where, “+” signifies upper-bound while “-“ denotes lower-bound. However, the stiffness ratio of aggregate and matrix shall be less than 10 for practical use of the variational method (Hill 1963, Hashin 1983).

3.1.2.3. Approximate method

There are many approximate analytical methods for homogenization. Here only self-consistent method is discussed. The strain field of linear composite material with two

phases is divided in two parts: homogeneous strain field ε and fluctuating strain field ε^* . Polarized stresses in two phases are set to equivalent by introducing a transformed strain field ε^T .

$$C_M(\varepsilon + \varepsilon^* + \varepsilon^T) = C_A(\varepsilon + \varepsilon^*) \quad (3.21)$$

where, C_M is the stiffness of matrix; C_A is the stiffness of aggregate. The fluctuating strain ε^* can be determined if the transformation strain is assumed constant in aggregate, or it is approximated by Fourier series expansions (Nemat-Nasser et al. 1981). For linear elastic two-phase composite material, relations shown in Equations (3.22-3.23) can be derived. Bulk modulus \bar{K} and shear modulus \bar{G} can be solved during iteration (Hashin 1983).

$$\frac{V_M}{\bar{K} - K_A} + \frac{V_A}{\bar{K} - K_M} = \frac{3}{3\bar{K} + 4\bar{G}} \quad (3.22)$$

$$\frac{V_M}{\bar{G} - G_A} + \frac{V_A}{\bar{G} - G_M} = \frac{6(\bar{K} + 2\bar{G})}{5\bar{G}(3\bar{K} + 4\bar{G})} \quad (3.23)$$

3.1.3. Numerical approach

Analytical approach reaches its limit in handling linear elastic composite material with complicated microstructure, much less with nonlinear composite material (Hollister & Kikuchi 1992). Developments of computer and numerical techniques lead homogenization to numerical approach, which can be regarded as the extension of experiment and has the ability to represent many boundary conditions and attain stress and strain fields easily.

3.1.3.1. Specimen testing method

Since this homogenization method is analogous to specimen testing in lab, it is called as specimen testing method, in which boundary conditions are prescribed. In the

following section, the implementation of several prescribed boundary conditions in FEM is discussed.

Mixed boundary condition

One type of prescribed boundary condition called mixed boundary condition are shown in Figure 2.8, which is feasible to get the average stiffness for linear and nonlinear RVE. The applied boundary conditions will generate average strain $\bar{\epsilon}_x$. By assuming isotropic composite material, the modulus of elasticity can be determined approximately via Equation (3.24) (Kurukuri 2005, Kim et al. 2009, Kim et al. 2011). For nonlinear problem, stress-strain curve will be created step by step. The accuracy can be improved by increasing RVE size (Hollister & Kikuchi 1992).

$$E_x = \frac{\sigma_x}{\epsilon_x} \quad (3.24)$$

Homogeneous boundary condition

Homogeneous boundary condition is described by Equations (3.1-3.2). The translated displacement boundary condition on the four edges is described by Equations (3.25-3.26).

$$\bar{\epsilon} = \begin{bmatrix} \bar{\epsilon}_{11} & \bar{\epsilon}_{12} \\ \bar{\epsilon}_{21} & \bar{\epsilon}_{22} \end{bmatrix} \quad (3.25)$$

$$\begin{bmatrix} u_1 \\ u_2 \end{bmatrix}_{(CD,DA,AB,BC)} = \begin{bmatrix} \bar{\epsilon}_{11}x_1 + \bar{\epsilon}_{12}x_2 \\ \bar{\epsilon}_{21}x_1 + \bar{\epsilon}_{22}x_2 \end{bmatrix}_{(CD,DA,AB,BC)} \quad (3.26)$$

where, $\bar{\epsilon}$ is average strain; u_1 , u_2 are displacement constraints on each node (x_1 , x_2) in 1-st and 2-nd direction; edges CD, AB, DA, BC are shown in Figure 3.2.

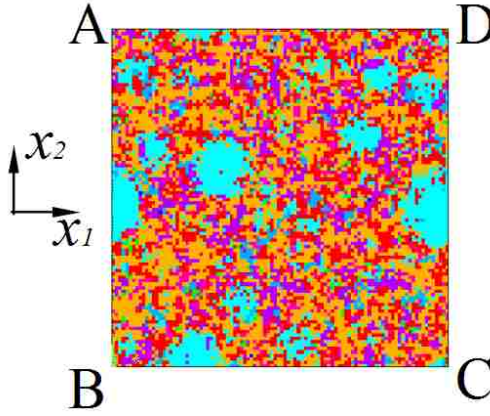


Figure 3.2: RVE (Specimen)

Periodic boundary condition

Periodic boundary condition is simplified by Equation (3.5). The translated displacement boundary condition on the four edges is presented by Equations (3.27-3.28).

$$\begin{bmatrix} u_1 \\ u_2 \end{bmatrix}_{(CD)} - \begin{bmatrix} u_1 \\ u_2 \end{bmatrix}_{(AB)} = L_{RVE} \begin{bmatrix} \bar{\varepsilon}_{11} + \bar{\varepsilon}_{12} \\ \bar{\varepsilon}_{21} + \bar{\varepsilon}_{22} \end{bmatrix}_{(CD-AB)} \quad (3.27)$$

$$\begin{bmatrix} u_1 \\ u_2 \end{bmatrix}_{(AD)} - \begin{bmatrix} u_1 \\ u_2 \end{bmatrix}_{(BC)} = L_{RVE} \begin{bmatrix} \bar{\varepsilon}_{11} + \bar{\varepsilon}_{12} \\ \bar{\varepsilon}_{21} + \bar{\varepsilon}_{22} \end{bmatrix}_{(AD-BC)} \quad (3.28)$$

The periodic boundary condition used here is simplified by setting u_1 and u_2 at edges AB and BC zeros arbitrarily. Assuming the composite material as isotropic, Equations (3.29-3.32) can be used to find the modulus of elasticity E and Poisson's ratio ν .

$$\begin{bmatrix} \bar{\sigma}_{11} & \bar{\sigma}_{12} \\ \bar{\sigma}_{21} & \bar{\sigma}_{22} \end{bmatrix} = \begin{bmatrix} C_{11} & C_{12} \\ C_{21} & C_{22} \end{bmatrix} \times \begin{bmatrix} \bar{\varepsilon}_{11} & \bar{\varepsilon}_{12} \\ \bar{\varepsilon}_{21} & \bar{\varepsilon}_{22} \end{bmatrix} \quad (3.29)$$

$$\begin{bmatrix} \bar{\sigma}_{11} & \bar{\sigma}_{12} \\ \bar{\sigma}_{21} & \bar{\sigma}_{22} \end{bmatrix} = \begin{bmatrix} \frac{E}{1-\nu^2} & \frac{E\nu}{1-\nu^2} \\ \frac{E\nu}{1-\nu^2} & \frac{E}{1-\nu^2} \end{bmatrix} \times \begin{bmatrix} \bar{\varepsilon}_{11} & \bar{\varepsilon}_{12} \\ \bar{\varepsilon}_{21} & \bar{\varepsilon}_{22} \end{bmatrix} \quad (3.30)$$

$$\nu = \frac{C_{21}}{C_{11}} \quad (3.31)$$

$$E = C_{11}(1 - \nu^2) \quad (3.32)$$

where C_{11} , C_{12} , C_{21} , and C_{22} are stiffness tensors; $\bar{\sigma}_{11}$, $\bar{\sigma}_{12}$, $\bar{\sigma}_{21}$, and $\bar{\sigma}_{22}$ are average stress tensors.

3.1.3.2. Multiscale method

Multiscale method is based on asymptotic and periodic assumptions. The relation between average stress and strain of RVE is established by solving periodic boundary conditions. Either average stress or average strain can be regarded as input, correspondingly, average strain or average stress will be the output (Suquet 1985; Michel et al. 1999). In multiscale method, periodic boundary condition is solved through minimizing strain energy in RVE by penalty method or Lagrange multipliers method follows Suquet (1985) and Michel et al. (1999).

3.1.3.3. Coupled multiscale method

In some senses, coupled multiscale method is similar to substructure technique in FEM (Fish & Shek 2000), in which global structure is divided into many substructures simulated separately to overcome computer limitation (Logan 2006). The compatibility at the sharing nodes of global structure and substructure shall be ensured, and this idea is followed in the coupled multiscale method proposed by Fish and Shek (2000). Figure 3.3 shows substructure and RVE in a global structure. The first case is that the substructure shares the same number of nodes with global structure along the interface. Compatibility can be achieved by seamless transfer of displacement and force via sharing nodes. However, in second case, compatibility of RVE and global structure is difficult to be

achieved. As shown in Figure 3.3, the shared nodes of global structure and substructure (RVE) are only four. Except the four nodes, displacement and force along the substructure (RVE) edges are unknowns and cannot be transferred. Asymptotic assumption and interface element are introduced to solve the problem. The key issue in coupled multiscale method is to determine the actual and compatible boundary condition applied on substructure (RVE). Computation is reduced significantly by considering one RVE rather than many different substructures.

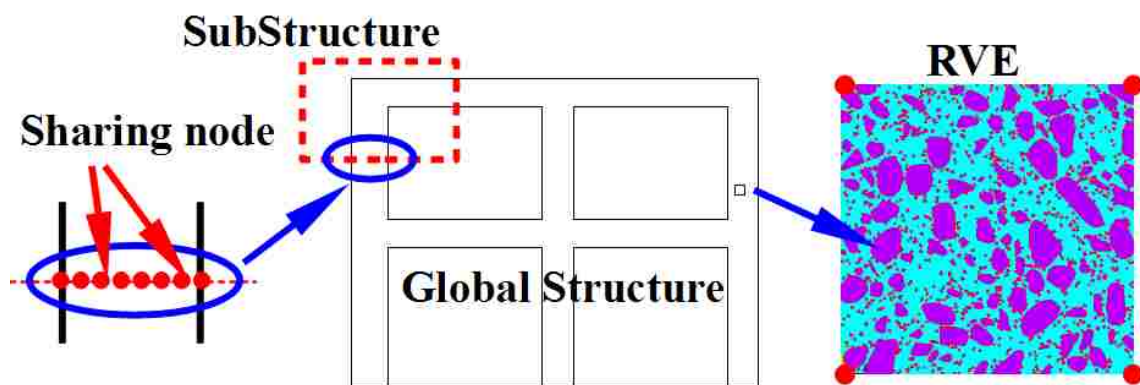


Figure 3.3: RVE, substructure and global structure

3.2. Reconstruction of Concrete RVE

3.2.1. Non-uniqueness of two-point correlation function in heterogeneous composites

Although two-point correlation function includes much more information than standard one-point correlation function such as volume fraction, the relationship between image and two-point correlation function is still not unique. It was proved that a two-phase heterogeneous material cannot be completely specified by a two-point correlation function alone (Jiao, Stillinger & Torquato 2007). On the other hand, for microstructures sharing the same two-point correlation function, it does not necessarily mean these microstructures are same material, nor the same mechanical property (Jiao, Stillinger & Torquato 2008).

Figure 3.4 shows materials A & B, and their two-point correlation functions. Material A is different from material B, which can be proved by the big aggregate in material A. Their two-point correlation functions are same as shown in Figure 3.4 (c). In Figure 3.5, images 1 & 2 are generated by a microstructure (re)construction algorithm and parameters used are same, therefore, images 1 & 2 are same material. Their two-point correlation functions are also same as shown in Figure 3.5 (c).

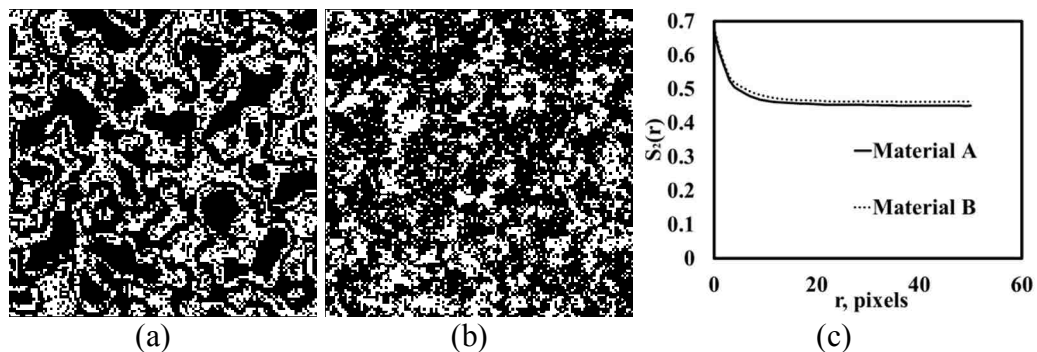


Figure 3.4: (a) Material A; (b) Material B; and (c) their two-point correlation functions (Images from paper published by Jiao et al. 2008)

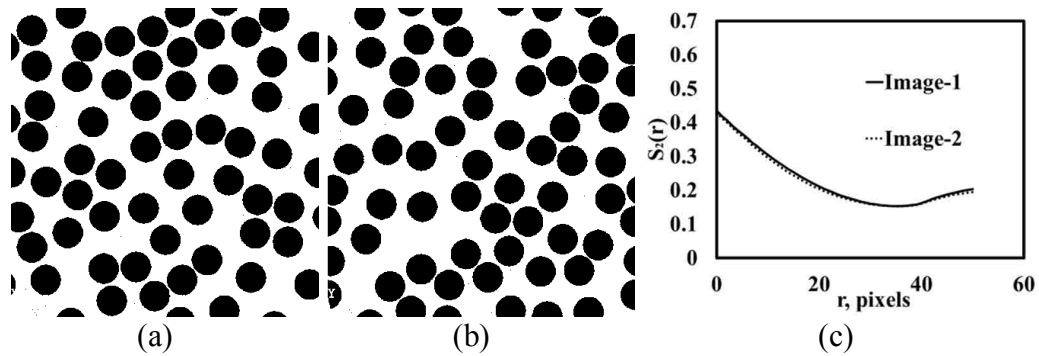


Figure 3.5: (a) Image 1; (b) Image 2; and (c) their two-point correlation functions

However, in Figure 3.6, RVEs 1, 2, 3 & 4 are cut from a concrete member, while difference can be seen in their two-point correlation functions. Are RVEs 1, 2, 3 & 4 same materials? Before answer this question, let's look Figures 3.7 & 3.8. In Figure 3.7 (a) & (b), RVE 3 and image 3 are different materials and they have different two-point correlation functions. In Figure 3.8, image 4 & 5 are cut from image 1. We can say image 4 & 5 are same materials. But they have different two-point correlation functions, which could be attributed by the small size of images 4 & 5. Whether two images are same material depends on the definition of material. Maybe it is reasonable that, only those microstructures built by the same rule can be regarded as same material. If the size of image is big enough, two-point correlation function is a necessary but not enough condition to specify a material. If the size of image is relative small, two-point correlation function is only a tool to check the similarity of images.

Between image and one-point/two-point correlation function, uniqueness can only be achieved by introducing additional boundary conditions. The typical example is concrete mix, which is a standard one-point correlation function, along with the prescribed boundary conditions, such as shape and size of aggregate, properties of cement and aggregate, etc., the bearing strength of concrete can be predicted with acceptable

accuracy. For two-point correlation function of concrete image, additional boundary conditions could be aggregate particle size distribution (PSD), aggregate shape, lineal-path function, two-point cluster function, and so on. Working together with enough boundary conditions, two-point correlation function can uniquely define a concrete image, vice versa.

For case that different images having same two-point correlation functions, if prescribed boundary conditions are not enough, same mechanical properties are not expected from those different images. Because two-point correlation function alone cannot prove images same, and different images always give different mechanical properties. Just like the standard one-point correlation function (volume fraction), two-point correlation function is the necessary but not enough condition in image definition. Therefore, in this dissertation, two-point correlation function is used to check the similarity of images, while helps from prescribed boundary conditions are indispensable.

In conclusion, only exactly same images can give exactly same mechanical properties. A heterogeneous material cannot be specified by a two-point correlation function alone. For images cut from a heterogeneous material, if they are big enough, they shall have same two-point correlation functions. But same two-point correlation function does not necessarily mean the images are from same material. In view of that images from same material have same two-point correlation functions, microstructures can be reconstructed based on a target two-point correlation function. Those generated microstructures sharing same two-point correlation function can be used to quantify the uncertainty from randomness of material itself. To ensure the reconstructed material is

same with target material, other boundary conditions like particle size distribution shall be considered in the process of (re)construction and/or as checkpoints.

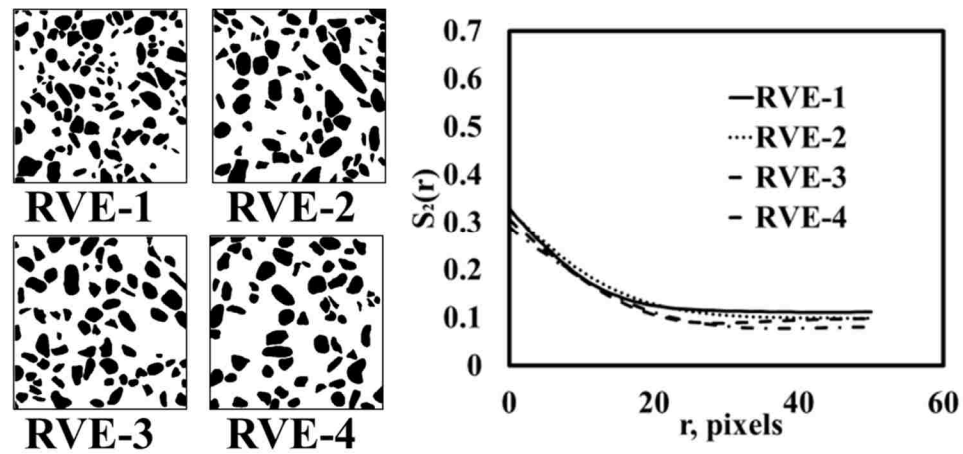


Figure 3.6: Concrete RVE 1, 2, 3 & 4 and their two-point correlation functions

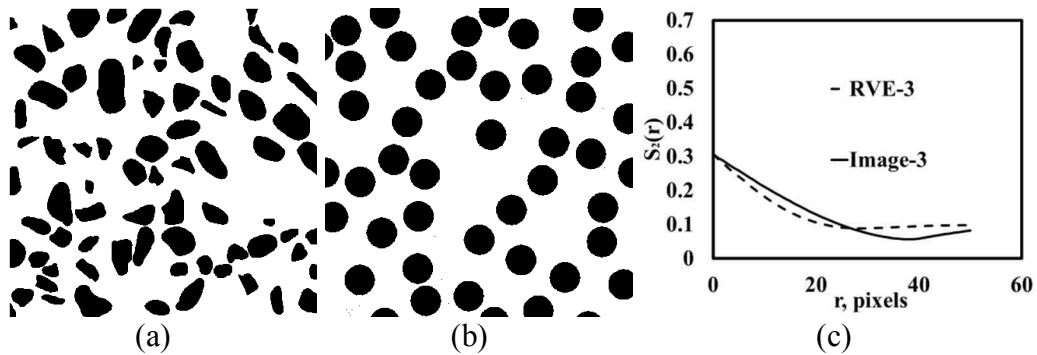


Figure 3.7: (a) RVE 3; (b) Image 3; and (c) their two-point correlation functions

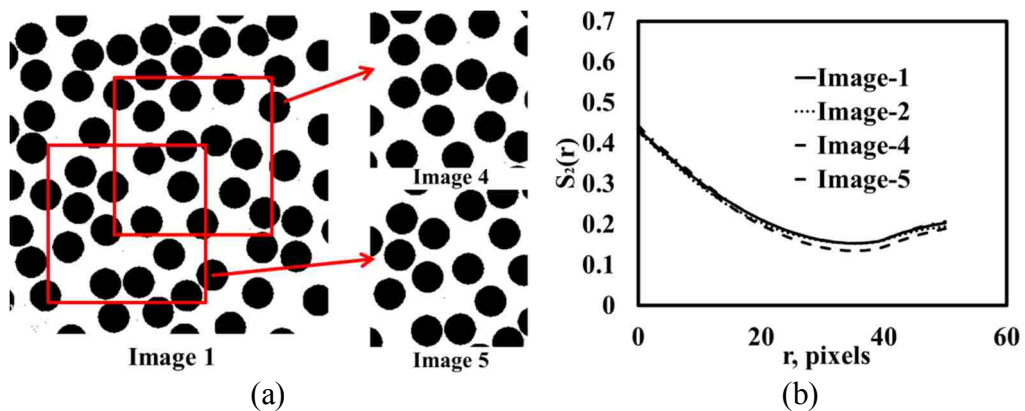


Figure 3.8: (a) Image 1, 4 & 5; and (b) their two-point correlation functions

3.2.2. Reconstruction of concrete RVE

For concrete, uncertainty is inevitable due to its random microstructure and the variations of properties of phases. In order to study concrete, it is necessary to determine concrete's mechanical properties, such as the average value and probability density function (PDF). While experiment is good to get the bearing strength, it is defective to study the uncertainty in concrete serviceability. The reasons are the long duration needed in test, and that experiment cannot depict the microstructural evolution in concrete durability. Numerical approach is presented here to reconstruct concrete RVE sharing similar statistical geometrical descriptors with realistic concrete, and the reconstructed RVEs are used to study concrete serviceability.

To reconstruct the microstructure of heterogeneous material based on limited information (such as volume fraction, two-point correlation function) is a challenging problem. It shall be ensured that the generated microstructures are categorized as the same material with target image. Referring to the discussion in section 3.2.1, same material means that the microstructures are constructed by the same rules, just as images 1 & 2 in Figure 3.5. While we know the characteristics of concrete, such as volume fraction, two-point correlation function, aggregate shape, aggregate particle size distribution, etc., we do not know the intrinsic rules to build it.

Naturally, to reconstruct the microstructure of material, there are two directions: One is focused on finding the intrinsic rules used to build material, and the other lays emphasis on the development of optimizing algorithm to match low-order correlation functions. If the size of reconstructed microstructure is big enough, correlation functions of the reconstructed microstructure shall be same with target material, and same macro

mechanical property is also expected. However, the common size of concrete is too small to escape from the uncertainty due to random microstructure while the uncertainty shall be quantified to study concrete. Just as discussed before, two-point correlation function per se cannot determine image, even actual concrete RVEs (these RVEs are same concrete, i.e., they are cut from a concrete member) do not have same two-point correlation functions. Therefore, if the correlation functions (two-point correlation function is one of them) of generated concrete are within a certain range, we can say the generated concrete RVEs are acceptable. It is worthy to note that, in (re)construction of RVE, the ultimate goal is to find the intrinsic rules to build concrete rather than the exact matching of correlation functions from target concrete image. The reason is, as shown in Figure 3.6, common size concrete cannot present effective correlation functions as standards. The alternative solution is to combine concrete images as a big enough image, whose correlation function can be regarded as standard for (re)construction. The generated microstructure then will be cut in common size.

The proposed method to reconstruct concrete is named by cell operation which includes two steps: one is to regenerate aggregate, and the second is to disperse these aggregate randomly into cement paste based on volume fraction, average distance and particle size distribution. In (re)construction, the intrinsic rules to build concrete are assumed first. Then parameters included in the assumed rules are tuned to match the correlation functions from target concrete image. Figure 3.9 (a) is a typical concrete section with aggregate. First, the original image is processed to make aggregate stand out. The image processing is based on aggregate featured colors. Because different phases

may have the same colors, manual operation sometimes is necessary. Figure 3.9 (b) shows the concrete section image processed.

The outline characteristics of aggregate are contained in aggregate sections, and those with complete shape can be regarded as cells. There are 9 aggregate particles with complete shape and they are flagged in Figure 3.9 (b). Following is the detailed procedures on how to operate these 2D cells to generate aggregate. Each cell is saved as a separated image file ready for operation by an algorithm coded in C++. The C++ program randomly selects a cell from the 9 cells. The selected cell will be scaled in 2 directions S_x , S_y , and rotated in θ_z . Then a random strait line passes the centroid of the operated cell and divides the cell into two halves as shown in Figure 3.10 (a). The right half will be kept as the leaf to make up aggregate particle. Other leaves are created using above mentioned process. The number of leaves needed to constitute an aggregate particle depends on the outline characteristics of cells. For the 9 cells, generally they have 3~4 angles hence 3~4 leaves are needed for an aggregate particle. Parameter θ_y is adopted to control the number of leaf randomly. Similarly, aggregate size distribution is controlled randomly by scale factor S_x and S_y .

Each leaf's height h is different as shown in Figure 3.10 (b). In order to put them together, an operation is necessary to scale leaves and make them same in h as shown in Figure 3.10 (b). The leaves are rotated in y direction to generate aggregate as shown in Figure 3.11. To connect the leaves, the outline could be certain curves, such as sinusoid, to represent the irregular shape of aggregate. The value of S_x and S_y is 0.6~1.2, and θ_z is between 0~360 degrees. The generated aggregate particles are dispersed into cement paste matrix randomly to achieve target volume fraction considering particle size

distribution. Two-point correlation function is used to check the similarity between (re)constructed RVE and original concrete image. S_x , S_y and θ_y , except θ_z , can be chosen as optimization parameters.

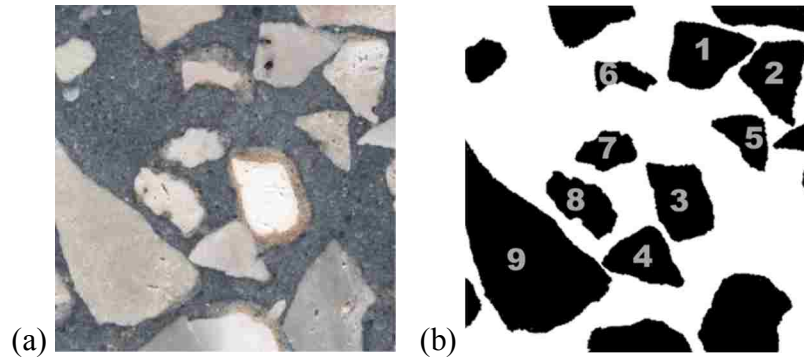


Figure 3.9: (a) Original concrete 2D section image; (b) Aggregate after being processed

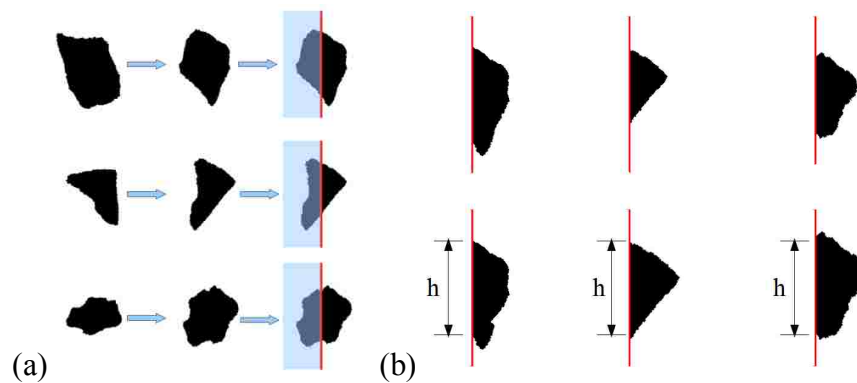


Figure 3.10: Operation of leaves

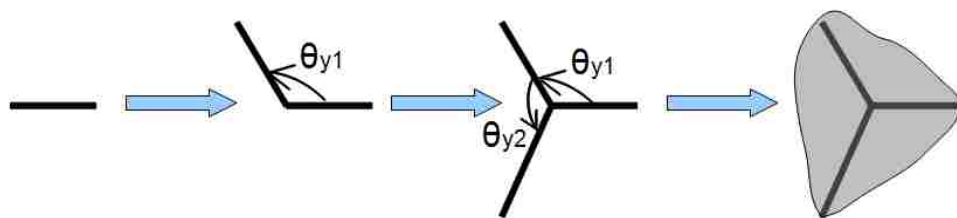


Figure 3.11: Aggregate generated by leaves

Figure 3.12 shows the original concrete section image, generated concrete image by cell operation and their two-point correlation functions. It can be observed from Figure 3.12 that the proposed operation algorithm works very well and can help to

generate large number of random concrete images with random microstructures that share similar statistical geometrical descriptors.

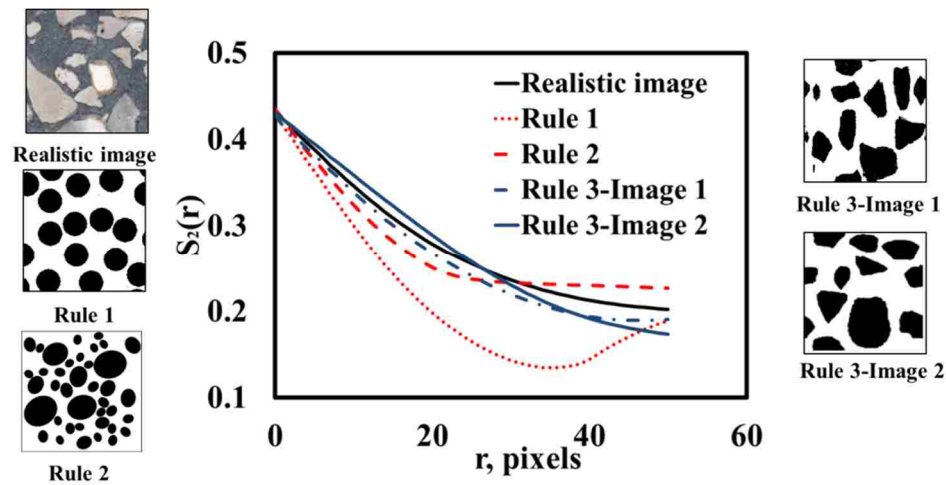


Figure 3.12: Two-point correlation functions of concrete image generated by different rules (Rule 1: Aggregate denoted by circles of same diameter; Rule 2: Aggregate denoted by ellipses considering particle size distribution; Rule 3: Cell operation method considering the irregular shape of aggregate, particle size distribution and aggregate volume fraction)

3.3. Reconstruction of Cement Paste

Cement paste microstructure is time-related due to chemical reaction. The location and volume fractions of phases such as calcium hydroxide (CH), calcium silicate hydroxide (C-S-H), etc., will develop with time. So (re)construction of cement paste is achieved via a cement hydration algorithm with the capacity to develop microstructure and consider cement chemistry and phase changes.

3.3.1. HYMOSTRUC[®]

HYMOSTRUC[®] is a cement hydration model developed at Delft University of Technology in Netherland (van Breugel 1995a & 1995b). In this model, cement particle is assumed as sphere and dispersed randomly in the water based on water-cement ratio.

Cement hydration starts from outer surface and the reactants are divided into outer product and inner product by the original cement particle outer surface as shown in Figure 3.13. HYMOSTRUC[®] also can predict the modulus of elasticity of cement paste based on the degree of cement hydration. However, the generated hydration microstructure is difficult to be meshed in FEM circumstance.

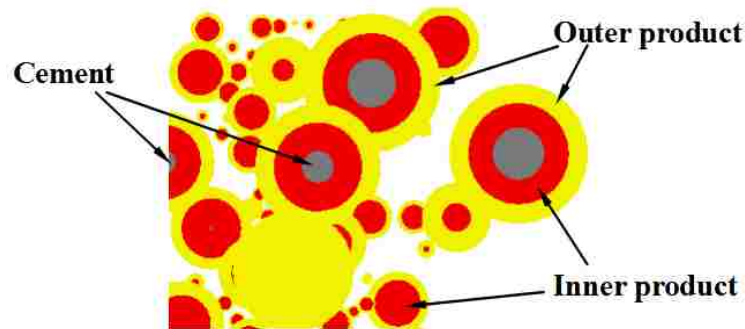


Figure 3.13: Cement hydration and microstructure development in HYMOSTRUC[®]

3.3.2. CEMHYD3D

A three-dimensional cement hydration and microstructure development modeling package CEMHYD3D was developed by Bentz from the National Institute of Standards and Technology (NIST) (Bentz 1997 & 2005). Based on measured cement particle size distribution (PSD), spheres with different diameters are generated to express cement particles in a cubic considering water cement (W/C) ratio. Meeting with water, cement particles will gather and this phenomenon is realized by a flocculate mechanism (Figure 3.14 (a)). Then cement clinker phases (C_3S , C_2S , C_3A and C_4AF) are assigned to cement particles based on the actual 2D image of cement particles (Figure 3.15). With target phase volume fractions, surface area and particle size distribution (PSD) being achieved, resultant microstructure is shown in Figure 3.14 (b). Microstructure at certain hydration age is generated by CENHYD3D as shown in Figure 3.14 (c). Cement hydration is

achieved by particle dissolution mechanism in chemical reaction (Bentz 1997). The generated microstructure of cement paste at different hydration age will be transferred to the homogenization algorithm (FEM model) to describe the property of cement paste.

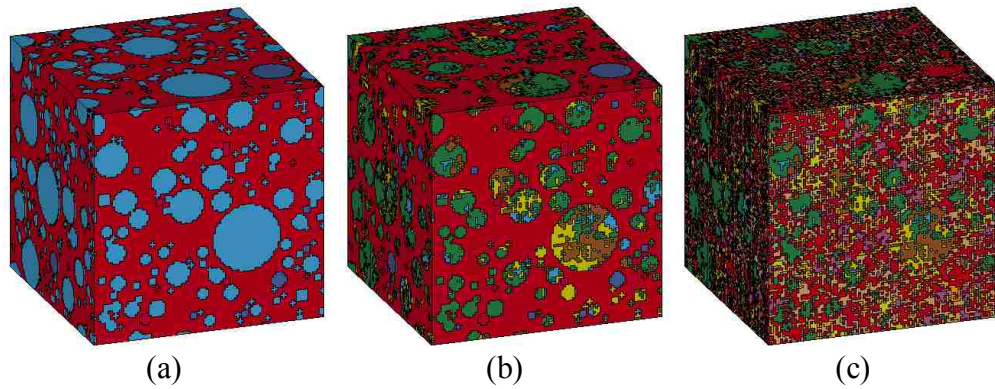


Figure 3.14: Construction of cement paste microstructure

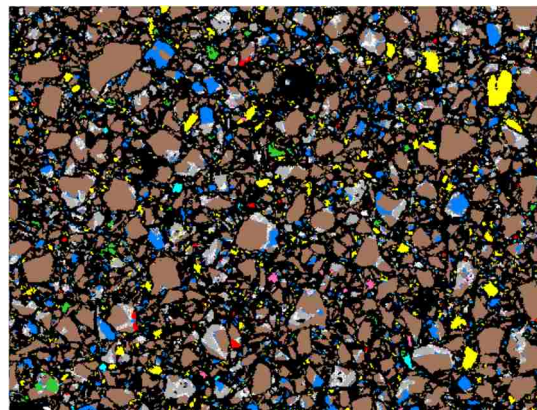


Figure 3.15: Two-dimensional processed scanning electron microscopy (SEM)/X-ray of cement particles (Bentz, 2005)

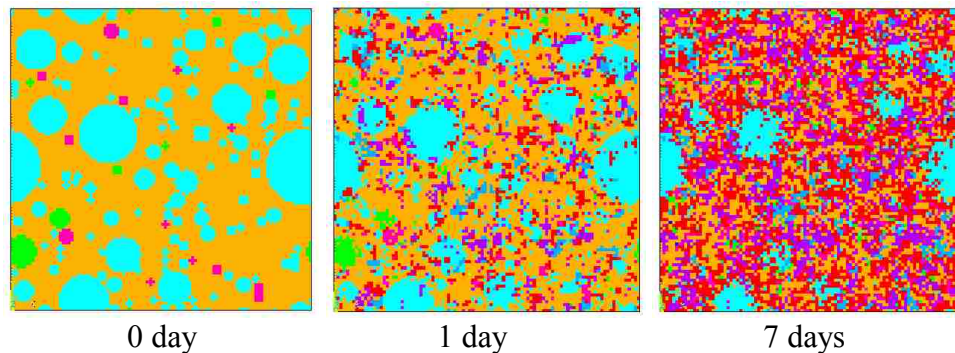


Figure 3.16: Microstructures of cement paste during hydration

Chapter 4. Application of Homogenization Method to Model Cement Paste

4.1. Model I

4.1.1. Introduction

Cement paste represents a major component in concrete and governs its strength and stiffness. Research in the last three decades has revealed how the microstructure of hydrated cement paste, including calcium silicate hydrate (C-S-H), calcium hydroxide (CH) and ettringite, participates in concrete strength (Taylor 1997, Mehta et al. 2006). Research has also shown how the addition of pozzolanic materials such as silica fume (microsilica) and fly ash helps to change concrete microstructure by converting the weak CH crystals into strong C-S-H (Takemoto et al. 1980). Microsilica and fly ash particles are on the same order of magnitude as cement particle size (microsilica particles are about 0.1 to 100 μm , fly ash particles are about 10 to 50 μm and cement particles are about 30 μm (Aïtcin 1998)), which allows the use of relatively high amounts of pozzolans (10 to 30%) in concrete as supplementary materials and as replacement for cement. The significant shrinkage and the high possibility of early-age cracking due to restrained autogenous shrinkage associated with using microsilica limits pozzolanic materials use in practical applications to 8 to 12% of the cement weight (Aïtcin 1998). The slow reactivity of fly ash limits fly ash use in concrete in which relatively early strength gain is desired.

The section 4.1 has been published in “Homogenization model examining the significance of nanoparticles on concrete strength and stiffness”, Journal of the Transportation Research Board (TRB), No. 2141, 28-35, 2010.

More recently, nanosilica was introduced as a new pozzolanic material that can be used to enhance concrete strength (Lin et al. 2005, Qing et al. 2007). However, scale plays an important role in the effect of nanosilica on concrete behavior. To understand this scale effect, consider that commercially available nanosilica particles are typically 3 to 30 nm in diameter. If 10 nm is an average diameter of nanosilica particles, then an average microsilica particle of 10 μm has a particle size of three orders of magnitude (10^3) larger than a nanosilica particle. This means that for the same weight ratio of cement from both materials, there will be nine orders of magnitude (10^9) nanosilica particles compared with microsilica particles, and the surface area of nanosilica will be six orders of magnitude (10^6) higher than that of microsilica. This simple arithmetic indicates that the reactivity of nanosilica will be much higher than that of microsilica. However, there will always be a fair number of nonreacted nanosilica particles in concrete due to the limited amount of water, which cannot cover the entire surface area of the nanosilica particles. This work provides insight on this issue and its significance for the properties of cement pastes.

In this dissertation, we suggest a model of cement paste with and without nanosilica as a heterogeneous material; the model includes various subphases, including one with nanosilica. The objective is to examine the response of the heterogeneous microstructure of cement paste with different levels of nanosilica by using microstructural homogenization techniques. The target of homogenization is to replace the classical composite mix rule with a robust model in which the heterogeneous material response is not just a function of the volume fraction and elastic modulus of its phases but is affected by the constitutive model of each phase. A number of homogenization

techniques to model composite materials have been developed (Ju et al. 1994). Concrete was successfully modeled by using this approach in which aggregate was assumed as a randomly dispersed material in the cement paste matrix (Kurukuri 2005). Torquato (2002) further suggested the use of linear correlation functions measured from scanning micrographs to model multiphase composites.

The homogenization technique is a modeling approach based on the assumption of continuum mechanic that one can upscale the properties of the constituent phases at a small scale (nano to micro) to predict the behavior of the composite at a larger scale (macro). The process starts by the selection of a representative volume element (RVE) that can statistically represent the geometric and physical characteristics of the composite to be modeled. The RVE should satisfy the scale separation principle (Bear and Bachmat, 1990) that the characteristic length of the heterogeneity is an order of magnitude less than the characteristic size of the RVE. The basic premise of modeling the RVE therefore involves the use of an averaging technique to determine apparent and intrinsic average properties of the composite materials (Dormieux et al. 2006).

The approach described here uses the finite element (FE) method to develop the RVE of hydrated cement paste with and without nanosilica. The use of a cement and silica hydration model (Yajun et al. 2004, van Breugel 1995a, van Breugel 1995b) to predict the volume fraction of the RVE phases modeled using the FE method is discussed. The RVE model is randomly generated by using the phase volume fraction information, and then used to predict the stress-strain curve of the cement paste. On the basis of the validated stress-strain behavior, the effect of nanosilica on the behavior of cement paste is

examined. Emphasis is on the role of nanosilica and the ability of the cement paste to absorb energy up to failure.

4.1.2. Methods

Cement Paste Homogenization

To meet the scale challenge in modeling the different phases of the cement paste, the various microstructural phases (i.e., C-S-H, CH, ettringite, undehydrated particles, and so forth) are lumped into two main phases: hydrated and unhydrated cement phases following standard classification (Neville 2005). The fractions of these two phases depend on the degree of hydration of cement paste and water-cement ratio (Powers et al. 1946). Unhydrated nanosilica particles (1- to 10-nm diameters) are considered as the third phase by considering the pozzolanic reactivity and estimating the ratio of nonreacted nanosilica. The capillary pores (10- to 50-nm diameters) are then considered as the fourth phase. These four phases can simulate the behavior of the cement paste with and without nanosilica. Even more interesting is that the four phases can describe the dynamics of hydration and the significance of the nanosilica volume fraction for the hydration products. Below, the four phases and their anticipated dynamics are described in further detail.

Four-Phase RVE

Phase I: This phase is a solid phase that represents C-S-H, CH, ettringite and other hydration products, including the gel pores (0.5- to 2.5- nm diameters). In this phase, C-S-H is assumed to be the major strength contributor. Therefore, the strength and stiffness of Phase I is a function of the C-S-H volume ratio in the solid hydrated phase. Moreover, there exists a threshold volume of pozzolanic materials beyond which changes

in strength and stiffness of this phase do not occur. This threshold is a function of the amount of CH formed in the original microstructure and the reactions of the pozzolanic materials. The RVE strength contribution of Phase I increases with time as more unhydrated particles become hydrated with the availability of external curing.

Phase II: This phase is the unhydrated solid phase. Further hydration due to favorable hydration conditions (e.g., high relative humidity) will reduce the volume fraction of Phase II as more unhydrated particles become hydrated. Note that the stress-strain relationship of Phase II will play a major role in determining the mechanical characteristics of the cement paste. If microsilica exists in the mixture (as in the case study considered here), unhydrated microsilica particles will exist in Phase II.

Phase III: This phase represents the nonreacted nanosilica particles. While Phase III can be incorporated in Phase II as part of the unhydrated particles, Phase III is intentionally separated from Phase II to be able to examine the effect of flocculating nanosilica particles (clusters) on the mechanical characteristics of cement paste. The upscaling mechanism is needed (i.e. separate nanoscale and microscale RVEs) for multiscale homogenization (Bear & Bachmat 1990, van Breugel 1995b, Bentz et al. 2000). However, the separation of nanosilica as a phase in the proposed RVE does not affect the robustness of the model due to the significantly low fraction of nanosilica in the mix. Separating the nanosilica phase is performed for providing insight on the nonreacted nanosilica existence in the RVE. The role of the pozzolanic threshold on the simulation is emphasized. At a nanosilica volume fraction below the pozzolanic threshold, Phase III will not exist in the simulation as all the nanosilica particles would have reacted. When the nanosilica volume fraction exceeds the threshold, Phase III will appear and participate

in the simulation. The increase in the nanosilica volume fraction will result in a considerable increase of nonreacted nanosilica particles in the RVE.

Phase IV: This phase is the porosity phase. Porosity will decrease as pozzolanic reaction continues. This is attributed to the pozzolanic conversion of CH to C-S-H when favorable hydration conditions exist. Porosity changes will alter the stress-strain relationship of the cement paste composite.

Volume Fractions of the Four Phases

To calculate the volume fraction of each phase, the hydration processes of Portland cement and the silica (micro and nano) are separated. The volume fractions of the three phases associated with cement hydration are calculated first and are then adjusted based on the pozzolanic reaction. This is shown schematically in Figure 4.1. The methods used in the calculation of the volume fractions of the RVE four phases are discussed as following.

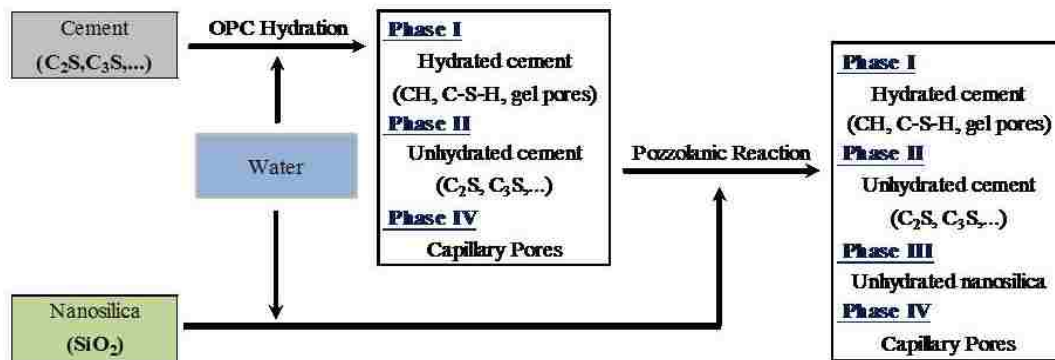


Figure 4.1: Schematic representation of cement hydration and pozzolanic reaction to develop the volume fractions of the phases for a cement paste RVE.

Cement Hydration

In this hydration process, the volume of hydrated cement (V_{hc}) is calculated after Neville (2005) as

$$V_{hc} = 2.14V_c \text{ (ml)} \quad (4.1)$$

where, V_c is the volume of cement used for hydration calculated as

$$V_c = \alpha_c \frac{W_c(w/c)}{1.323} \text{ (ml)} \quad (4.2)$$

where α_c is the degree of ordinary cement hydration, which can be calculated using HYMOSTRUC[®] model after van Breugel (1995a & 1995b) by considering particle size distribution, the chemical composition of the cement, the water-cement ratio and the actual reaction temperature. W_c is the weight of cement in g. w/c is water/cement ratio. The volume of unhydrated cement V_{uc} is calculated as $W_c/3.15 - V_c$ (liter). The volume of the segmented capillary pores V_{cp} is then calculated by subtracting the volume of hydrated cement and unhydrated cement from total volume as $\{W_c/3.15 + W_c(w/c)\} - (V_{hc} + V_{uc})$ in liter.

Pozzolanic Reaction

The volume stoichiometries of the pozzolanic reaction were assumed after Bentz et al. (2000). On the basis of this assumption, the volume change in hydrated cement can be calculated as

$$\Delta V_{hc} = 2.42\alpha_p V_{SF} \text{ (milliliter)} \quad (4.3)$$

where α_p is the pozzolanic reaction degree. V_{SF} is the volume of silica fume (microsilica). To determine α_p , diffusion-controlled pozzolanic reaction rate after Barnes (1983) is considered as

$$K_D t_i = (d_n / 2)^2 [1 - (1 - \alpha'_{pn})^{1/3}]^2 \quad (4.4)$$

where K_D is diffusion rate parameter. t_i is time. d_n is the diameter of a microsilica particle. α'_{pn} is pozzolanic reaction degree of the silica fume particle. On the basis of Equation

(4.4) and considering the glass phase content of the silica particles, the pozzolanic reaction degree of a microsilica particle having the diameter d_n can be calculated as

$$\alpha_{pn} = 1 - \left(1 - \frac{\beta_{GP} \sqrt{K_D t_i}}{d_n / 2} \right)^3 \quad (4.5)$$

where β_{GP} is glass phase content of microsilica. By weighted summation of the pozzolanic degree of a microsilica particle, the pozzolanic reaction degree α_p is determined as

$$\alpha_p = x + \sum_{d_n > 2\delta_p} y_n \alpha_{pn} \quad (4.6)$$

where y_n is the percentage of a particle and x is the percentage of microsilica particles having less diameter than two times the penetration depth δ_p , which is calculated as

$$\delta_p = \sqrt{K_D t_i} \quad (4.7)$$

Therefore, when cement hydration and pozzolanic reaction are combined, the final volumes of hydrated cement, unhydrated cement, capillary pores, and remaining microsilica will be $V_{hc} + \Delta V_{hc}$, V_{uc} , $V_{cp} - \Delta V_{hc}$ and $V_{SF}(1 - \alpha_p)$, respectively. In modeling nanosilica hydration, two interacting factors were considered: the size of the nanosilica particles (1- to 50- nm) and the surface area of the nanosilica particles when added to the mix. The first factor should enable all nanosilica particles to be fully hydrated when they come in contact with water, according to all hydration models (Yajun & Cahyadi 2004; van Breugel 1995a; Bentz et al. 2000), and given its much lower size compared to the penetration depth computed in Equation (4.7). Nevertheless, the second factor considers the significance of the very small size of the nanosilica particles in producing a very large surface area that cannot be covered by the water in the mix (especially at low water-

cement ratios). Therefore, the hydration of nanosilica is modeled by computing an equivalent microsilica volume that has the same surface area of the nanosilica. The nonreacted microsilica fraction was then computed by using the amicrosilica hydration model described above, and the nonreacted fraction of that equivalent microsilica was converted back to nanosilica to represent the nonreacted nanosilica in Phase IV of the cement paste. Experimental investigations by using scanning electron microscopy (SEM) are necessary to confirm or negate that assumption. Experimental data on the reactivity of nanosilica are limited in the literature.

Constitutive Models for the Four Phases

While the constitutive model of the solid phase (Phase I) and the nanosilica phase (Phase III) can be extracted from the literature, the constitutive model for Phase II is unknown. To determine the mechanical properties of Phase II, first Phase II is assumed as linear elastic-plastic material. Then the stress-strain curve of Phase II is identified by matching the simulated stress-strain curve of cement paste to the one extracted from nanoindentation. The verified FE model is then used to examine the effect of nanosilica volume fraction on the mechanical properties of cement paste. The constitutive models for the four phases are summarized here.

Phase I This phase represents the ‘hydration gel’, including all the hydration products: CH, C-S-H, ettringite and the gel pores. The maximum strength of 120 MPa is used for Phase I by considering Power’s equation with gel space ratio as 1 representing capillary pore-free cement paste (Powers 1960). The modulus of elasticity of Phase I is assumed as 10 GPa after Constantinides and Ulm (2004). A linear elastic-plastic constitutive model was adopted as shown in Figure 4.2. Poisson’s ratio of 0.21 was

assumed in range with data reported in the literature (Haecker et al. 2005). Sensitivity analysis proved that the strength of the cement paste is strongly influenced by the maximum strength of Phase I. Further investigations are needed to correlate the mechanical properties of this phase to the intrinsic mechanical properties of the hydration products such as C-S-H and CH at packing density.

Phase II For Phase II of unhydrated cement and capillary pores, a linear elastic-plastic model was adopted. Poisson's ratio of Phase II was also assumed to be 0.21. The parameters of the constitutive model of Phase II were to be modified during the simulation process such that the stress-strain of the composite cement paste modeled by the RVE meets that extracted from experiments.

Phase III The nanosilica particles were assumed to be linear elastic with modulus of elasticity as 70 GPa (Schackelford 2005). As individual particles were used in this phase and distributed randomly in the RVE model, no special efforts to account for particle flow or packing under stress were considered.

Phase IV The capillary pores are considered as void without stiffness and with zero strength.

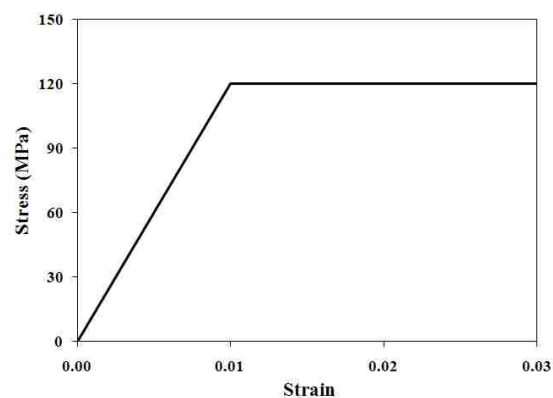


Figure 4.2: Stress-strain curve for Phase I (Hydrated cement)

Finite Element Model of the RVE

A three-dimensional FE model of the RVE is developed to predict the constitutive relationship of the cement paste and to extract its fundamental mechanical characteristics. The RVE is a cubic FE model including 8000 ($20 \times 20 \times 20$) cubic elements developed under ANSYS® finite element environment (ANSYS 2007) as shown in Figure 4.3.

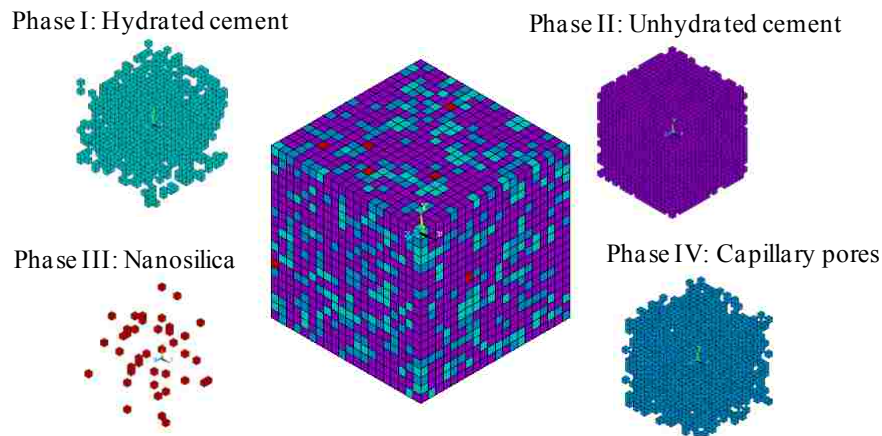


Figure 4.3: Finite element (FE) model representing the four phase RVE model.

The RVE was modeled by using ANSYS® SOLID45, which is a solid element with eight nodes, each having three degrees of freedom and translations in the x , y and z directions at each node. Elements are randomly assigned to be certain phase within the volume fraction defined for each phase. This allows for dealing with the RVE as isotropic material. Periodic boundary condition is used to represent the RVE after Kurukuri (2005). In the FE model, displacements are applied and the average strain and stress of the different phases are computed at each loading step. Specimen testing homogenization method is used here to avoid the challenge in computing the strain energy tensors when nonlinear phases are considered (Khisaeva & Ostoja-Starzewski 2006). The stiffness of

Phase I in the $n+1$ step of the computation is based on the average strain in Phase I in the n^{th} step.

Identifying Phase II Constitutive Model using Nanoindentation Data

A cement paste including nanosilica was mixed and cast. The mix proportions for this cement paste are provided in Table 4.1. The nanoindentation experiment was performed after 7 days of curing in a standard water-lime bath. The specimen was extracted from the cement paste cast cube by slicing 50mm×50mm×50mm cubes with a diamond blade saw. The specimen was then cast in a fast-set acrylic epoxy. After the epoxy hardened, the specimen surfaces were ground with a mechanical polishing wheel with a grit size of 120 for a total of ten minutes. The specimen surface was then ground with grits of 240, 600, 1000, 1500 and 2000 in respective order for a total of five minutes at each scale. During the grinding process, specimens were continuously rinsed with running water. The specimen was then placed in an ultrasonic bath with distilled water to displace lodged particles, after which it was polished for a total of two minutes with a microcloth impregnated with a colloidal silica polishing suspension to achieve a surface roughness of 60 nm. After polishing, the specimen was placed in the ultrasonic bath and then placed in a distilled water bath until the time of nanoindentation.

Table 4.1: Mixture ingredients of cement paste for nanoindentation (kg/m³)

| Cement | Microsilica | Nanosilica | Water |
|--------|-------------|------------|-------|
| 975 | 78 | 7 | 159 |

The nanoindentation test was performed using an instrumented nanoindenter (NanoTest™ 600 indenter platform from Micro Materials, Inc., Wrexham, UK). The designated indentation locations on specimens were selected using a high-magnification light microscope attached to the NanoTest 600 platform (1000×). Nanoindentations were

performed by using a 50- μm -diameter spherical indenter tip. This tip was used instead of the typical Berkovich indenter tip reported by others for nanoindentation of cementitious materials (Constantinides & Ulm 2004, Zhu et al. 2007) in order to observe the composite cement performance at the nanoscale (indentation depth is in the range of 100 nm) rather than observing the mechanical performance of the microstructural phases. Ten indentations spaced at 30 μm were performed along a straight line. The maximum indentation load was set to 0.5 mN and the indentation load was applied at a constant loading rate of 0.025 mN/second. A typical loading and unloading curves is shown in Figure 4.4.

On the basis of nanoindentation observation, the stress-strain curve of the cement paste can be extracted after Kalidindi and Pathak (2008). The modulus of elasticity of the cement paste can be calculated as

$$E_s = (1 - \nu_s^2) \left(\frac{1}{E_r} - \frac{1 - \nu_i^2}{E_i} \right) \quad (4.8)$$

where E_i and ν_i are the modulus of elasticity and Poisson's ratio of the nanoindenter, respectively. ν_s is Poisson's ratio of the cement paste assumed as 0.25. E_r is the reduced modulus of elasticity calculated as

$$E_r = \frac{S\sqrt{\pi}}{2\beta\sqrt{A_p}} \quad (4.9)$$

where β is a geometry correction factor of 1 for sphere indenter. S is the contact stiffness defined as the slope of the unloading in Figure 4.4. S can be determined as

$$S = \frac{3P_t}{2h_e} \quad (4.10)$$

where P_t is the maximum load and h_e is the elastic rebound as shown in Figure 4.4. A_p is the area of contact calculated as

$$A_p = 2\pi r_i h_p \quad (4.11)$$

where r_i is the radius of the indenter and h_p is the plastic depth as shown in Figure 4.4. By using nanoindentation data analysis, the average modulus of elasticity of the cement paste is calculated as 3.06 GPa. The resulting modulus of elasticity seems to be lower than those reported by Constantinides and Ulm (2003) and Mondal et al. (2007). This can be explained by the significant difference between the mixes tested here and those reported by these other researchers. The major difference is represented by the significantly high silica content and very low water-cement ratio of the cement paste examined here. Additional macroscale experiments of the cement paste confirmed the reported cement paste to have a modulus of elasticity of 4 GPa, which is comparable to the 3.06 GPa identified by nanoindentation. The average nanoindentation parameters for the cement paste are presented in Table 4.2.

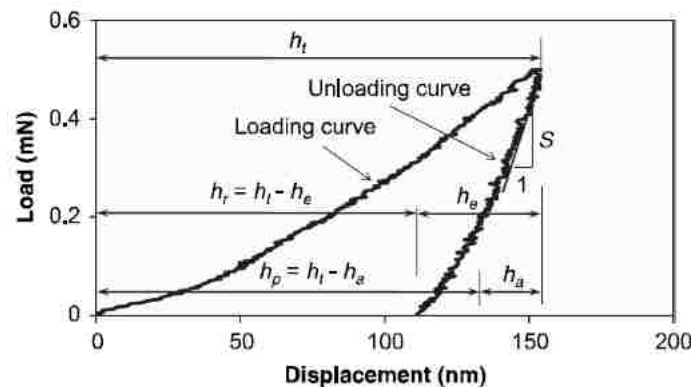


Figure 4.4: A typical loading and unloading curve in nanoindentation

Table 4.2: Average nanoindentation parameters of the cement paste as observed in nanoindentation

| Nanoindenter | | | Nanoindentation results | | | | Calculated values | | |
|--------------|---------|-------------------------|-------------------------|------------|------------|-----------|---------------------------|-------------|-------------|
| E_i (GPa) | ν_i | r_i (μm) | P_t (mN) | h_e (nm) | h_p (nm) | S (N/m) | A_p (μm^2) | E_r (GPa) | E_s (GPa) |
| 1141 | 0.07 | 25 | 0.5 | 45 | 130.5 | 16667 | 20.5 | 3.26 | 3.06 |

The strains in the elastic region are determined by using the unloading curve after Kalidindi et al. (2008) as

$$\varepsilon_e = \frac{h_t - h}{2.4\sqrt{R_e}(h_t - h)} \quad (4.12)$$

where h_t is the total indenting depth as shown in Figure 4.4. R_e denotes the effective radius defined as

$$1/R_e = 1/R_i + 1/R_s \quad (4.13)$$

where R_i and R_s are the radius of the indenter and the specimen, respectively. As R_s for elastic loading of a flat sample will be infinity, R_e is considered as R_i . However, more accurate calculation can be done if R_e is considered as a function of indentation depth and material properties (Kalidindi et al. 2008). Finally, the corresponding stresses in the elastic region are calculated by multiplying the elastic strains by E_s . Therefore, the maximum strength is determined by multiplying the strain calculated by Equation (4.12) by E_s for $h \leq h_e$. For plastic region, the final strain is determined by considering $h = 0$ in Equation (4.12). The above method allows realizing the “true” stress-strain of the indented material. However, it should be noted that the final strain does not necessarily represent the failure strain of the material, as the indentation process does not necessarily result in failure of the indented material.

4.1.3. Results and Discussion

Identifying Phase II Characteristics

The stress-strain curve of the cement paste composite as extracted from the nanoindentation test is shown in Figure 4.5(a). The volume fractions of the four phases for the cement paste used in nanoindentation are calculated by using the method

described using Equations (4.1-4.7), considering a degree of hydration of 22% as simulated by HYMOSTRUC[®]. As discussed above, the cement paste was modeled as a four-phase composite: Phase I, hydrated cement; Phase II, unhydrated cement; Phase III, nanosilica; and Phase IV, capillary pores. The volume fractions of the four phases for the specimen made of the mix presented in Table 4.1 are determined as 14.7%, 62.5%, 0.5% and 22.3% respectively. The RVE model was developed and the constitutive model of the cement paste was simulated. The stress-strain of Phase II was optimized such that the final stress-strain of the cement paste composite modeled by the RVE met the experimentally observed stress-strain extracted from nanoindentation experiments. The final stress-strain curve as modeled using the RVE model is shown in Figure 4.5(a). The optimal stress-strain of Phase II that produced this constitutive model for the cement paste is shown in Figure 4.5(b).

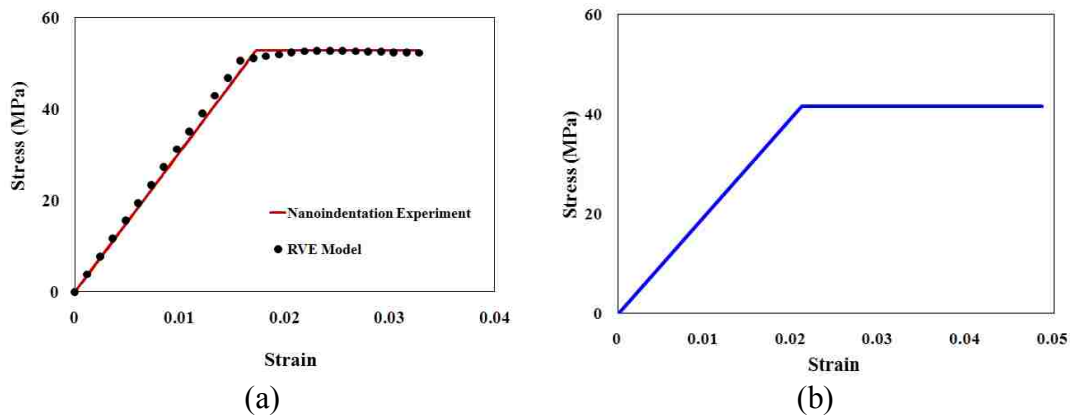


Figure 4.5: (a) Final stress-strain curves of cement paste composite extracted from nanoindentation and simulated by using the RVE model (b) Identified stress-strain curve for Phase II.

Significance of Nanosilica

The validated RVE model and constitutive models for the four phases were then used to identify the effect of nanosilica on the behavior of cement paste. Nanosilica

additions of 0%, 2%, 4% and 10% of the total cement weight were considered while all the other mix constituents were fixed as listed in Table 4.1. The volume fractions of the four phases computed by using the hydration model described above were presented in Figure 4.6. The 10% case is hypothetical because it is practically difficult to produce a cement paste mix with 10% nanosilica and such a low water-cement ratio. These volume fractions were then used in building four RVE models, as shown in Figure 4.6, to extract the stress-strain curves of the composite cement paste. The FE analysis was conducted, and the composite cement paste RVE was assumed to reach its maximum strain when the strain of Phase I or Phase II reached its maximum value.

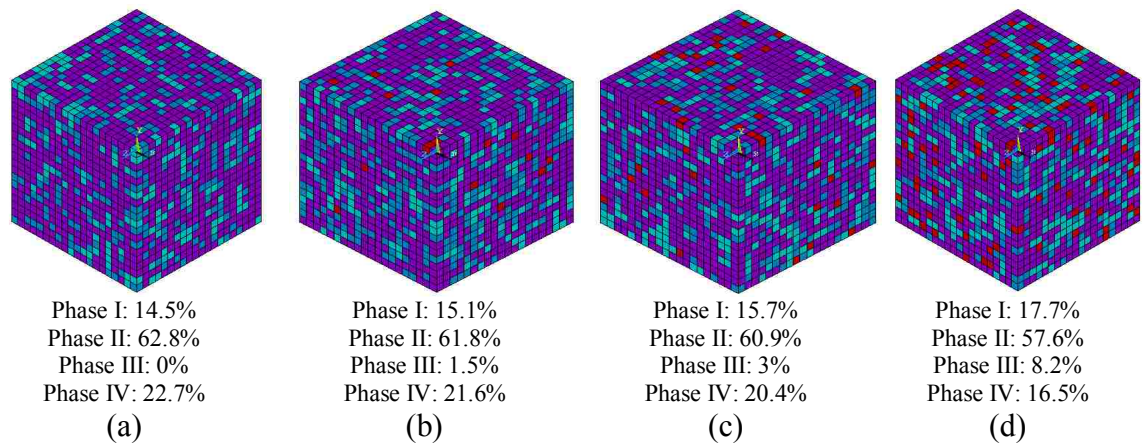


Figure 4.6: RVE models for four cement pastes using (a) 0% (b) 2% (c) 4% and (d) 10% nanosilica showing the four phases in all the models identified using hydration model described above.

The stress-strain curves of the four cases with the four nanosilica ratios are shown in Figure 4.7(a). It is obvious from these curves that the addition of nanosilica increased the stiffness and strength of the cement paste. No observation on the ductility (maximum strain at failure) can be concluded here because the maximum strain extracted is related to maximum strain in Phase II, which is affected by the nanoindentation observation. The maximum strain therefore is less than the true maximum strain of such cement paste

composite. This can be overcome by obtaining the maximum strain of these mixtures from macroscale experiments.

Nevertheless, the strength (maximum stress) and stiffness (slope of the linear part of the stress-strain curve) is clearly increasing as the nanosilica content in the paste increases. This can be explained by the ability of nanosilica to increase the volume fraction of the Phase I mainly contributing to strength and stiffness of the cement paste composite. Finally, the ability of nanosilica to affect the toughness of the cement paste (ability to absorb energy to failure) is evaluated by computing the area under the stress-strain curves. This significance is shown in Figure 4.7 (b). Computationally, the addition of nanosilica produces a slight increase the cement paste and concrete toughness.

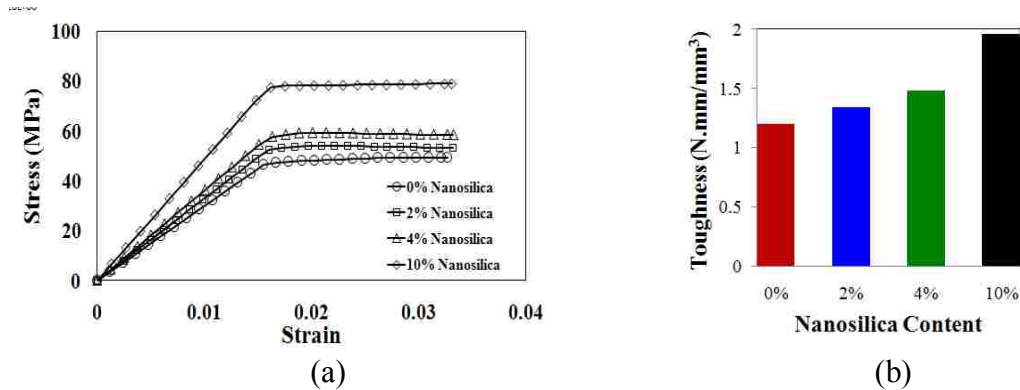


Figure 4.7: Significance of nanosilica on the behavior of cement paste (a) stress-strain relationship (b) toughness calculated as the area under the stress-strain curve.

4.1.4. Conclusion

A homogenization model was developed to examine the effect of nanosilica particles on cement paste behavior. A four-phase cement paste RVE was simulated by using the FE method with the aid of hydration models by others. The unknown constitutive model of the unhydrated cement paste (Phase II) was identified by getting the RVE model simulation to meet the stress-strain of the cement paste as extracted from

nanindentation experiments. The validated FE model for the RVE was then used to examine the effect of nanosilica on the strength and stiffness of cement paste. It was concluded that, computationally, the nanosilica seems capable of increasing cement paste strength and stiffness. Moreover, a slight increase in toughness (representing the energy absorbed to failure) can also be realized when nanosilica content is increased. Further work is needed to confirm these computational findings.

4.1. Model II

To consider cement paste microstructure and hydration, a homogenization model of cement paste was developed via a 3D cement hydration and microstructure development modeling package CEMHYD3D (Bentz 2005). Through a study on the significance of pozzolanic material on cement paste, the proposed model is validated by nanoindentation test.

From nanoindentation experiment, mechanical properties of material can be attained, such as hardness H , Poisson's ratio ν and modulus of elasticity E , by using the analytical method presented in the literature (Doerner & Nix 1986; Oliver & Pharr 1992). However, the conventional approach was derived on the basis of stringent assumptions: indenter is linear elastic with ideal geometrical shape, specimen shall be an infinite half space, and materials of indenter and specimen are incompressible (Poon et al. 2008). These assumptions cannot be satisfied. Therefore, mechanical properties measured from nanoindentation are load-dependent, which is called as indentation size effect (ISE) in the literature (Oliver & Pharr 1992; Pharr et al. 2009; Huang et al. 2010). Generally, for hardness and modulus of elasticity, the measured value decreases when indentation depth or load increases (Oliver & Pharr 1992, Chen & Bull 2006, Pharr et al. 2009, Huang et al. 2010). But more complicated relation between measured properties and indentation load/depth was observed (Voyiadjis & Peters 2010).

Although different correction methods were presented to erase the load-dependence (Oliver & Pharr 1992; Poon et al. 2008; Huang et al. 2010), in this

dissertation, these methods will not be adopted due to the complexity, and a linear relationship between modulus of elasticity and indentation load is assumed.

4.2.1. Nanoindentation test and results

Three cement paste specimens with 0%, 1% and 3% nanosilica were prepared. The mixes are shown in Table 4.3. At age of 7 days, nanoindentation tests were carried out on the three specimens. For each specimen, 20 indentations using spherical indenter at 0.5, 1 and 1.5 mN spaced by 5 μm with 10 indents using Berkovich indenter at 1.0 mN spaced by 5 μm were performed as shown in Figure 4.8.

Table 4.3: Mixes of cement paste specimens (kg/m^3)

| Specimen | Cement | Water | Nanosilica |
|---------------|--------|--------|------------|
| 0% Nanosilica | 539.0 | 269.51 | 0 |
| 1% Nanosilica | 533.3 | 269.32 | 5.33 |
| 3% Nanosilica | 522.2 | 268.93 | 15.67 |

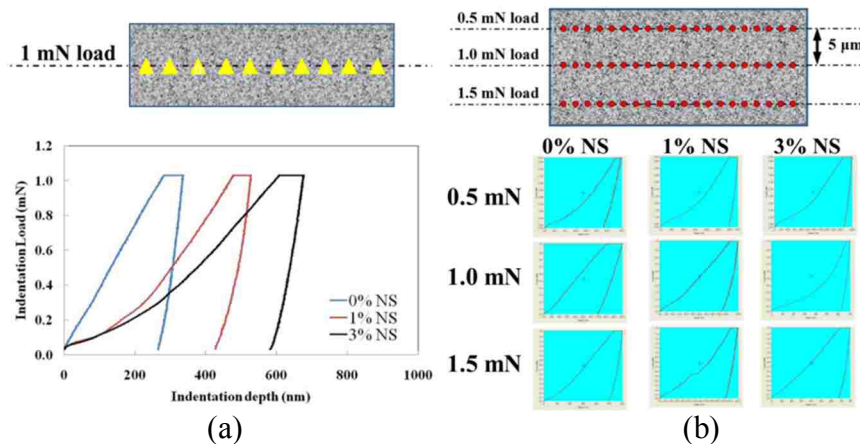


Figure 4.8: Nanoindentation using (a) Berkovich indenter and typical load-depth curves; (b) spherical indenter and typical load-depth curves.

4.2.1.1. Results from nanoindentation using Berkovich indenter

Berkovich indenter will detect certain phase; hence Young's modulus of LD C-S-H and HD C-S-H can be determined by deconvolution of nanoindentation test results

(Constantinides & Ulm 2004). Young's modulus of C-S-H E_{C-S-H} at the packing density 1 is then extrapolated from the E_{C-S-H} at the packing density 0.63 (LD) and 0.76 (HD). Based on the assumption that Berkovich indenter indents one phase, the observed experimental frequency density (EFD) can be considered as a combination of EFDs of some material phases. The observed EFD obeys to the probability density function (PDF) $p(x)$ as

$$p(x) = \sum_{i=1}^n f_i p_i(x) \quad \text{with} \quad \sum_{i=1}^n f_i = 1 \quad (4.14)$$

where f_i represents the surface fraction occupied by phase i on the indented surface; $p_i(x)$ is a PDF of each phase i ; n is the number of phases. Deconvolution of $p(x)$ into the number of n $p_i(x)$ and the corresponding f_i , can be conducted by minimizing the standard error R between EFD and $p(x)$ as

$$R = \sum_{j=1}^m \frac{\left(\text{EFD}_j - \sum_{i=1}^n f_i p_i(x_j) \right)^2}{m} \quad \text{with} \quad \sum_{i=1}^n f_i = 1 \quad (4.15)$$

where EFD_j is the experimental frequency density at the j -th bin. $p(x_j)$ is the value of PDF at point x_j ; m is the number of bins used to construct the EFD distribution. The deconvolution results are shown in Figure 4.9 and Table 4.4.

Table 4.4: Young's modulus of HD and LD C-S-H determined using deconvolution

| Item | 0% nanosilica | | | 1% nanosilica | | | 3% nanosilica | | |
|----------|---------------------|------------------------|----------|---------------------|------------------------|----------|---------------------|------------------------|----------|
| | μ_{LD} (GPa) | σ_{LD} (GPa) | f_{LD} | μ_{LD} (GPa) | σ_{LD} (GPa) | f_{LD} | μ_{LD} (GPa) | σ_{LD} (GPa) | f_{LD} |
| LD C-S-H | 10 | 3.1 | 80% | 11 | 8 | 80% | 15 | 5 | 40% |
| HD C-S-H | 20 | 4 | 20% | 25 | 6 | 20% | 33 | 4.2 | 60% |

f , volume fraction of C-S-H;
LD, low density;
HD, high density;
 μ , average value;
 σ , standard deviation.

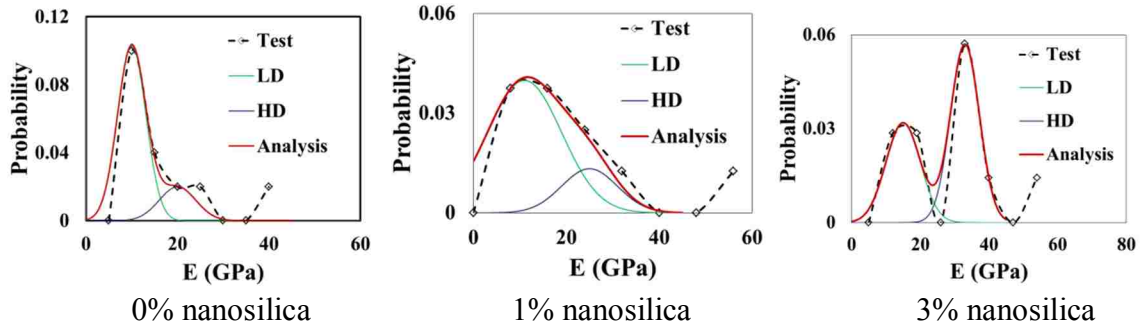
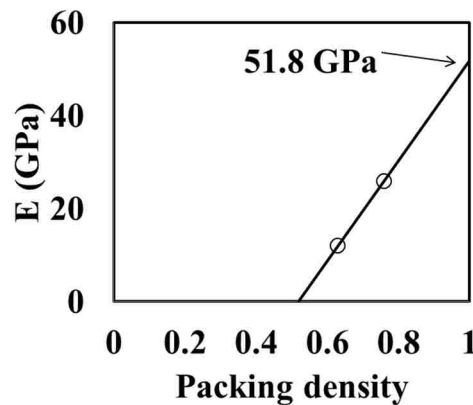


Figure 4.9: Deconvolution results

Referring to Constantinides & Ulm (2007), the packing density of low density (LD) C-S-H is 0.63 and high density (HD) C-S-H is 0.76. E_{C-S-H} of at 100% packing density can be extrapolated 51.8 GPa as shown in Figure 4.10.

Figure 4.10: E_{C-S-H} of at 100% packing density

Young's modulus of cement paste can also be determined using Berkovich nanoindentation results based on C-S-H's modulus of elasticity E_{C-S-H} and volume fraction X . The Power's like model suggested by Dr. Kim is presented as

$$E_C = E_{CSH} X^\gamma \quad (4.24)$$

where, E_{C-S-H} is 51.8 GPa. X attained from CEMHYD3D is 39.7%, 40.7% and 37.7 for 0%, 1% and 3% nanosilica specimen, respectively. From the experiments, the value of γ is 2.47. The modulus of elasticity of cement paste is determined and listed in Table 4.5.

Table 4.5: Modulus of elasticity of cement paste estimated from nanoindentation using Berkovick indenter

| Case | 0% NS | 1% NS | 3% NS |
|-----------------------------|-------|-------|-------|
| Modulus of elasticity (GPa) | 5.30 | 5.57 | 5.01 |

4.2.1.2. Results from nanoindentation using Spherical indenter and discussion

Young's modulus of cement paste E_c can be determined by calculating the expected value from the PDF of E

$$E_c = p_i E_i \quad (4.16)$$

where, E_i is Young's modulus from i -th indentation and p_i is the probability of i -th Young's modulus. PDF of E can be generated by assigning the experimental cumulated probability (ECP) to the rank ordered E results. The resulted Young's modulus from nanoindentation tests of three loading cases (0.5, 1.0 and 1.5 mN) are projected to "zero indentation" or "zero loading" to extract Young's modulus of cement paste E_c .

Unlike Berkovich indenter, spherical indenter indents a random composite as shown in Figure 4.11. Therefore, Young's modulus is approximated as

$$E_i = \sum_{j=1}^n a_j e_j \quad (4.17)$$

where, E_i is Young's modulus from i -th indentation; a_j is the surface fraction of j -th phase in contact area; e_j is Young's modulus of j -th phase. And there is

$$E_c = \sum_{i=1}^m \sum_{j=1}^n p_i a_{ij} e_j \quad (4.18)$$

where, the term $a_{ij} e_j$ represents Young's modulus of elasticity of the j -th phase as realized from the i -th indentation based on the assumption that the indented surface can represent the whole material.

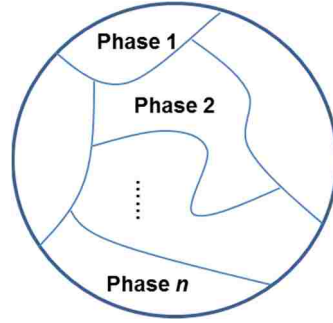


Figure 4.11: Spherical indenter indents a random composite

The maximum elastic strain is calculated as

$$\varepsilon_{\max, elastic} = \frac{h_t - h_p}{2.4a} \quad (4.19)$$

$$a = \sqrt{2R_i h_p - h_p^2} \quad (4.20)$$

where, h_t is the total depth; h_p is the plastic depth; a is the radius of contact area of indenter and R_i is the radius of indenter. The meanings of other signs refer to Figure 4.4.

The total energy per unit volume is calculated by assuming all applied energy is absorbed in the volume under contact area to depth of $2.4a$

$$\Pi_{Total} = \frac{W_{Applied}}{2.4\pi a^3} \quad (4.21)$$

Using lognormal distribution, the expected values of mechanical properties are determined as shown in Table 4.6.

The characteristic properties at “Zero load” E_z can be determined with the linear relationship

$$E_z = E_p - P\alpha \quad (4.22)$$

where, α will be determined by minimizing the standard error R as

$$R = \sum_{i=1}^N \frac{[\Phi^{-1}(E_{z,i}) - ECP(E_{z,i})]^2}{N} \quad (4.23)$$

where, Φ is the CDF and ECP is the experimental cumulated probability. Using Equations (4.22-4.23), the modulus of elasticity at load P can be projected to the corresponding modulus of elasticity at load zero E_z as shown in Figure 4.12. Finally, the processed average results are listed in Table 4.7 and the corresponding stress-strain curves derived are shown in Figure 4.13.

Table 4.6: Results from nanoindentation using Spherical indenter

| Load | Case | Π_{Total} | Π_{Elastic} | $\epsilon_{\text{elastic}}$ | E | h_t |
|--------|--------|----------------------|------------------------|-----------------------------|------|-------|
| | | (MJ/m ³) | (MJ/m ³) | (10 ⁻³) | GPa | Nm |
| 0.5 mN | 0% NS | 5.99 | 3.34 | 15 | 5.92 | 201 |
| | 1% NS | 5.03 | 3.01 | 10 | 7.13 | 581 |
| | 3% NS | 4.96 | 1.8 | 10 | 4.97 | 635 |
| 1.0 mN | 0% NS | 6.88 | 2.01 | 12.5 | 4.21 | 375 |
| | 1% NS | 6.26 | 1.81 | 11.5 | 4.67 | 346 |
| | 3% NS | 4.44 | 1.53 | 9.7 | 3.98 | 545 |
| 1.5 mN | 0% NSa | 7.51 | 3.23 | 13.5 | 5.36 | 271 |
| | 1% NS | 10.01 | 4.44 | 14 | 7.42 | 1033 |
| | 3% NSa | 7.08 | 1.87 | 10 | 5.42 | 836 |

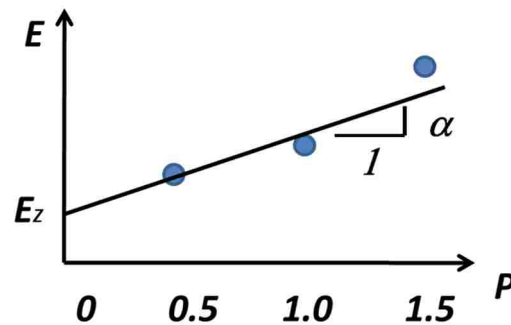
Figure 4.12: Assumed linear relationship between E and indentation load P

Table 4.7: Average results from nanoindentation using Spherical indenter

| Case | Π_{Total} | Π_{Elastic} | $\epsilon_{\text{elastic}}$ | E |
|-------|----------------------|------------------------|-----------------------------|------|
| | (MJ/m ³) | (MJ/m ³) | (10 ⁻³) | GPa |
| 0% NS | 7.65 | 2.74 | 12.7 | 5.28 |
| 1% NS | 8.09 | 2.87 | 11.7 | 5.84 |
| 3% NS | 6.66 | 1.82 | 11.5 | 4.89 |

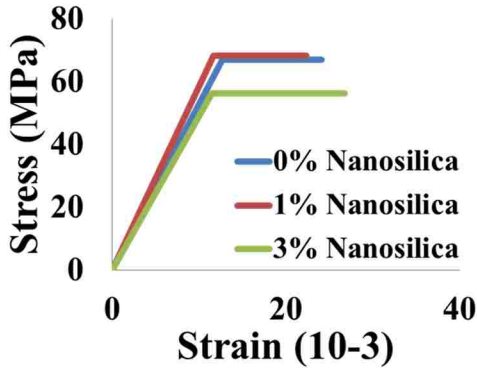


Figure 4.13: Stress-strain curves of cement paste from nanoindentation

4.2.2. Homogenization model of cement paste

Three cement paste hydration models with 0%, 1% and 3% nanosilica are established by CEMHYD3D. Hydration is simulated and microstructure of cement paste at 7 days is generated as shown in Figure 4.14. Then the generated cement paste microstructure is transferred to FEM package ANSYS® to extract its fundamental mechanical characteristics. Cement paste RVE has dimension of $100 \mu\text{m} \times 100 \mu\text{m} \times 100 \mu\text{m}$. The modulus of elasticity is determined by statistical analysis of 100 (2D) slices cut from RVE as shown in Figure 4.15. Each slice is treated as a 2D RVE and modeled by element type PLANE42 in ANSYS®, which is a plane element with four nodes, each having two degrees of freedom (DOF): translations in the x and y directions at each node. In the 2D RVE, all phases are assumed to be fully bonded. Applying prescribed boundary conditions, modulus of elasticity was gotten and the CDF for three cases are shown in Figure 4.16. The simulated and test results are listed in Table 4.8. It can be found that the homogenization model of cement paste is validated by the nanoindentation tests.

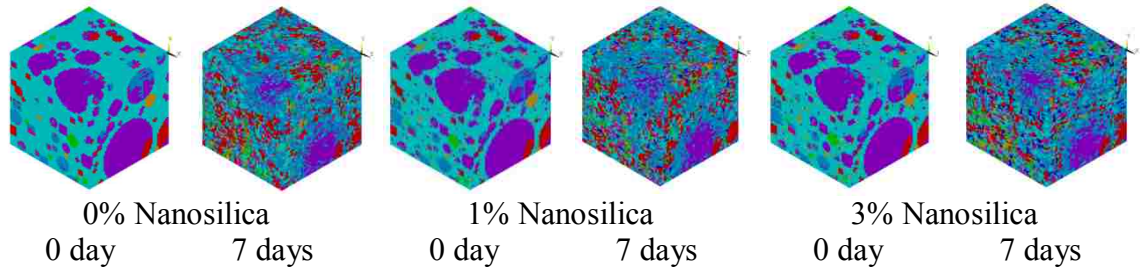


Figure 4.14: Cement paste microstructure

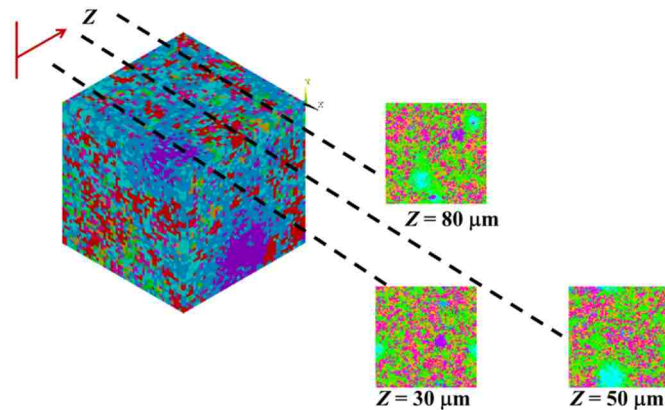


Figure 4.15: RVE slices

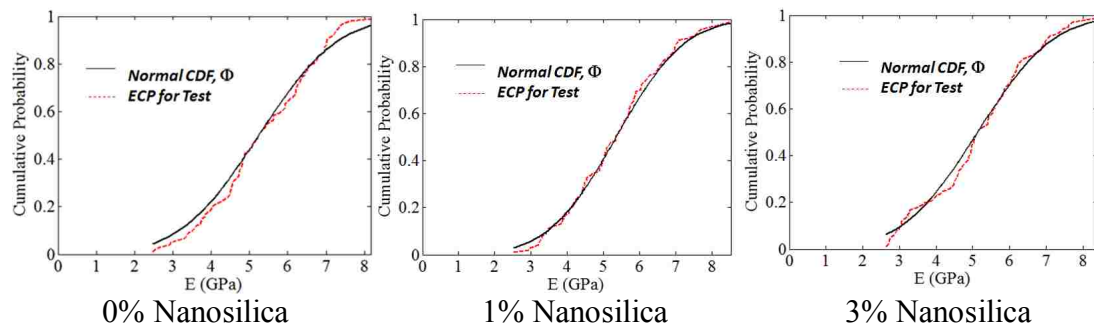


Figure 4.16: CDF of the modulus of elasticity attained from 2D RVEs

4.2.3. Results and conclusion

The proposed methods of experiments and analysis can accurately measure and simulate the behavior of cement paste. A comparison between the three methods is presented in Table 4.8.

Table 4.8: Modulus of elasticity of cement paste estimated from two nanoindentation methods and cement paste homogenization model

| Case | Berkovich indentation | Spherical Indentation | Microstructural Simulation |
|-------|-----------------------|-----------------------|----------------------------|
| | GPa | GPa | GPa |
| 0% NS | 5.30±0.18 | 5.28±5.24 | 5.25±1.51 |
| 1% NS | 5.57±0.19 | 5.84±5.57 | 5.35±1.45 |
| 3% NS | 5.01±0.17 | 4.89±4.51 | 5.13±1.73 |

Chapter 5. Application of Homogenization Method to Model Concrete

5.1. Model I: Serviceability Prediction Using Concrete Homogenization

5.1.1. Introduction

Composite behavior of concrete can be modeled by homogenization method. A representative volume element (RVE) of concrete microstructure including three phases as cement paste, aggregate and ITZ is developed by using the finite element model. Cement hydration models are used to predict the properties of the cement paste phase. Intrinsic characteristics of concrete including modulus of elasticity and cracking strength can be predicted from the homogenization model. It is shown that random generation of the RVE by using Monte Carlo simulation can compute uncertainty in concrete characteristics. Probabilistic analysis of RC beam deflection using the random concrete characteristics predicted from homogenization model allows realization of uncertainty in deflections on RC beams. Concrete homogenization enables a unique opportunity to bridge the gap between concrete materials and structural modeling that is necessary for realistic serviceability prediction.

The properties of concrete including compressive strength, modulus of elasticity and cracking strength have relatively large variation than other structural materials due to the inherent uncertainty in concrete microstructure. Concrete characteristics can be determined experimentally or predicted by numerical simulation using composite homogenization techniques. Composite homogenization is based on realization of the

The section 5.1 has been published in “A homogenization approach for uncertainty quantification of deflection in reinforced concrete beams considering microstructural variability”, *Structural Engineering and Mechanics*, An International Journal, Vol. 38, No. 4, 503-516, 2011.

interaction of the microstructure constituents to predict composite properties. A number of homogenization techniques to model particulate composites have been developed (Ju and Chen 1994; Torquato 2002). The homogenization process is developed by selecting a representative volume element (RVE) of the composite microstructure to simulate the mechanical characteristics of the composite. The RVE shall satisfy the scale separation principle (Hashin 1983). The basic premise of modeling the RVE is to utilize a robust averaging technique to determine apparent and intrinsic properties of the composite materials (Dormieux et al. 2006).

5.1.2. Concrete homogenization

Concrete was successfully modeled by using this approach in which aggregate particle was assumed as sphere randomly dispersed in the cement paste (Kurukuri 2005). The model will follow this assumption in performing concrete homogenization. Concrete is considered a three phase material: cement paste, aggregate (coarse and fine) and interfacial transition zone (ITZ). Selection of the three phases was based on their unique microstructural features and intrinsic properties (Mehta and Monterio 2006). The properties of the cement paste are predicted by using cement hydration models with time dependent strength growth considered (van Burgel 1995). RVE characteristics include the volume fraction of cement paste and aggregate, size distribution of the aggregate and the constitutive models of the cement paste and the aggregate. If RVE is randomly generated, intrinsic characteristics of concrete can be predicted. The work is extended here to utilize the basic characteristics of the concrete extracted from RVE to model deflection of a RC beam. A two-dimensional finite element model of RVE is developed to predict the constitutive relationship and the fundamental characteristics of concrete. Random

generation of RVE by using Monte Carlo simulation enables computing uncertainty of concrete characteristics and RC beam deflection. The RVE is a 50mm×50mm FE model including 250,000 elements developed under ANSYS[®] finite element environment as shown in Figure 5.1.

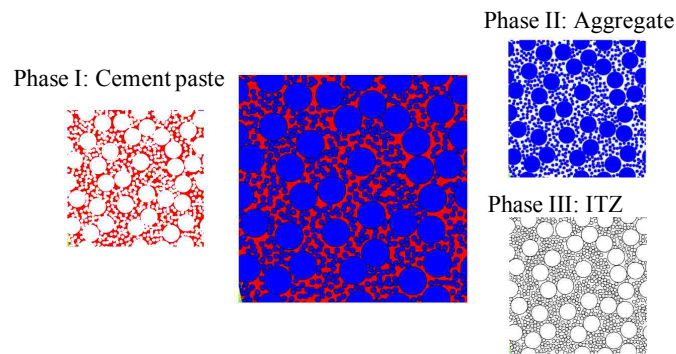


Figure 5.1: A three phase RVE modeled using the finite element method.

The RVE was modeled using PLANE42, which is a plane element with 4 nodes, each having two degrees of freedom (DOF): translations in the x and y directions at each node. Periodic boundary condition is used to represent the RVE after Kurukuri (2005). Displacements are applied to the model and the average strain and stress of the different phases are computed at each load step. Specimen testing homogenization method is used here to avoid the challenge in computing the strain energy tensors when nonlinear phases are considered (Khisaeva et al. 2006).

5.1.3. Case study

Deflection test of a RC beam having concrete compressive strength f'_c of 26 MPa was reported by Christiansen (1988). A concrete mix (Portland cement: 236 kg/m³, Silica fume 79 kg/m³, Water: 192 kg/m³, Fine aggregate 700 kg/m³ and coarse aggregate 1143 kg/m³) is considered for its ability to provide similar compressive strength of 26 MPa.

RVE to simulate this concrete is generated. Using cement hydration models, the volume fractions of Phase I (Cement paste), Phase II (aggregate) and Phase III (ITZ) are predicted to be 21%, 69% and 10% respectively. The properties of Phase I was determined using HYMOSTRUC[®] model after van Burgel (1995a & 1995b). Circles with diameters of 1 mm and 6 mm were used to represent the mean coarse and fine aggregate particles (Phase II). The thickness of ITZ is modeled as 100 μm . The elastic constitutive models in tension and compression were used for Phase I: cement paste (peak stress 30 MPa and peak strain 0.01) and Phase II: aggregate (peak stress 70 MPa and peak strain 0.001). The tensile strength and stiffness of Phase III is determined through iterative process such that the composite concrete model has an elastic tensile strength of $0.62\sqrt{f'_c}$ MPa. The elastic model for Phase III for tension is determined to have a peak stress 1 MPa and peak strain 0.001. For the compression constitutive model, Phase III is assumed to have linear elastic behavior peak stress of 10.5 MPa and peak strain of 0.00015 such that the composite concrete model achieves a compression modulus of elasticity of $4730\sqrt{f'_c}$ MPa.

By applying periodic boundary condition on RVE until the average strain of Phase III reaches its peak strain, the stress-strain curve is obtained and the tensile strength and modulus of elasticity of the composite concrete are determined as shown in Figure 5.2. The cumulative probability distribution functions (CDF) of the tensile strength (average 2.95 MPa with standard deviation 0.05 MPa) and modulus of elasticity (average 24.9 GPa with standard deviation 0.5 GPa) are then extracted by performing 100 random generation of RVE as shown in Figure 5.3. It is noticeable that the variation of f_r and E_c

from the RVE are produced without considering the variation in cement paste constituent material properties but by considering the random distribution of aggregate only.

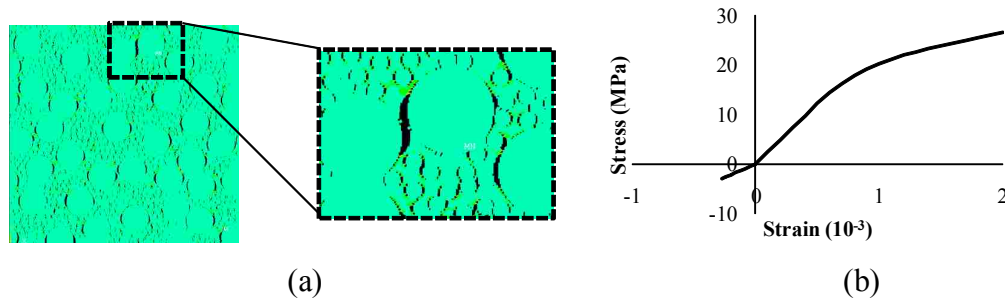


Figure 5.2: (a) Strains and crack distribution in RVE due to tensile stresses and (b) the corresponding stress-strain of RVE for compression (+) and tension (-)

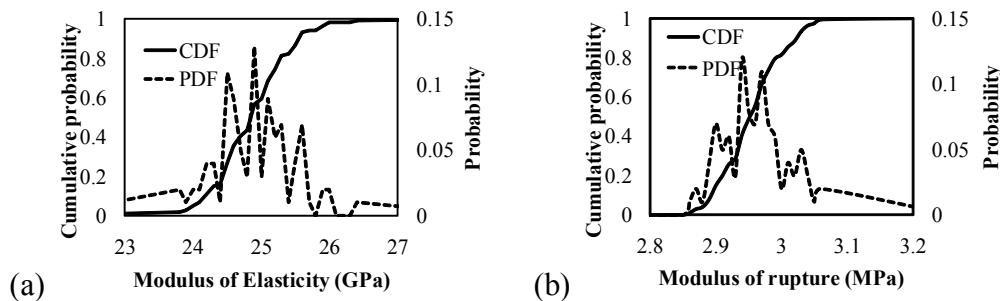


Figure 5.3: PDF and CDF for (a) E_c and (b) f_r generated from random generation of RVE

Using the CDFs of f_r and E_c as shown in Figure 5.3, the variation of deflection is quantified using Monte Carlo simulation. For random sampling of f_r and E_c , 1000 random variates for f_r and E_c were generated by the inverse transformation from the standard uniform variate. The deflection test for a simply supported RC beam made of this concrete with third-point loading is considered (Christiansen 1988). The beam considered had 7.5 meters span, 280 mm thick and 170 mm wide. The reinforced steel areas for compression and tension are 452 mm^2 , respectively. The bottom concrete cover to the reinforcement is 31 mm. The beam is subjected to a distributed load of 1.143 kN/m and two concentrated load of 2.27 kN. For this beam, the test result of the instantaneous deflection at the mid-span was measured as 14.2 mm. The deflections were calculated by

using the cracked plane frame analysis follows Ghali and Favre (2002). The resulted deflection histogram is shown in Figure 5.4 with the average of 14.6 mm and the coefficient of variation (COV) of 1.7%. Although a relatively low COV of deflection 1.7% is determined from the above analysis, this can be considered as a part of the total uncertainty of deflection due to inherent random distributions of aggregate in the cement paste matrix. Additional uncertainty due to random variations in constituent material properties is not considered. It is worth noting that the distribution of aggregate in the cement paste can be described by using lineal correlation functions as geometrical descriptors of the concrete microstructure (Torquato 2002).

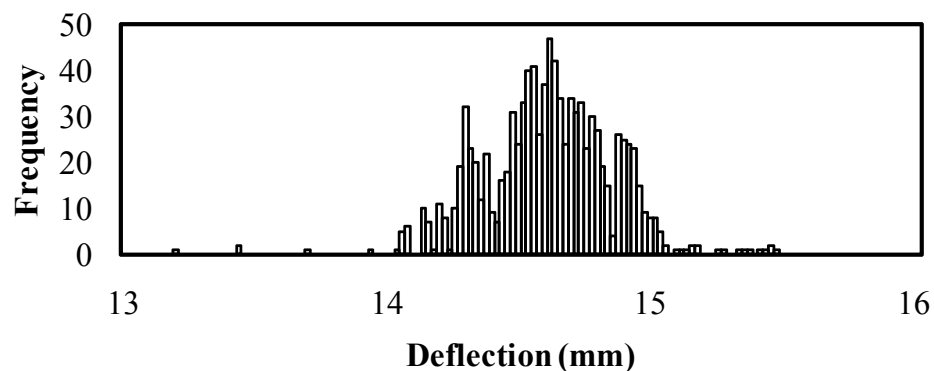


Figure 5.4: Histogram of deflections

5.1.4. Conclusions

A homogenization model is developed to examine the significance of random distribution of concrete phases on the uncertainty of concrete deflection. The inherent randomness of phase distribution of concrete matrix is considered by performing Monte Carlo simulation of the RVE model. The probabilistic properties of concrete (tensile strength and modulus of elasticity) predicted by the random RVE were used to predict the deflection histogram for a reinforced concrete beam tested by others. It is possible to

realize the uncertainty in deflection by considering homogenization of concrete. On the other hand, the relatively low COV of deflection 1.7% indicates that RVE size used here is big enough to be representativeness. However, the homogenization model cannot consider the realistic mesostructure of concrete, which will be addressed in Model II.

5.2. Model II: Estimating Uncertainty in Concrete Deflection Using an Enhanced Concrete Homogenization Approach

5.2.1. Introduction

Deflection of reinforced concrete (RC) beams is affected by the mechanical property of concrete, which directly affects the structural stiffness of the element and indirectly define the moment redistribution due to cracking. Therefore, it is important to incorporate uncertainty of the mechanical properties of concrete in deflection calculations for robust prediction of RC deflection. In this dissertation, inherent variations of mechanical properties of concrete are evaluated using the finite element (FE) method. Considering concrete as discrete particles of aggregate and cement paste connected by interfacial transition zone (ITZ), a nonlinear representative volume element (RVE) of concrete is developed based on concrete section images. Tension and compression behaviors in concrete are simulated by modeling the cohesive response of ITZ and considering contact mechanics within the RVE. The concrete RVE is validated with a theoretical concrete constitutive model based on compressive strength. The proposed RVE model is then used to describe the constitutive properties of concrete. The mechanical properties of cement paste and ITZ are used as sources of uncertainties in concrete. The homogenization approach allows for considering uncertainties due to concrete microstructure randomness. These uncertainties are reflected in the macro properties of concrete derived from the RVE. The deflection variations of RC beams are then propagated from the variations in macro properties of concrete using Monte Carlo

The section 5.2 has been published in “Quantifying deflection variation in RC beams propagated from microstructural variability in concrete using homogenization technique”. ACI Special Publication for Andrew Scanlon Symposium, 2011.

(MC) simulation based on a nonlinear FE beam model incorporating cracking and tension stiffening.

Acceptable deflection in flexural reinforced concrete (RC) members is necessary for desirable performance during their use. Due to inherent uncertainty of mechanical properties in concrete, the variation of the deflection is inevitable and it is important to incorporate uncertainty of concrete properties in deflection prediction for satisfactory use of RC members. The need to consider uncertainty in concrete properties for deflection prediction has been suggested by many researchers. The principle of error propagation was applied to predict the variation in the final deflection of prestressed concrete elements and reported a coefficient of variation (COV) of 10% final measured deflection (Zundeleovich et al. 1974). The probability to exceed the mean deflection provided from code deflection computations would be about 50% with the assumption that slab deflections are normally distributed (Thompson & Scanlon 1988). A probabilistic approach to control deflection was compared to the current deterministic approach for design for safety (Scanlon 1992). By showing the wide variation of concrete properties incorporated in deflection calculation (i.e. modulus of elasticity, modulus of rupture, and time-dependent parameters), it was suggested that a practical probability limit could be generated using a measure of the associated damage to serviceability due to excessive deflections (Fling 1992). Using deflection computation model, it was also shown that a COV of 20% in concrete cracking strength can result in COV of 30% in instantaneous deflection (Reda Taha & Hassanain 2003). Monte Carlo (MC) simulation was used to evaluate the variation of deflections due to uncertainty in material properties and dimensions involved in the computation of deflections, and a wide variation range of

deflection was reported as a result of the variability in design parameters, applied moment/cracking moment ratio, reinforcement ratio and live load/dead load ratio (Choi et al. 2004). The sensitivity of modulus of rupture and modulus of elasticity to deflection of RC beam was investigated (Kim & Reda Taha 2009). Considering the aspect that our lack of knowledge is a part of uncertainties in concrete properties, it was proposed to include both non-random (epstemic) with random uncertainties for deflection prediction of RC beams (Kim et al. 2010).

Homogenization of a composite material is based on the interaction of the microstructure constituents to predict composite properties. A number of homogenization techniques to model particulate composites have been presented (Ju & Chen 1994; Torquato 2002; Dormieux et al. 2006; Kim et al. 2010). Representative volume element (RVE) of a composite microstructure is used for the homogenization process to simulate the mechanical characteristics of the composite material. In a composite material with random microstructural inclusions as in concrete, RVE would rather be considered a statistical volume element (SVE) due to its stochastic aspect (Ostoja-Starzewski 2006). It is challenging to select an appropriate SVE with sufficient size compared to the inclusion size (e.g. aggregate particles) to be an acceptable RVE. This is achieved by minimizing or optimizing the stochastic effect of inclusion on the mechanical properties of the composite material. The size challenge in producing RVE in particulate composite is related to the need to satisfy the scale separation law that is a necessary condition to meet continuum assumption (Hill 1956 & 1963; Kanit et al. 2003). For concrete homogenization, the construction of concrete RVE was made by satisfying representativeness and geometrical similarity between the size of RVE and the

representative volume size conventionally used to measure concrete properties such as a $\phi 152.4\text{mm} \times 304.8\text{mm}$ cylinder for the compressive and tensile strength. Representativeness is a quantitative definition of RVE size to meet the accepted accuracy of composite properties predicted from RVE (Kurukuri 2004; Le Pape et al. 2009; Wu et al. 2010).

In this dissertation, a concrete RVE is developed by converting concrete section image into finite element environment. The proposed RVE recognizes concrete as a cluster of discrete particles of cement paste and aggregate linked by interfacial transition zone (ITZ). The properties of concrete, which are modulus of elasticity, compressive strength and tensile strength, are extracted from the finite element (FE) analysis of the RVE. The deflection of the RC beam is then calculated with the concrete properties attained from the RVE analysis. A nonlinear FE beam model incorporating tension stiffening of concrete is used to quantify deflection of the RC beam. Considering the variability in the microstructural mechanical properties of cement paste and ITZ, the variation of deflection of the RC beam is quantified using MC simulation. As a result, it can be realized that concrete homogenization approach can be a robust approach to bridge the gap between concrete materials and structural modeling for realistic serviceability prediction.

5.2.2. Methods

Concrete homogenization

Considering the dimension ratio of the RVE matrix and inclusion sizes, it has been shown that the predicted modulus of elasticity of a concrete has a variation of 2% for the range of the dimension ratio between 2.5 and 17.5 (Kurukuri 2004). Successful

uses of RVE for predicting macroscale properties of concrete were reported with the dimension ratio of 6.7 to 15 (Le Pape et al. 2009; Wu et al. 2010; Kim et al. 2009). For the geometrical similarity of inclusion (aggregate in concrete), it is one of the prerequisites to ensure that the constructed RVE has the same mechanical properties with real material (Torquato 2002; Le Pape et al. 2009; Sumanasooriya et al. 2009). However, as it is difficult to assign the irregular shape of aggregate in RVE, most concrete RVE in the literature was generated with the aggregate shape of sphere or overlapping spheres without considering similarity to concrete microstructure (Kim et al 2009; Kim et al. 2011). In this study, RVE is constructed from a concrete section image as shown in Figure 5.5 to ensure geometrical similarity of aggregate. RVE size is selected as 71.1 mm×71.1 mm considering the largest aggregate size of 10.2 mm from the concrete section image, which gives the dimension ratio of 7.0.

Construction of RVE

Using image processing of the concrete section as shown in Figure 5.5, the 71.1mm×71.1mm concrete RVE was constructed as a FE model. The size of RVE is determined by inscriptional square of ϕ 101.6 mm cylinder section as shown in Figure 5.5. The RVE is developed based on concrete as a cluster of discrete particles of cement paste and aggregate linked by ITZ. Due to the limitation of element number, not each fine aggregate particle can be treated as one element (Cusatis et al. 2003a & 2003b). If necessary, two or more fine aggregate particles will be combined together and represented as one aggregate element to achieve the target volume fraction. Therefore, for ITZ between fine aggregate particles and cement paste, rather than the exactly interfacial transition zones, ITZ here shall be considered as equivalent ITZ extracted from a specific

domain including fine aggregate particles. As shown in Figure 5.5, nearly all elements are surrounded by ITZ and only a few cement paste elements' neighbor is cement paste. Hence, for simplicity, all cement paste elements are surrounded by ITZ.

Concrete RVE model is built under LS-DYNA[®] FE environment. 5765 elements are included in the model (4028 elements for aggregate, 1757 elements for cement paste). In LS-DYNA[®], cement paste and aggregate are modeled using solid element type 1 and isotropic elastic material (material type 001). ITZ is modeled using cohesive and contact mechanisms in LS-DYNA[®] including a traction-separation law with quadratic mixed mode delamination criterion and a damage formulation. By applying appropriate boundary conditions, the three-dimensional (3D) model is converted to the two-dimensional (2D) plane stress state. In order to extract the constitutive of concrete, mixed boundary conditions are applied on the 2D RVE (Böhlke et al 2010).

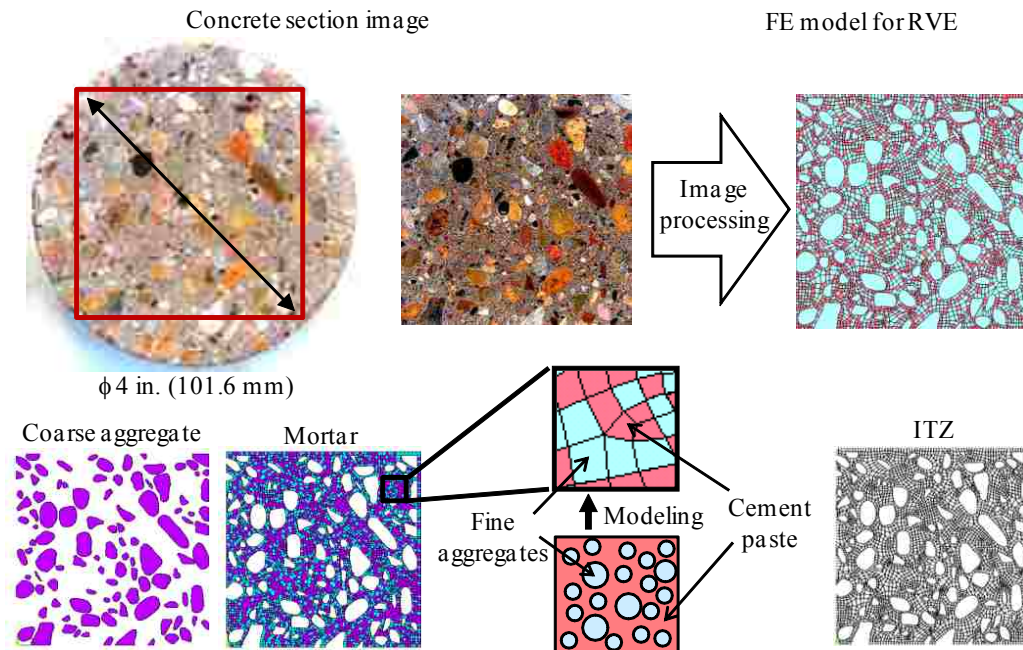


Figure 5.5: FE model for concrete RVE from a concrete section image having three phases as aggregate, cement paste and ITZ.

Debonding and contact models in ITZ

Considering the different mechanical properties of concrete in tension and compression, the process of debonding and contact mechanics between aggregate and cement paste particles in ITZ shall be carefully modeled. The debonding and contact models are combined here together in the ITZ. For debonding mechanism, Mode I and Mode II fracture modes are considered. While a relationship between the normal traction and gap distance is considered for Mode I fracture, a relationship between tangential traction and slip distance is considered for Mode II fracture. For both modes, the relationship is defined by a traction-separation curve as shown in Figure 5.6 (a). In this figure, σ is normal or tangential stress according to the debonding mode; σ_{max} is the normal or tangential bond strength; u is the contact gap or slip distance according to the debonding mode; u_f are the contact gap (slip) distances at the completion of debonding; G_F is the fracture energy equals to the area under the traction-separation curve. To consider the mixed contribution of Mode I and Mode II for the initiation and the completion of ITZ debonding, a power law was applied as

$$\left(\frac{\sigma_n}{\sigma_{n,max}} \right)^2 + \left(\frac{\sigma_t}{\sigma_{t,max}} \right)^2 = 1 \text{ (Debonding initiation)} \quad (5.1)$$

$$\left(\frac{u_n}{u_{fn}} \right)^2 + \left(\frac{u_t}{u_{ft}} \right)^2 = 1 \text{ (Debonding completion)} \quad (5.2)$$

where the subscripts n and t of the stresses and the distances in Equations (5.1-5.2) denote the normal and the tangential directions of the stresses and distances, respectively.

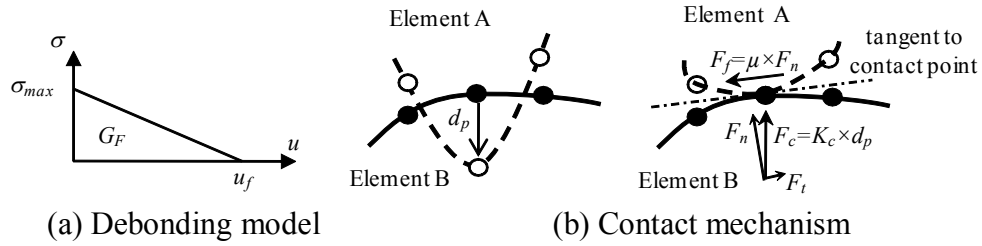


Figure 5.6: ITZ modeling using (a) debonding model of normal (tangential) stress to gap (slip) distance and (b) contact mechanism of segment-based penalty method.

Contact mechanism is to consider the compatibility of contact surface of two discrete elements. The complex contact behaviour of elements is simulated by segment-based penalty method (LS-DYNA Theory Manual 2007). In this method, contact surfaces are constituted of two surfaces connected by interface springs. A searching mechanism is introduced to detect penetration depth d_p between the two elements. When penetration occurs, contact force is generated to meet the compatibility of contact surface of two elements as shown in Figure 5.6 (b). The contact force P_c is calculated by penetration depth d_p according to contact stiffness K_c as

$$F_c = K_c d_p \quad (5.3)$$

The contact stiffness K_c is defined as

$$K_c = \alpha E_{AB} \text{ where } E_{AB} = \min(E_A, E_B) \quad (5.4)$$

where E_A and E_B is the modulus of elasticity of elements A and B, respectively, and α is a coefficient to represent the interaction between the two elements in contact. While the tangential component of the contact force to the contact surface generates shear force on the surface as shown in Figure 5.6(b), the normal component of that generates resisting friction force by Coulomb friction coefficient as

$$F_f = \mu F_n \quad (5.5)$$

where, F_f is the friction force and μ is the Coulomb friction coefficient. F_n is the normal

component of the contact force to the contact surface. The coefficients α and μ are dependent on the aggregate and cement paste used in concrete and can be calibrated to enable the RVE model to accurately simulate concrete behaviour.

Random sampling and uncertainty propagation

Many researchers have shown the efficiency of Monte Carlo (MC) simulation for modeling uncertainty in complex systems (Choi 2004) and for calibration of structural concrete design codes (Novak et al. 2003). Here MC simulation is used to quantify the variations (uncertainty) in concrete properties of compressive strength, modulus of elasticity and tensile strength propagated from the variations (uncertainty) in microstructural characteristics describing the bond strength of ITZ and the modulus of elasticity of the cement paste using a concrete RVE analysis. The variation in RC deflection is then drawn with the variation of the concrete properties attained from the RVE analysis using FE analysis. The multi-scale uncertainty propagation procedure considered in this study is schematically presented in Figure 5.7.

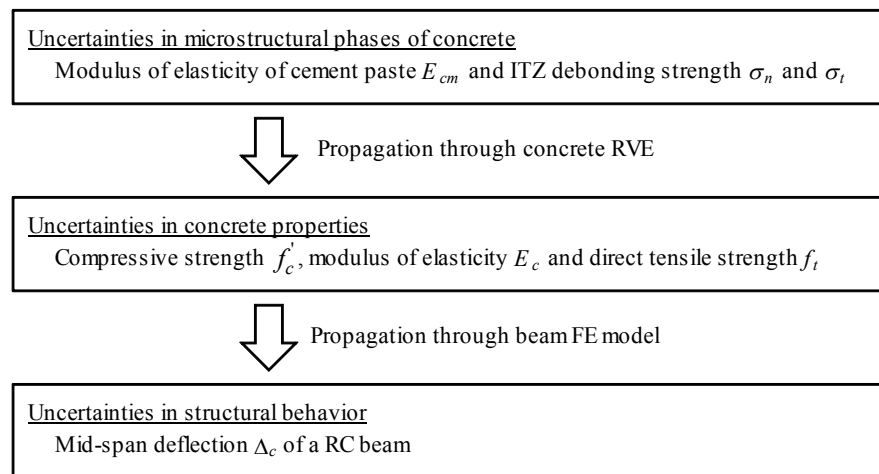


Figure 5.7: Schematic representation of the multiscale uncertainty propagation in concrete used in this study.

Assuming the bond strength of ITZ σ_{ITZ} and the modulus of elasticity of cement paste E_{cm} are independent of each other, the two variations in modulus of elasticity E_c are propagated from the variations of them. By generating the number of N random variates of σ_{ITZ} and E_{cm} from the corresponding distributions, the distributions of $E_{c,ITZ}$ and $E_{c,Ecm}$ are propagated from the distributions of σ_{ITZ} and E_{cm} respectively using concrete RVE as

$$E_{c,ITZ}^i = \text{RVE}(\sigma_{ITZ}^i, C_1) \quad \text{where } i = 1, 2, \dots, N \quad (5.6)$$

$$E_{c,Ecm}^i = \text{RVE}(E_{cm}^i, C_2) \quad \text{where } i = 1, 2, \dots, N \quad (5.7)$$

where $\text{RVE}()$ in Equations (5.5) and (5.6) represents the concrete RVE analysis to obtain E_c . C_1 and C_2 are constant parameters for the corresponding RVE analysis. The mean value c and the standard deviation s , $s_{E_c,ITZ}$ and $s_{E_c,Ecm}$ from Equations (5.1-5.3), respectively, are then calculated from the distributions. The distribution of E_c is thus formulated by combining the two distributions of $E_{c,ITZ}$ and $E_{c,Ecm}$. The error propagation theory based on the first order second moment (FOSM) method is used to combine two independent distributions (Reda Taha & Hassanain 2003). The mean of the E_c distribution is determined as

$$c_{E_c} = \text{RVE}(c_{\sigma_{ITZ}}, c_{E_{cm}}, C_3) \quad (5.8)$$

while the standard deviations is determined as

$$s_{E_c}^2 = \left(\frac{\partial \text{RVE}(\sigma_{ITZ}, C_1)}{\partial \sigma_{ITZ}} \right)^2 (s_{\sigma_{ITZ}})^2 + \left(\frac{\partial \text{RVE}(E_{cm}, C_2)}{\partial E_{cm}} \right)^2 (s_{E_{cm}})^2 = s_{E_c,ITZ}^2 + s_{E_c,Ecm}^2 \quad (5.9)$$

where the mean c_{E_c} , $c_{\sigma_{ITZ}}$ and $c_{E_{cm}}$ and the standard deviations s_{E_c} , $s_{\sigma_{ITZ}}$ and $s_{E_{cm}}$ are corresponding to the distributions of E_c , σ_{ITZ} and E_{cm} respectively. The procedure is repeated to get the distributions of the concrete compressive strength f'_c and the tensile

strength f_t propagated from the distribution of σ_{ITZ} and E_{cm} . The distributions are used to formulate the distribution of RC beam deflections using nonlinear FE analysis.

Considering the conventional relationships of f_c' to f_t and f_c' to E_c , the random variates of them are generated conditionally with the coefficient of correlation ρ of 0.9798 for the two variables having linear square root relationship (Reda Taha & Hassanain 2003). Therefore, after generating a standard uniform variate, it is shared to generate random variates of f_c' , f_t and E_c . Details for conditional sampling can be found elsewhere (Ang & Tang 2006). The distribution of mid-span deflection of RC beam Δ_c is propagated from the distributions of f_c' , f_t and E_c using the FE beam model as

$$\Delta_c^i = \text{FE}_{\text{beam}}(f_c', E_c, f_t, \text{constant parameters}) \quad \text{where } i = 1, 2, \dots, n \quad (5.10)$$

where $\text{FE}_{\text{beam}}()$ in Equation (5.10) represents the FE analysis of RC beam to get Δ_c . n is the number of generated standard uniform variates.

5.2.3. Case study

The deflection tests of four identical RC beams with different concrete compressive strengths (Washa 1947) were selected for the case study to obtain the variation in deflection according to the variation in the concrete compressive strength. The third-point bending tests of a simple support RC beam in Figure 5.8 were done by others (Washa 1947) to observe the mid-span deflection due to an applied moment M_a of 2.022 kN-m.

The mean deflection of 40.3 mm with the corresponding COV of 8% was the result of considering the mean concrete compressive strength of 29.5 MPa with the corresponding COV of 5%. The selected RC beam has span-to-depth ratio L/d of 69.2

and tension steel reinforcement ratio of 1.59%. The dimensions of the RC beams are presented in Table 5.1.

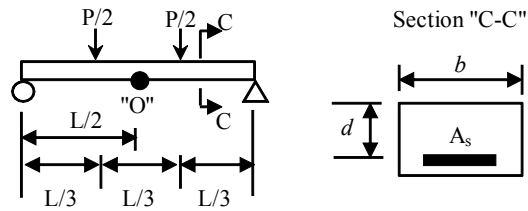


Figure 5.8: Description of deflection test set-up

Table 5.1: The RC beam considered in the case study and the corresponding deflection observations

| ID* | L (m) | b (mm) | d (mm) | A_s (mm ²) | M_a (kN-m) | f'_c (MPa) | Δ_c (mm) |
|--|---------|----------|--------------------|--------------------------|--------------|--------------|-----------------|
| B/D | 5.3 | 305 | 58.7 | 285 | 2.022 | 28.6 | 38.1 |
| B/S | | | | | | 31.8 | 37.1 |
| C/D | | | | | | 28.8 | 42.4 |
| C/S | | | | | | 28.7 | 43.7 |
| | | | Mean | | | 29.5 | 40.3 |
| | | | Standard deviation | | | 1.54 | 3.2 |
| *Beam identifications (ID) in first column are referenced from the original research (Washa 1947). | | | | | | | |

Concrete properties using representative volume element (RVE)

A mixture proportion of concrete presented in Table 5.2 is selected considering the ability to provide the same compressive strength (Zheng et al. 2001) with a mean concrete compressive strength for the deflection tests (Washa 1947) presented in Table 5.1. $\phi 101.6\text{mm} \times 203.2\text{mm}$ cylinders were cast to get a concrete section image from a cross section. RVE is generated based on the randomly selected section image shown in Figure 5.5.

Table 5.2: Mixture proportions of a concrete used to generate RVE (kg/m³)

| Cement | Water | Fine aggregate | Coarse aggregate |
|--------|-------|----------------|------------------|
| 307 | 212 | 785 | 1046 |

Cement paste and aggregate properties

Using a validated 3D cement hydration and microstructural development model HYMOSTRUC[®] (van Breugel 1995a & 1995b), the modulus of elasticity of cement paste for the mixture proportion in Table 5.2 at the hydration age of 28 days was calculated as 8.9 GPa. For the modulus of elasticity of the aggregate, 120 GPa was used. Cement paste and aggregate were modeled as linear elastic materials. As the developed RVE is based on concrete as discrete particles of cement paste and aggregate linked by ITZ, all cracking is assumed to occur in the ITZ. The volume fractions of 31% and 69% for cement paste and aggregate, respectively, were based on the mixture proportions in Table 5.2.

ITZ Properties

As ITZ is modeled as a surface, no volume fraction of that is considered in the RVE. The characteristics of ITZ were found by modeling such that the stress-strain curve of the RVE meet a theoretical stress-strain curve of a concrete with characteristic compressive strength of concrete of 29.5 MPa (Loov 1991).

$$\frac{f_c'}{f_c} = \frac{\varepsilon_c}{\varepsilon_{c0}} \left(\frac{1 + k + \frac{1}{\eta - 1}}{1 + k(\varepsilon_c / \varepsilon_{c0}) + \frac{(\varepsilon_c / \varepsilon_{c0})^\eta}{\eta - 1}} \right) \quad (5.11)$$

where f_c and ε_c are stress and strain respectively. ε_{c0} is the strain when the stress is f_c' and 0.0022 is used for normal concrete. k and η are coefficients and 0 and 4 are used for normal concrete. The theoretical stress-strain curve is shown in Figure 5.9 (a).

By applying uniaxial compression to the RVE, the stress-strain curve was matched to the theoretical stress-strain curve as shown in Figure 5.9(a) with the R-

Squared value of 0.9755. The determined ITZ characteristics for normal and tangential traction-separation curves of ITZ are presented in Figure 5.9 (b). The normal and tangential bond strengths of ITZ agree well with other findings (Kim et al. 2011). The mechanical properties of microstructural phases for the RVE are summarized in Table 5.3.

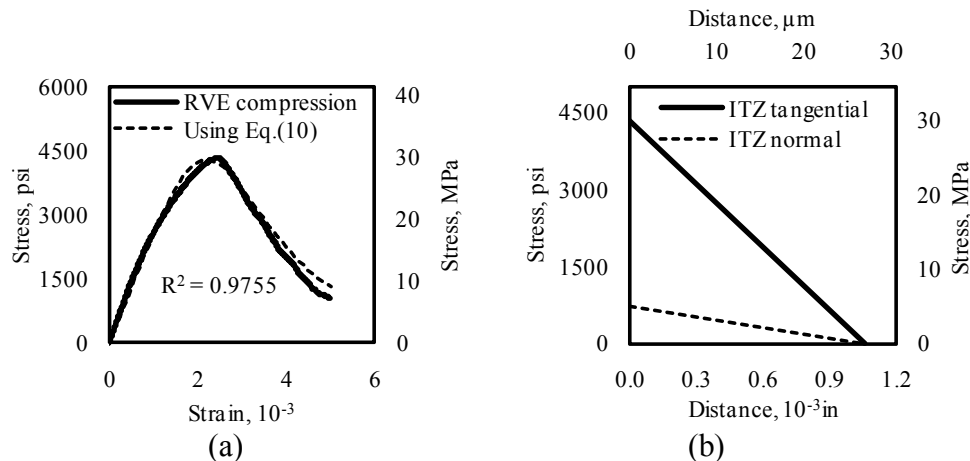


Figure 5.9: RVE model (a) Theoretical and simulated stress-strain curves, (b) ITZ properties necessary to match theoretical and simulated stress-strain curves.

Table 5.3: Mechanical properties of microstructural phases in the RVE

| Phases | Volume fraction | Modulus of elasticity (GPa) | $\sigma_{t,max}$, (MPa) | $\sigma_{n,max}$, (MPa) | u_f , (μm) |
|--------------|-----------------|-----------------------------|--------------------------|--------------------------|---------------------------|
| Cement paste | 31% | 8.9 | - | - | - |
| Aggregate | 69% | 120 | - | - | - |
| ITZ | None | - | 30 | 5 | 27 |

The constitutive models of concrete are then determined by applying uniaxial compression and tension to the RVE presented in Figure 5.10 (a) and (b), respectively. As shown in Figure 5.10(a), the concrete compressive strength of 30.0 MPa is determined at the peak strain ε_{c0} of 0.0024 and the modulus of elasticity E_c is determined as 20.0 GPa. From Figure 5.10(b), the tensile strength f_t of 1.82 MPa is determined. The determined properties are compared with those from Equation (5.11) in Table 5.4.

It is worth noting that the determined tensile strength compares well to the direct tensile strength (Canadian Highway Bridge Design Code 2000) rather than the flexural strength f_r (ACI 318). The tensile strength can be calculated as 2.17 MPa, which is apparently close to the RVE prediction of 1.82 MPa, using the direct tensile strength computation as Equation (5.12).

$$f_t = 0.4\sqrt{f'_c} \quad (5.12)$$

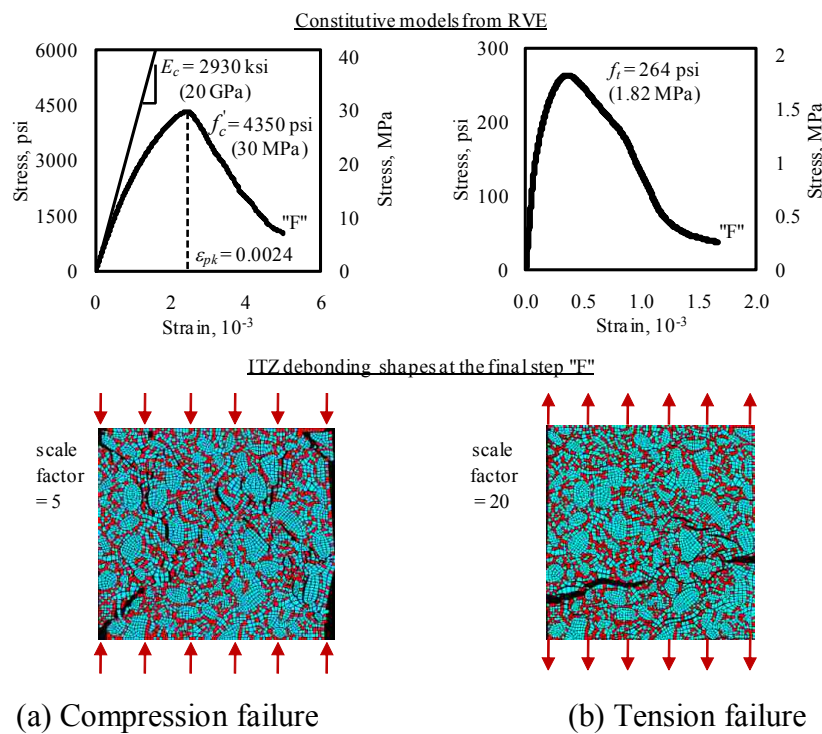


Figure 5.10: Constitutive model and ITZ debonding by applying (a) compression and (b) tension to RVE.

Table 5.4: Comparison of concrete properties predicted from RVE with corresponding values from Eq. (5.11)

| Characteristic | f'_c , (MPa) | ϵ_{pk} | * E_c , (GPa) |
|---|----------------|-----------------|-----------------|
| Target values from Equation (5.11) | 29.5 | 0.0022 | 17.3 |
| RVE Prediction | 30.0 | 0.0024 | 20 |
| Error | 1.6% | 9.1% | 13.2% |
| *The target value E_c can be evaluated at $\epsilon_c = 0$ of derivative of Equation (5.11) | | | |

Deflection of RC beam using FE analysis

FE analysis of a beam is conducted using LS-DYNA[®] to compute deflection of an RC beam. Reinforcement is modeled as smeared into concrete elements as shown in Figure 5.11. Total of 9720 solid elements are used and 1620 elements among them include reinforcement with the ratio of 0.0732 to have tension steel reinforcement ratio of 1.59% for the beam section. The material type 085 in LS-DYNA[®] is used for concrete. Concrete properties predicted from the RVE in Table 5.4 are used. To consider crack in concrete, the Winfrith concrete model is used (Broadhouse 1995). The mechanical properties for concrete cracking model include Poisson's ratio ν_c of 0.21, crack width w_c of 0.12 mm and aggregate size a_d of 10.1 mm. For the reinforcement steel, modulus of elasticity E_s of 200 GPa, Poisson's ratio ν_s of 0.21, yielding strength f_{sy} of 248 MPa, hardening modulus E_{st} of 300 MPa and ultimate elongation before rebar failure ε_s of 0.30. The mechanical properties used for FE analysis are summarized in Table 5.5. The mid-span deflection at the applied moments M_a of 2.022 kN-m was computed using the FE model as 43.1 mm.

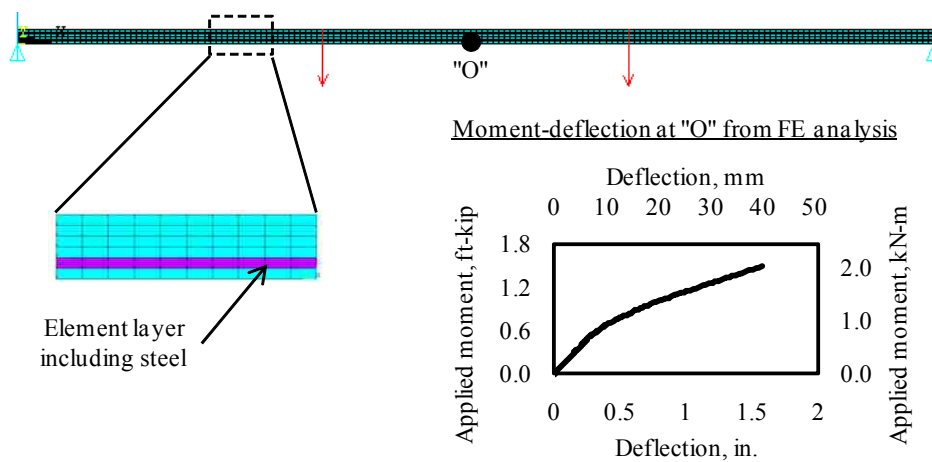


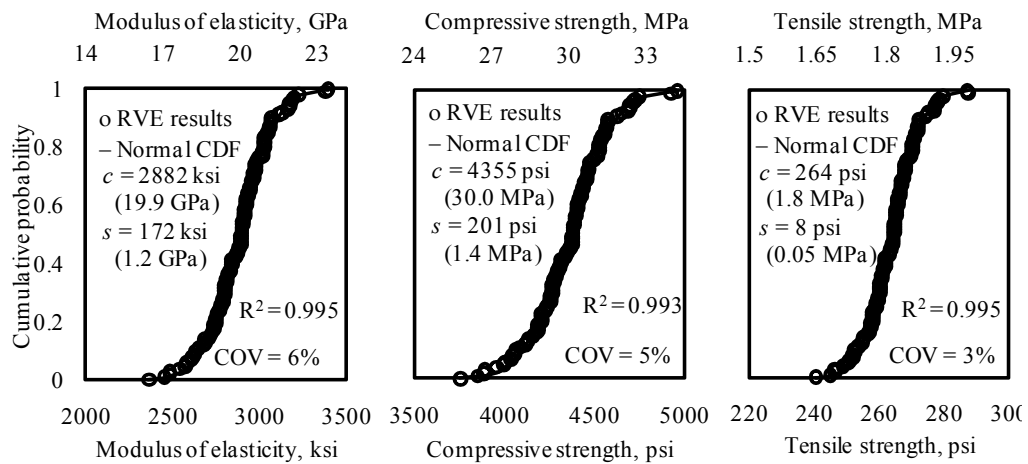
Figure 5.11: FE model dimensions and deflection prediction.

Table 5.5: Mechanical properties used for FE beam analysis

| Concrete | | | Steel | | | | |
|----------|--------------|--------------|---------|---------------|-----------------|---------------|------------------|
| ν | w_c , (mm) | a_d , (mm) | ν_s | f_y , (MPa) | ε_s | E_s , (GPa) | E_{st} , (MPa) |
| 0.21 | 0.12 | 10.1 | 0.21 | 248 | 0.3 | 200 | 300 |

5.2.4. Results and discussion

To consider microstructural variability, the normal distributions of the modulus of elasticity of cement paste E_{cm} and the bond strength of ITZ, $\sigma_{n,max}$ and $\sigma_{t,max}$ are selected as random variables. By generating 100 random variates of E_{cm} from the normal distribution with a COV of 10%, three distributions of the concrete properties, modulus of elasticity E_c , compressive strength f'_c and tensile strength f_t are propagated through the constructed RVE used to simulate concrete constitutive models in the case study. The resulted distributions are presented in Figure 5.12 as the cumulative density function (CDF) with the corresponding normal CDF. The R-squared values between the simulated CDF and a normal CDF are calculated to examine the errors between the two distributions. All three distributions showed good agreement with the corresponding normal distribution with the R-squared value of 0.99.

Figure 5.12: CDFs for concrete properties propagated from E_{cm} variation using a RVE.

For the microstructural variability of the bond strength of ITZ, $\sigma_{n,max}$ and $\sigma_{t,max}$, 100 random variates are generated, respectively, from the normal distributions with a COV of 30%. Full positive correlation between $\sigma_{n,max}$ and $\sigma_{t,max}$ is considered. The three distributions of the concrete properties, modulus of elasticity E_c , compressive strength f'_c and tensile strength f_t are propagated from the distribution of $\sigma_{n,max}$ and $\sigma_{t,max}$ through the RVE. The resulted distributions are presented in Figure 5.13 as a CDF compared with the corresponding normal CDF. All three distributions showed good agreement with the corresponding normal CDF with the R-squared value of 0.98 for the modulus of elasticity and 0.99 for the compressive strength and the tensile strength.

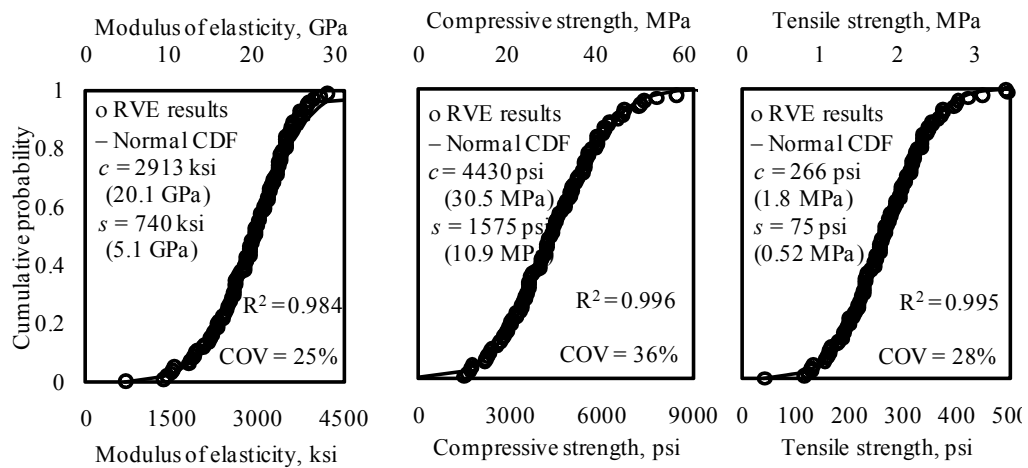


Figure 5.13: CDFs for concrete properties propagated from $\sigma_{n,max}$ and $\sigma_{t,max}$ variations using a RVE

Assuming the bond strength of ITZ σ_{ITZ} and the modulus of elasticity of cement paste E_{cm} are independent to each other, the two variations of concrete modulus of elasticity E_c in Figure 5.12 (a) and Figure 5.13 (a) are combined together using the error propagation theory in Equations (5.8-5.9). It is noticeable that as the propagated distributions are close to normal distributions as confirmed with the R-squared values, the use of the error propagation theory is more efficient than the use of MC simulation to

combine the two distributions. The mean value of the E_c distribution is determined as 20 GPa from the RVE analysis using the mean values of E_{cm} , $\sigma_{n,max}$ and $\sigma_{t,max}$ while the standard deviation is determined as 4.6 GPa. The procedure is repeated to combine the distributions of the concrete compressive strength f'_c in Figure 5.12 (b) and Figure 5.13 (b) and the tensile strength f_t in Figure 5.12 (c) and Figure 5.13 (c). The mean values and the standard deviations of the combined distributions of the concrete properties are represented in Table 5.6.

Table 5.6: Variations in microstructures and propagated variations in concrete properties and deflection

| Criterion | Considered variations in microstructures | | | Propagated variations in concrete | | | Propagated variation in deflection, (mm) |
|-----------|--|------------------------|------------------------|-----------------------------------|--------------|-------------|--|
| | E_{cm} , (GPa) | $\sigma_{t,max}$ (MPa) | $\sigma_{n,max}$ (MPa) | E_c (GPa) | f'_c (MPa) | f_t (MPa) | |
| Mean | 8.9 | 30 | 5 | 20.0 | 30.0 | 1.82 | 44.2 |
| Std* | 0.9 | 9 | 1.5 | 4.6 | 10.9 | 0.52 | 13.5 |
| COV | 10.0% | 30.0% | 30.0% | 22.8% | 36.4% | 28.7% | 30.6% |

*Std: standard deviation.

The variation in RC deflection is then quantified from the variation of the concrete properties attained from the RVE analysis. Using MC simulation, 1000 standard uniform variates were generated, the random variates of f'_c , f_t and E_c were generated conditionally with the coefficient of correlation of 0.9798. The distribution of mid-span deflection of RC beam Δ_c is propagated from the distributions of f'_c , f_t and E_c using FE beam model. The variation in deflection is presented as the simulated CDF and the frequency histogram shown in Figure 5.14 (a). The simulated deflection distribution is also presented as the relative frequency density (RFD) with the corresponding normal PDF in Figure 5.14 (b). The R-squared value between the simulated RFD and the corresponding normal distribution is calculated as 0.934. The mean deflection is

determined as 44.2 mm with the standard deviation of 13.5 mm, which provides COV of deflection of 30.6%.

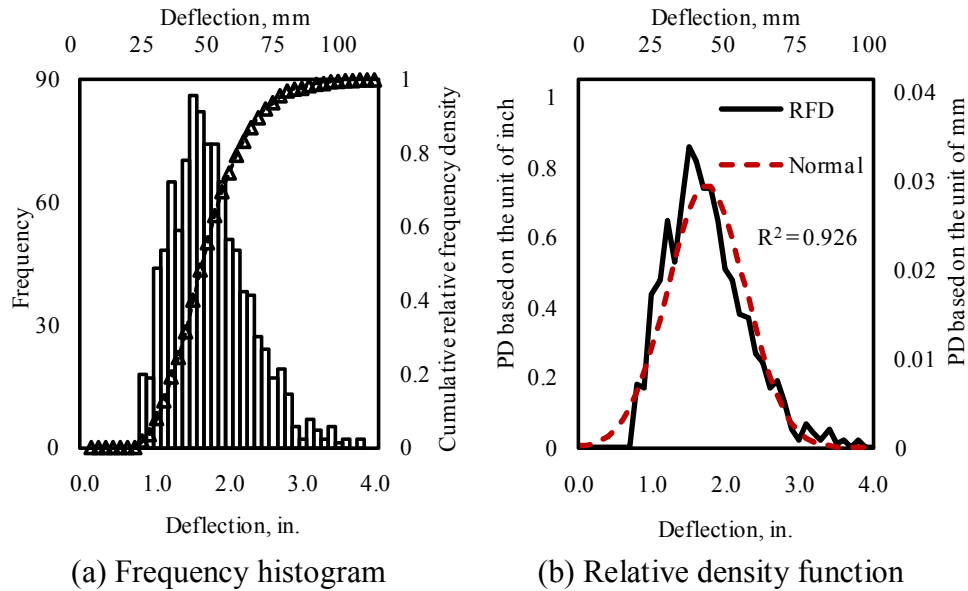


Figure 5.14: (a) Frequency histogram and (b) relative frequency density for deflection generated by the FE analysis considering concrete variation as predicted by the microstructural homogenization model. Results are compared to experimental PDF

The predicted mean of 44.2 mm compares well with the experimental measured deflection by others (Washa 1947) (Table 5.1) of 40.3 mm. However, the measured deflection had COV of 8% only, based on a COV of compressive strength of 5%. The FE model showed a COV of deflection of 30.6% based on a COV of compressive strength of 36.4%. It is obvious that the simulated deflection and compressive strength incorporated much higher variability than that observed experimentally. This is attributed to the fact that compressive strength coefficient of variation extracted from the RVE model was based on the microstructural variability of the bond strength of ITZ based on coefficient of variation of the normal and tangential tractions $\sigma_{n,max}$ and $\sigma_{t,max}$, assumed to be 30%. This COV of the ITZ characteristics seems to be relatively high and were impossible to

verify. Further analysis showed that limiting the COVs of the ITZ characteristics and E_{cm} to 5% and 10%, respectively, would result in a COV of concrete compressive strength of 8.0% and the corresponding deflection of 6.3%, much closer to that reported experimentally. Moreover, the constitutive model of concrete based on the homogenization model was compared to a classical constitutive model of concrete (Loov 1991). This can be better compared to and validated against a stress-strain relationship determined experimentally of the same concrete material. Such validation can provide more confidence in the RVE model before its use for RC structural analysis. Furthermore, it is important to note that the RVE model extracted the variation of the concrete properties based on microstructural characteristic variation while neglecting the significance of microstructural randomness. While the significance of microstructural randomness shall result in a very low addition to concrete variation as the RVE selected was based on the length scale limits, it is believed that consideration of microstructural randomness might add to concrete variation. This can be performed by analysis of large number (>100) RVEs with random microstructures that achieve a minimum acceptable two-point correlation value with the multiple cross sections of this concrete. Further research is undergoing to include such variation into account.

The above method and case study provide a framework for quantifying uncertainty in serviceability limit states (e.g. deflection) of RC members by considering sources of inherent randomness in concrete microstructures. This quantified uncertainty might be integrated with other uncertainties in loading and structural geometry to provide a rational estimate for uncertainty in deflection and cracking of RC members. Furthermore, using the probabilistic distribution of deflection predicted in Figure 5.14(b),

the probability of exceeding deflection threshold can be quantified by reliability analysis. This might enable probabilistic design of serviceability limit states considering realistic assumptions of the materials behavior under service conditions.

Finally, the proposed method of analysis based on microstructural homogenization opens new frontiers in RC serviceability modeling not considered before. By introducing homogenization techniques for modeling reinforced concrete elements, we will be able to incorporate durability deterioration mechanisms in modeling the structural behavior of RC members. For example, if microstructural cross sections due to freeze-thaw cycles or exposure to sulphate solutions can be attained, damage in the concrete can be measured and can be modeled and incorporated in modeling serviceability of RC structures. This is an important step toward bridging the gap between concrete materials and structures modeling that can lead to more accurate modeling and better design.

5.2.5. Conclusions

A concrete homogenization approach is developed to examine the significance of random distribution and uncertain mechanical characteristics of concrete microstructure on the uncertainty of deflection of reinforced concrete beams. The inherent variability in concrete microstructures is considered by studying the variation in the cement paste stiffness and the characteristics describing the normal and tangential traction slip relationships in the ITZ. This enabled computing the uncertainty in concrete constitutive relationship under compression and tension. The uncertainties in concrete constitutive models are used to compute the variation in deflection of RC beams using MC simulation. It is shown that the proposed approach is capable of quantifying uncertainty

in RC deflection by homogenization of concrete microstructure. The use of microstructural homogenization enables examining the significance of durability effects on serviceability of RC structures.

5.3. Model III: Modeling ASR in Concrete Using Concrete Homogenization

5.3.1. Introduction

Alkali-silica reaction (ASR) is called “concrete cancer”. When alkali in cement, reactive silica in aggregate and water meet together, ASR will happen and produce gels which expand if water exists. Swelling of ASR gels presses other phases in concrete microstructure and induces stress. If the pressure is big enough, cracking and volume expansion can be created on macro concrete structures. The original loading path may be changed due to concrete cracking or due to concrete material damaged by ASR. Moreover, cracking will allow water and possibly chloride ions to ingress to concrete, causing corrosion of steel reinforcement and worsening the effect of freeze/thaw cycles. This environmental deterioration can significantly shorten concrete structure service life.

Since the first report of ASR by Stanton in 1940, researchers all over the world examined ASR. ASR research work can be categorized into three groups: First, to investigate ASR consequences on concrete specimens and structures, second, to explore the chemical-physical mechanisms of ASR and third to develop simulation methods, which combines chemical and mechanical modeling of ASR and apply these models to concrete structures.

Methods to prevent ASR were found during research. The methods are rooted in the three preconditions for ASR: adding admixtures with high silica content such as fly ash or silica fume, keeping concrete structure dry, and using nonreactive aggregate. Any of these three ways can mitigate or control ASR effectively. However, these prescriptions only work on new concrete structures but not on existing concrete structure with ASR

potential. This becomes critical for sensitive structures (e. g., nuclear power plant). The cost to demolish and rebuild such structure is significant. Researchers need to answer the question, for those structures subjected to ASR which was not considered in their design, can they survive for the next 50 years safely? Such challenge makes modeling and simulation of ASR necessary. This dissertation suggests that concrete homogenization can be of significant value for that challenge.

The details of chemical reaction of ASR are too complex and are not clear in the literature. Generally, it is believed that ASR will happen along the aggregate surface, when alkali from cement meets with silica from reactive aggregate. Water is used to transport reactants and so is indispensable. Like other chemical reactions, ASR can be accelerated by high temperature. The resultant of ASR is a kind of gel that swells significantly when absorbs water, changing the microstructure of concrete. However, the change of microstructure does not necessarily damage concrete. If the amount of ASR gel is very small, only voids in concrete will be filled and no stress is induced. During this period, concrete mechanical performance might be improved due to the reduced porosity. With the proceeding of ASR, large amount of ASR gels are generated, and particles in concrete microstructure will be detached by ASR gel expansion. For this stage, ASR deteriorates concrete, macro cracking and expansion can be observed and the concrete structure deforms.

Even if the whole concrete member is submerged under water and if the ASR process reactivity is consistent, it is reported that, in casting direction, ASR expansion is about 1.5 times of that in lateral direction. Grimal et al. (2008) attributed this phenomenon to the fact that voids tend to gather at the bottom and top of aggregate along

the casting direction due to microbleeding and sedimentation. ASR gels will occupy these voids and are apt to cause expansion in the casting direction. Researchers also reported that compression can reduce ASR expansion in the loading direction. For example, ASR expansion decreases gradually from surface to center in a concrete member. However, it is still unclear whether compression inhibits ASR itself or not. The mechanical test results from standard specimens (prisms, cylinders) perhaps cannot reflect the real states in concrete structures, because they might have different levels of ASR and different boundary conditions. Assuming ASR is not affected by stress, and ASR expansion can be regarded as imposed strain on concrete, mechanical consequences of ASR on concrete can be simulated as the superposition of damage in concrete material and interaction between concrete expansion and confinement from reinforcement and prestress.

In this dissertation, we will only focus on the mechanical simulation of concrete subjected to ASR. ASR expansion ratio is selected as a tentative controlling parameter. The mechanical properties are correlated to ASR expansion ratio through experiment, and this relationship will be used to validate the proposed homogenization model of concrete subjected to ASR. Later, the validated mechanical model will be combined with the chemical mechanism of ASR reported by other researchers. The complete chemical-mechanical simulation can be used by others to predict the mechanical performance of ASR-affecting concrete structures. It is worth noting that continuous cement hydration can compensate some of the negative effect of ASR. A cement hydration simulation package HYMOSTRUC[®] is used to consider cement hydration. The ASR simulation process is illustrated in the following section.

5.3.2. Methods

Homogenization model of cement paste

Construction of cement paste RVE and cement hydration are achieved by HYMOSTRUC[®] developed at Delft University of Technology in Netherland (van Breugel 1995). Knowing water to cement ratio, cement type, and cement particle size distribution (PSD), a 3D cement paste RVE will be generated by random spheres. Clinkers in cement paste are distributed. Then the cement paste RVE will experience hydration. In cement paste RVE, all phases are assumed to be fully bonded. This modeling of cement paste is validated by other researchers and by an earlier model described in this dissertation.

Homogenization model of concrete

Concrete is regarded as discrete particles connected by interfacial transition zone (ITZ). Cement paste and aggregate particles are assumed to follow linear elasticity. Properties of cement paste are derived from cement homogenization simulation. Aggregate's properties are determined by experiments reported in the literature (Comby-Peyrot et al. 2009). Because properties of ITZ are unknown, an optimization algorithm is developed to find the properties of ITZ by matching the concrete RVE stress-strain curve to a target stress-strain curve from the literature (Loov 1991). Detailed information on this process is described early in Chapter 5.2.2. The concrete RVE and boundary conditions used are shown in Figure 5.15. Because aggregate and cement elements are all linear elastic, in RVE, average strain is attained using Equation 5.13, and average stress equals the y -direction average stress approximately.

$$\varepsilon_A = \frac{d}{L_{RVE}} \quad (5.13)$$

where, ε_A is the average strain; d is the displacement applied; L_{RVE} is the length of RVE edge.

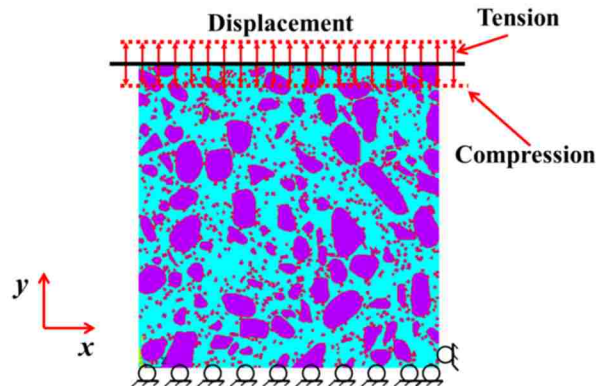


Figure 5.15: Concrete RVE and boundary conditions

However, the relationship between cement hydration and ITZ properties is unknown. Here, two different cases are assumed. One is that the properties of ITZ will change proportionally with the Young's modulus of cement paste as the cement hydration continues; and the other is that ITZ will remain constant with the properties determined at age of 28 days regardless of cement hydration. Different results from the two assumptions are compared.

Modeling of mechanical consequences of ASR on concrete

So far, the details of chemical mechanism of ASR cannot be figured out with complete certainty, and modeling of ASR has to compromise with this point and select a macro parameter widely used in experiment as ASR expansion ratio. ASR expansion ratio is the bridge to connect ASR and its mechanical consequences on concrete. Based on this parameter, constitutive and discrete models were proposed by researchers. In constitutive model, the target expansion ratio is applied directly on concrete elements as imposed strain. While in discrete model, the target macro expansion ratio is achieved by reactive aggregate elements only, which gives insight of the microstructural behavior of

concrete subjected to ASR expansion. Because it is believed that ASR gel generation and swelling are located along the aggregate surfaces, in the proposed model, ASR expansion is realized by expanding aggregate elements, as shown in Figure 5.16. The swelling of aggregate can produce cracks in concrete and damage ITZ. Deterioration of concrete due to ASR expansion is simulated.

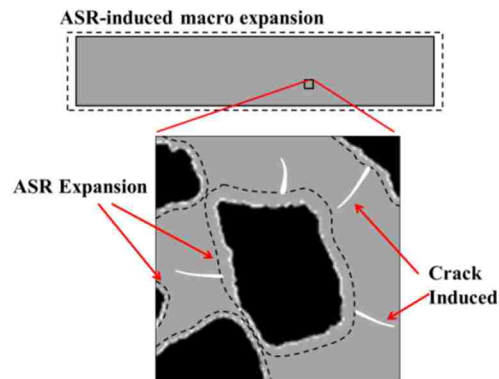


Figure 5.16: ASR-induced macro expansion achieved by expanding aggregate

In concrete RVE model, swelling of aggregate is implemented by thermal expansion of reactive aggregate elements. When target expansion ratio is reached, holding temperature, tensile or compressive displacement will be applied on RVE to get the average stress-strain curve. Internal stress in RVE can be induced by expansion of aggregate particles. Stress relaxation will happen but it is difficult to be measured. On the other hand, it is reported that complete stress relaxation never occurs (Suter & Benipal 2010). Stress relaxation is not considered in this model. The methods to extract stress-strain curve for RVE are elaborated as follows.

Methods to get stress-strain curve of RVE

At each sub-step, the average strain is determined by Equation (5.13), and average stress of RVE can be attained in view of strain energy based on Equation (5.14).

$$U = \frac{1}{2} \cdot \varepsilon_A \cdot \sigma_A \cdot \varepsilon_A \quad (5.14)$$

where, U is the total elastic strain energy, σ_A is the average stress. For RVE without ASR expansion, the typical displacement-strain energy curves are shown in Figure 5.17, and the derived stress-strain curve based on Equations (5.13 & 5.14) is shown in Figure 5.18.

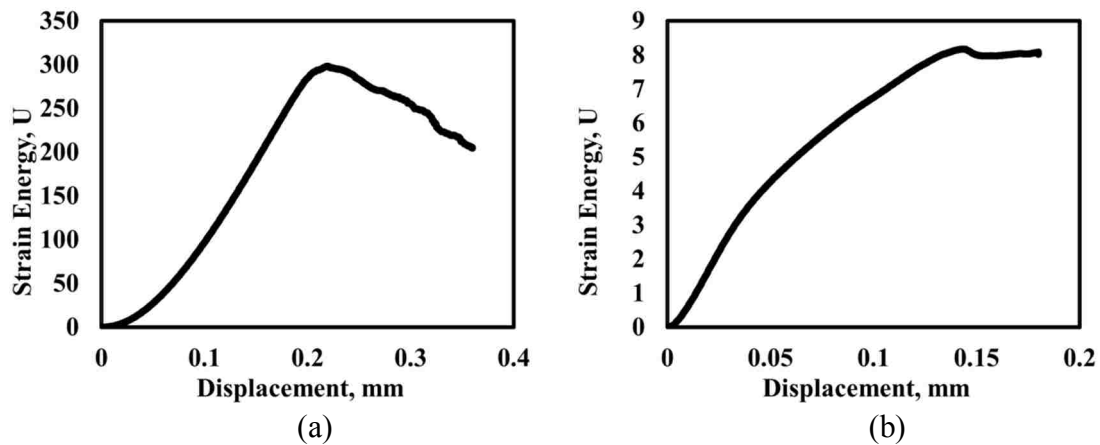


Figure 5.17: Displacement-strain energy curve; (a) in compression, and (b) in tension

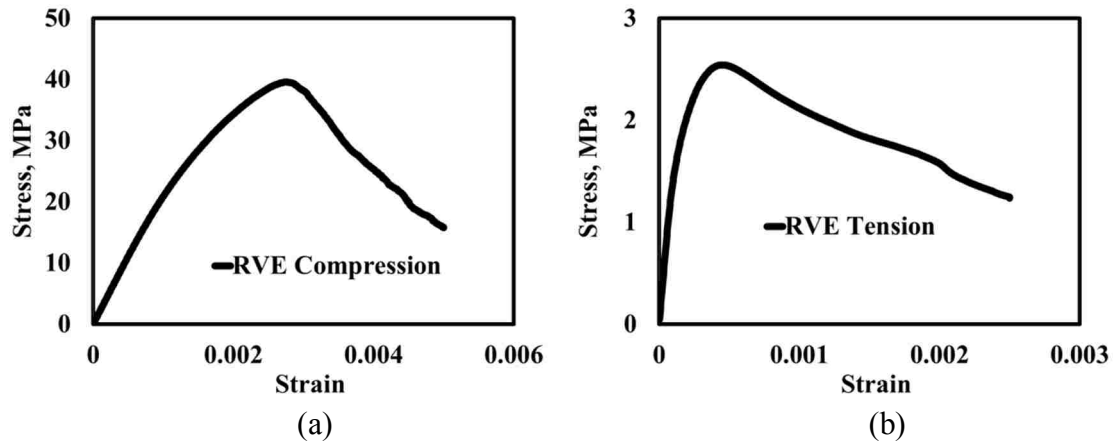


Figure 5.18: Stress-strain curve of RVE; (a) in compression, and (b) in tension

However, Equation (5.14) is challenged for RVE subjected to ASR expansion. The displacement-strain energy curve from RVE with ASR expansion is shown in Figure 5.19. Total strain energy is composed of two parts as described by Equation (5.15).

$$U_{Total} = U_t + U_d \quad (5.15)$$

where U_t is the strain energy caused by thermal expansion of aggregate elements; U_d is the strain energy caused by the displacement applied; U_{Total} is the total strain energy. In compression, U_d and U_t are separated by the dashed line shown in Figure 5.19 (a), and stress-strain curve can be attained via U_d . However, in tension, when ASR expansion ratio high (above 0.2%), U_{Total} decreases with tensile displacement as shown in Figure 5.19(b) & (c). Obviously, U_t decreases due to the tensile displacement applied on the expanded RVE. The decrease of U_t is mixed with increase of U_d and cannot be separated from each other. Stress-strain curve has to be gotten by another way, that is to average all elements' stress as Equations (5.13 & 5.16).

$$\sigma_A = \frac{\sum_{i=1}^N \sigma_{ei} A_{ei}}{A_{Total}} \quad (5.16)$$

where σ_A is the average stress of RVE; N is the total number of elements; σ_{ei} is the average stress of element i ; A_{ei} is the area of element i ; A_{Total} is the total area of RVE.

For RVE without ASR expansion, the typical difference between the two methods is shown in Figure 5.20. That average stress calculated based on strain energy is smaller than average stress calculated based on averaging each element's stress can be attributed by the open and slid in ITZ elements, which are similar with plastic strain.

Considering the average stress method, for RVE subjected to ASR expansion, in compression, RVE model will give stress-displacement curve as shown in Figure 5.21(a). Aggregate expansion starts from point A and ends at point B, with about 7 MPa internal stress induced. Compressive displacement is applied on RVE from point B, at point C, the average stress decreases to zero. Point D denotes the failure of RVE. For this case, the stress-strain curve of RVE will be calculated based on section CD in Figure 5.21 (a). The displacement-average stress curve in tension is shown in Figure 5.21 (b). Aggregate

expansion starts from point A and ends at point B, with about 7 MPa internal stress induced. Applied by tensile displacement, the average stress in RVE increases from B then decreases to failure point D. In tension case, the stress-strain curve of RVE is calculated based on section BD in Figure 5.21 (b). It is evident from Figure 5.21 that the average stress approach can yield acceptable results.

The proposed average stress approach will be used for simulation in next section and be validated by plain concrete test results with and without ASR published by other researchers.

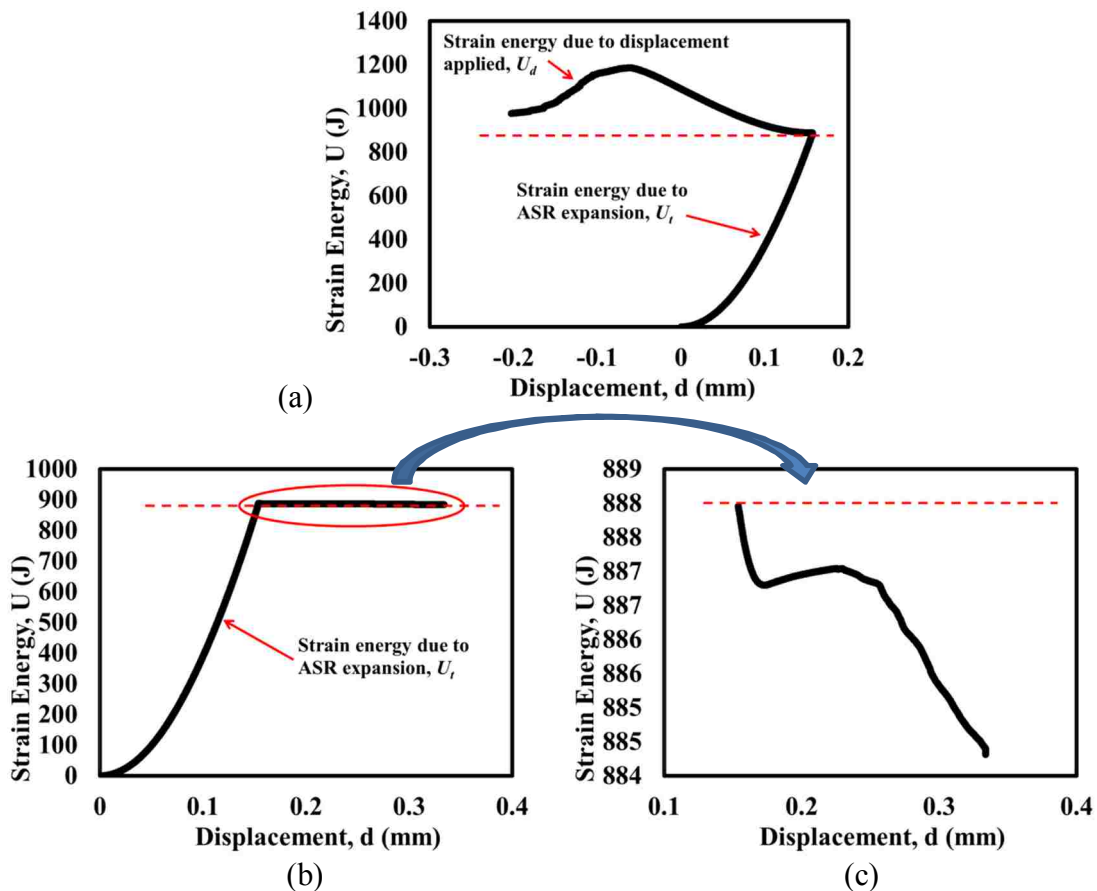


Figure 5.19: Displacement-strain energy curve of RVE; (a) Compression; (b) Tension; (c) Detailed information of displacement-strain energy curve in tension.

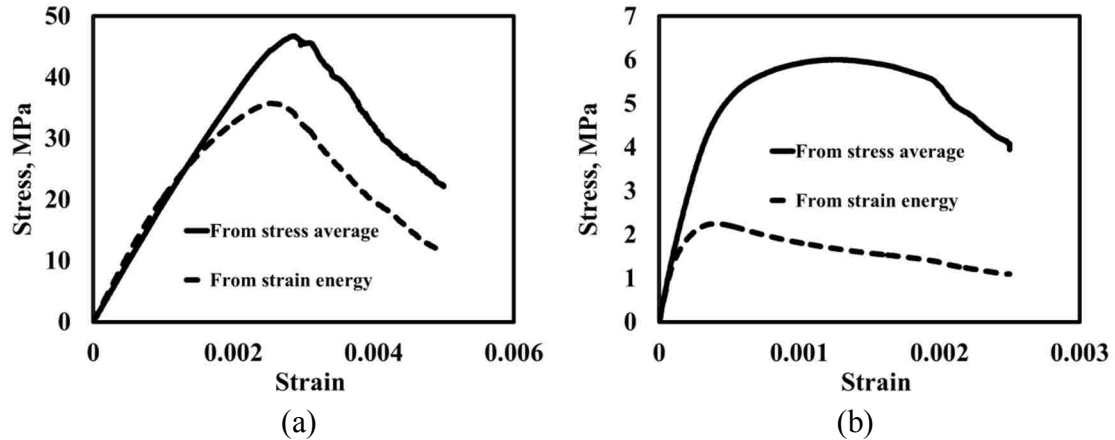


Figure 5.20: Stress-strain curve generated by the two methods; (a) Compression; (b) Tension

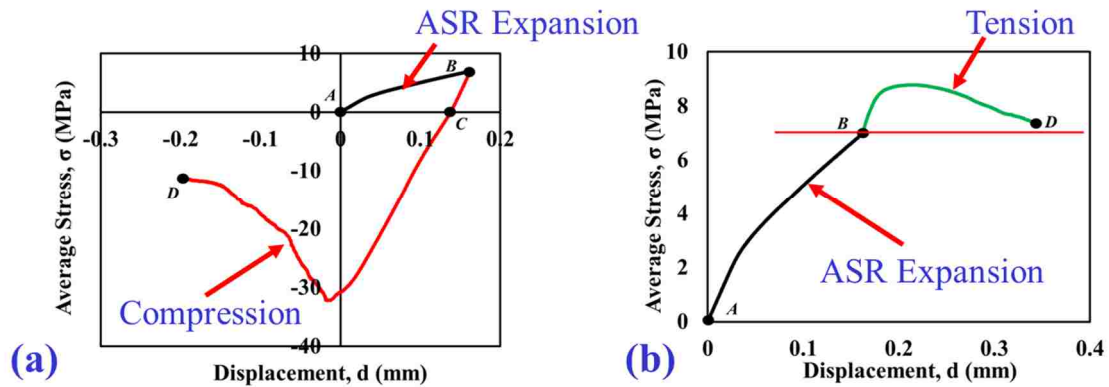


Figure 5.21: Displacement-average stress curve of RVE subjected to ASR expansion without stress relaxation; (a) compression; (b) tension

5.3.3. Case study

The concrete RVE and boundary conditions used in this study are shown in Figure 5.15. The proposed ASR model was validated by experimental results presented by Fan & Hanson (1998) and Asai et al. (2009). In the work done by Fan & Hanson, 40 reactive and 40 nonreactive concrete cylinders of dimension $\phi 100\text{mm} \times 200\text{mm}$ were cast to get the mechanical properties of concrete. In the experiment done by Asai et al. (2009), prisms of dimension $100\text{mm} \times 100\text{mm} \times 400\text{mm}$, cylinders of dimension $\phi 100 \times 200$ mm and

$\phi 150\text{mm} \times 200\text{ mm}$ were cast and cured in accelerated speed conditions. These specimens were tested at different ages. Concrete mix used in experiments is listed in Table 5.7. The test results such as ASR expansion ratio, compressive strength, modulus of elasticity and tensile strength were shown in Figures 5.22 & 5.23. In this dissertation, cases of concrete with ASR expansion ratio of 0.10% and 0.21% are simulated and compared with the experimental results.

Table 5.7: Mix of reactive concrete (kg/m^3)

| Item | Water | Cement | Coarse aggregate | Sand | Water reducer | Air entraining agen |
|----------------------------------|-------|--------|------------------|------|---------------|---------------------|
| Concrete mix by Fan et al. 1998 | 191 | 405 | 960 | 742 | 2.38 | 0.298 |
| Concrete mix by Asai et al. 2009 | 175 | 389 | 980 | 728 | -- | -- |

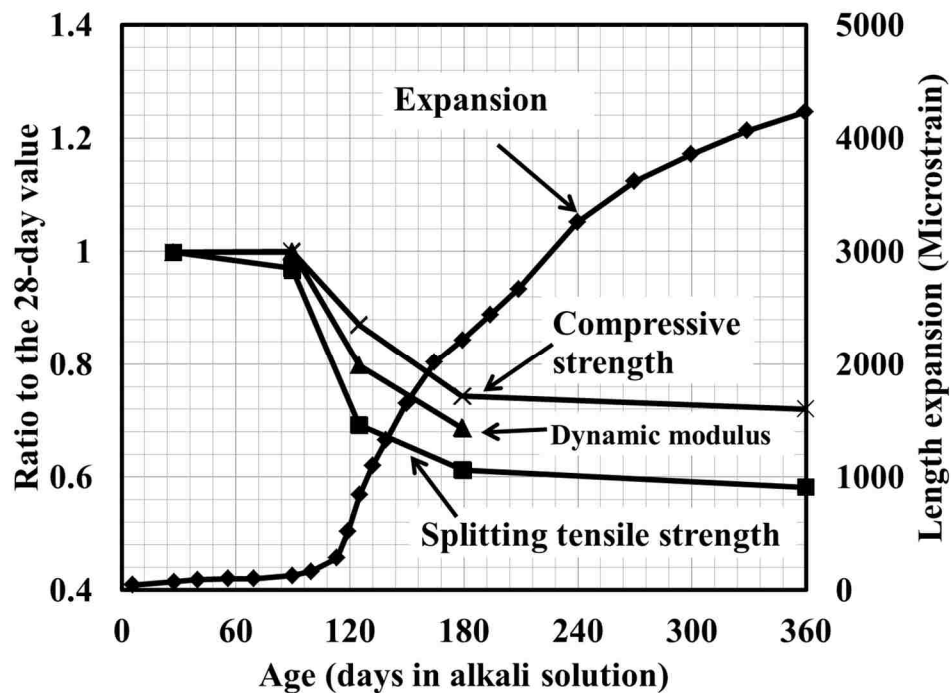


Figure 5.22: Experimental results presented by Fan et al. (1998)

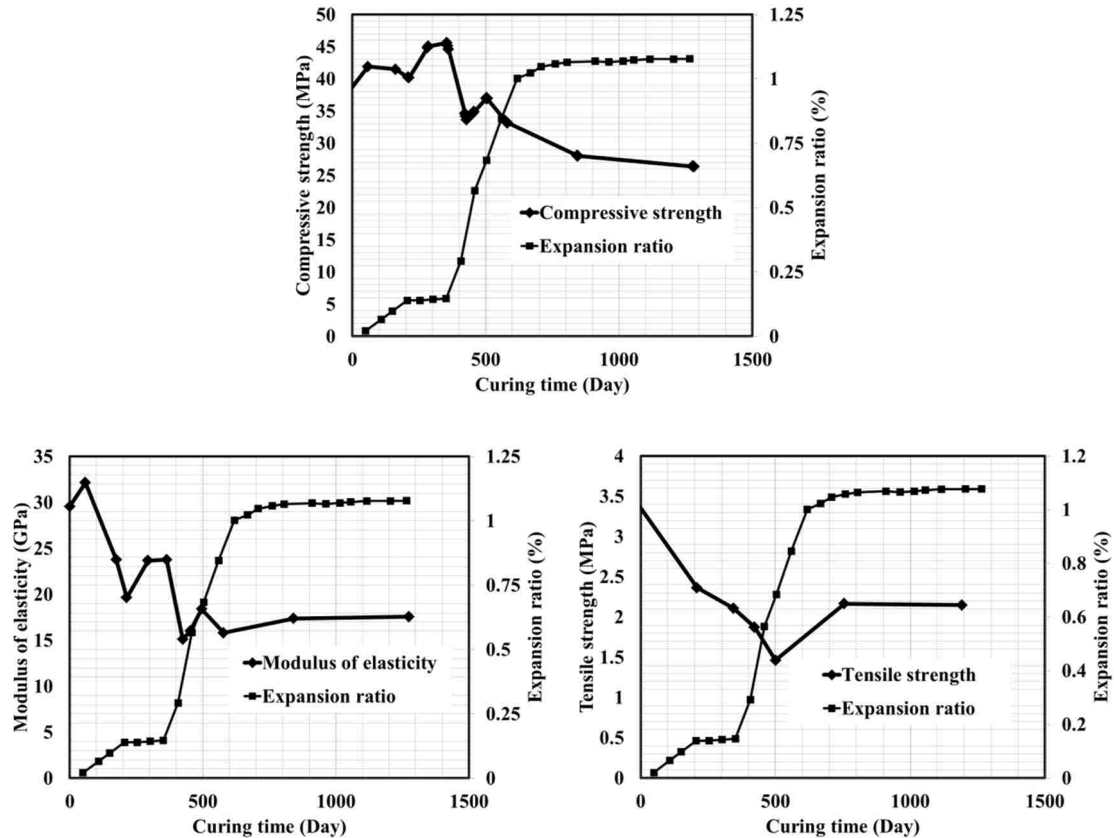


Figure 5.23: Experimental results from Asai et al. (2009)

5.3.4. Results and discussion

Based on the concrete mixes given, cement hydration is simulated by HYMOSTRUC[®] (van Breugel 1995a & 1995b). For concrete mix by Fan et al. (1998), the modulus of elasticity of cement paste at age of 28 days, 127 days (ASR expansion ratio 0.10%) and 180 days (ASR expansion ratio 0.21%) are generated as 10.0 GPa, 12.0 GPa and 13.0 GPa, respectively. For concrete mix by Asai et al. (2009), the modulus of elasticity of cement paste at age of 28 days, 150 days (ASR expansion ratio 0.10%) and 450 days (ASR expansion ratio 0.21%) are generated as 10.5 GPa, 12.3 GPa and 13.1 GPa, respectively. Then ITZ properties are determined through homogenization model of concrete, by matching the generated stress-strain curve to target stress-strain curve

defined as Equation (5.11). The stress-strain curve from RVE and the determined ITZ properties are shown in Figures 5.24 & 5.25. Constitutive models attained from RVE are shown in Figures 5.26 & 5.27.

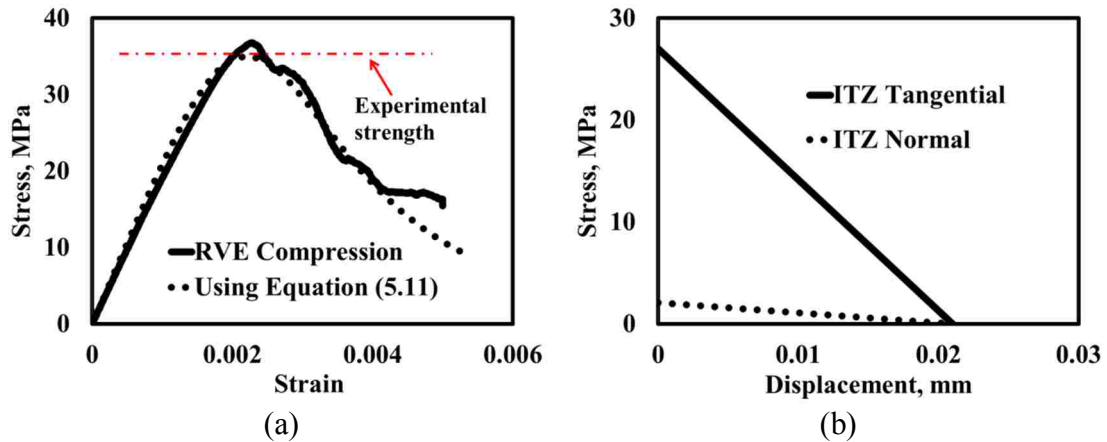


Figure 5.24: (a) Stress-strain curve of concrete and (b) ITZ properties determined for concrete mix by Fan et al. (1998)

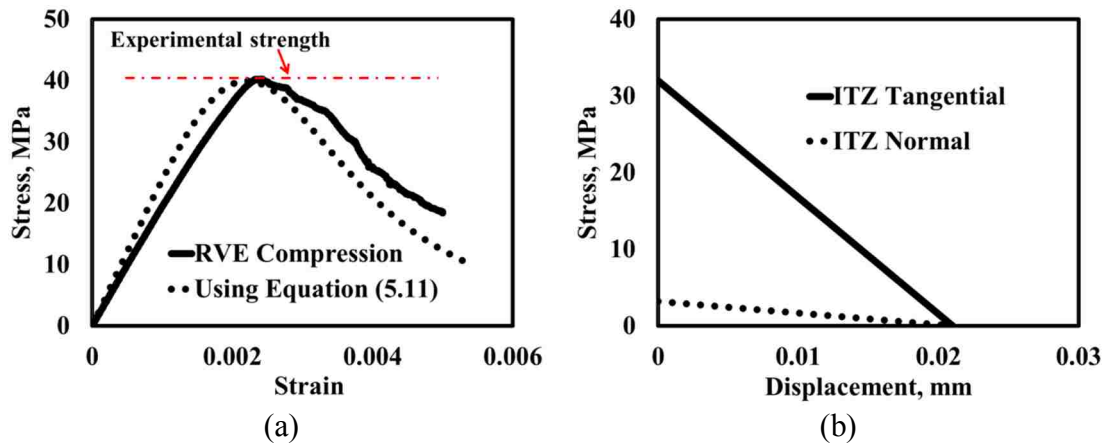


Figure 5.25: (a) Stress-strain curve of concrete and (b) ITZ properties determined for concrete mix by Asai et al. (2009)

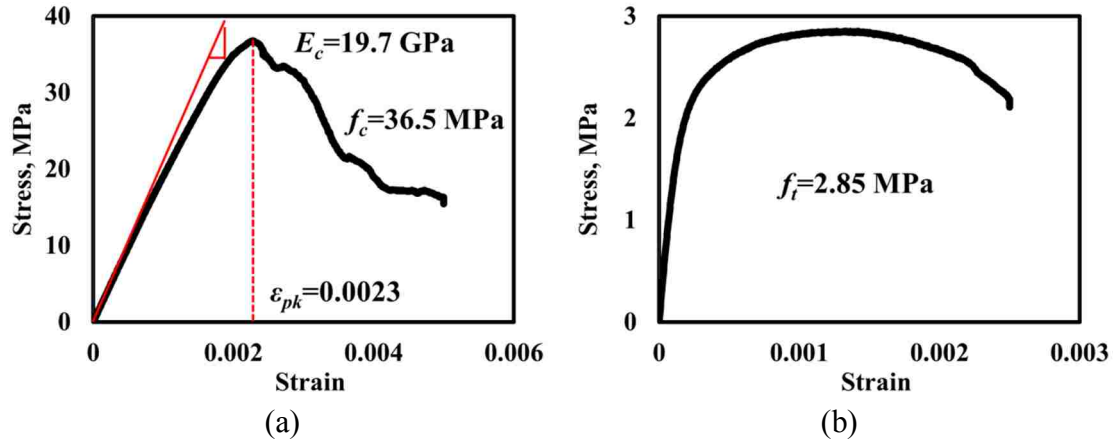


Figure 5.26: Constitutive models extracted from RVE for concrete mix by Fan et al. (1998) (a) compression; (b) tension

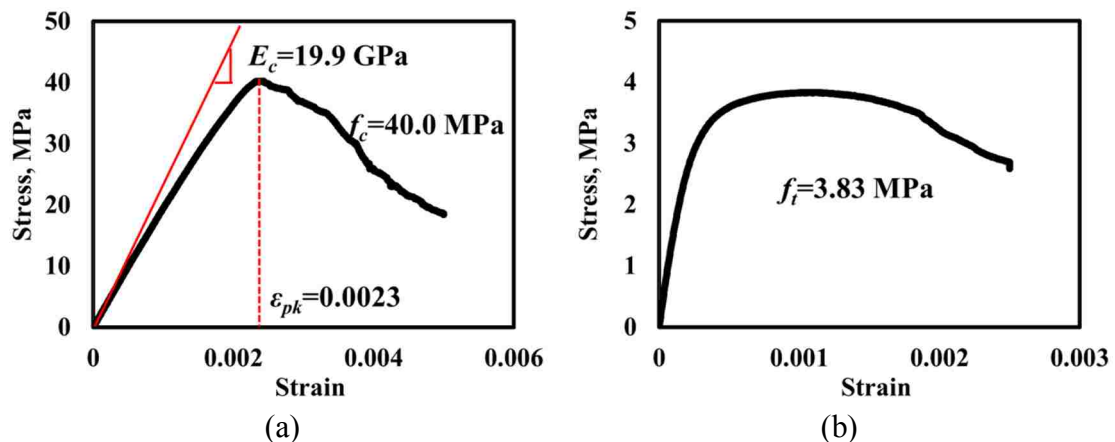


Figure 5.27: Constitutive models extracted from RVE for concrete mix by Asai et al. (2009) (a) compression; (b) tension

In simulation, aggregate elements were applied by expansion to achieve the target macro expansion ratio. Then the expanded RVE is applied by tension and compression displacement to extract the constitutive models in tension and compression, respectively. Figures 5.28, 5.29, 5.31 & 5.32 shows the generated stress-strain curves without ASR, with ASR and constant ITZ, with ASR and ITZ changed proportionally to the ratio of cement paste modulus of elasticity at age of 28 days and at age when ASR expansion ratio is 0.10% or 0.21%. The changed ITZ properties are shown in Figures 5.30 & 5.33.

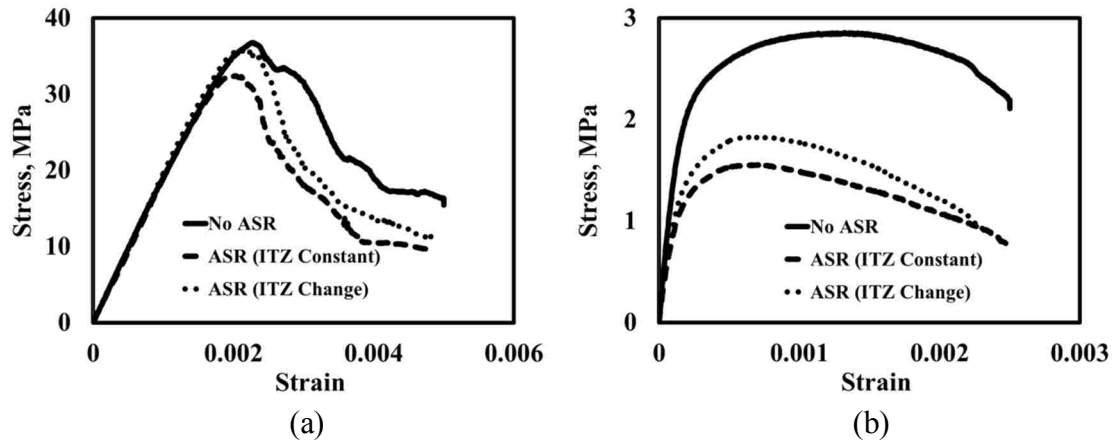


Figure 5.28: Stress-strain curve generated from RVE for concrete mix by Fan et al. (1998); (a) Compression; (b) Tension (ASR expansion ratio 0.10%)

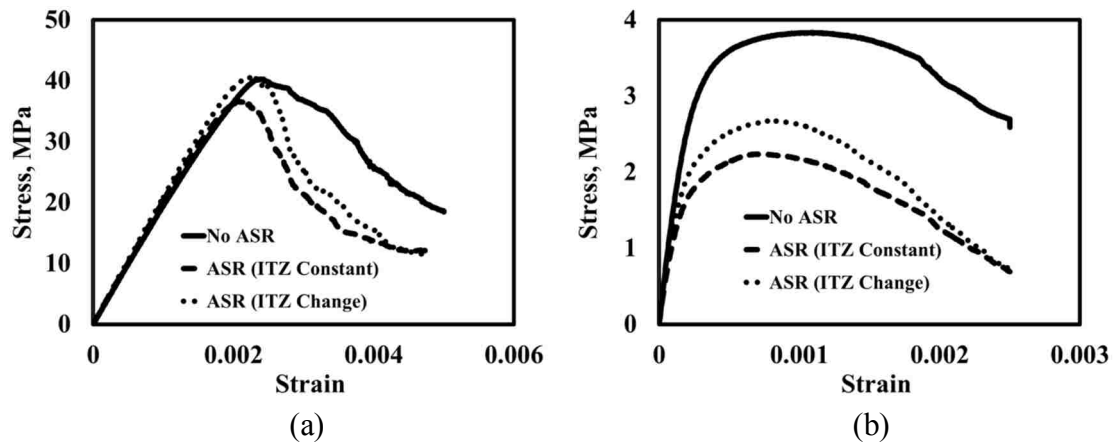


Figure 5.29: Stress-strain curve generated from RVE for concrete mix by Asai et al. (2009); (a) Compression; (b) Tension (ASR expansion ratio 0.10%)

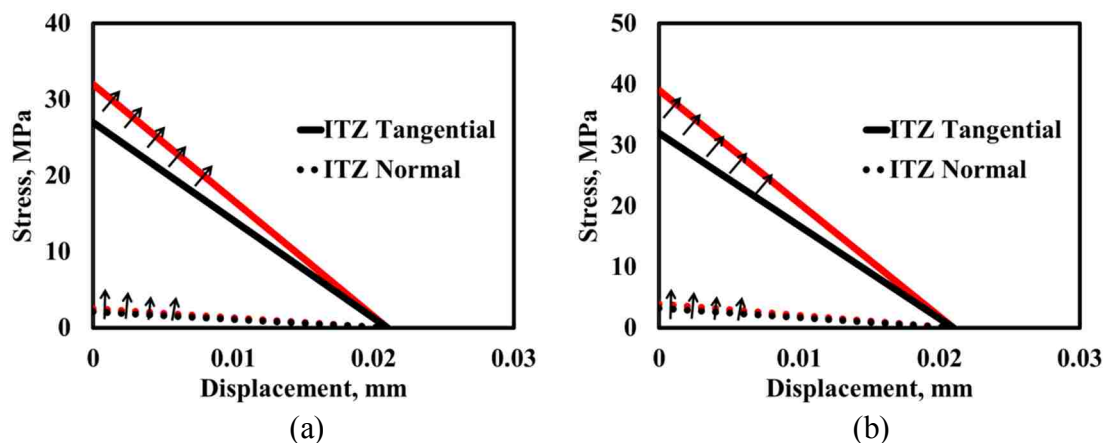


Figure 5.30: Change of ITZ properties used in (a) Concrete mix by Fan et al. (1998); (b) Concrete mix by Asai et al. (2009) (ASR expansion ratio 0.10%)

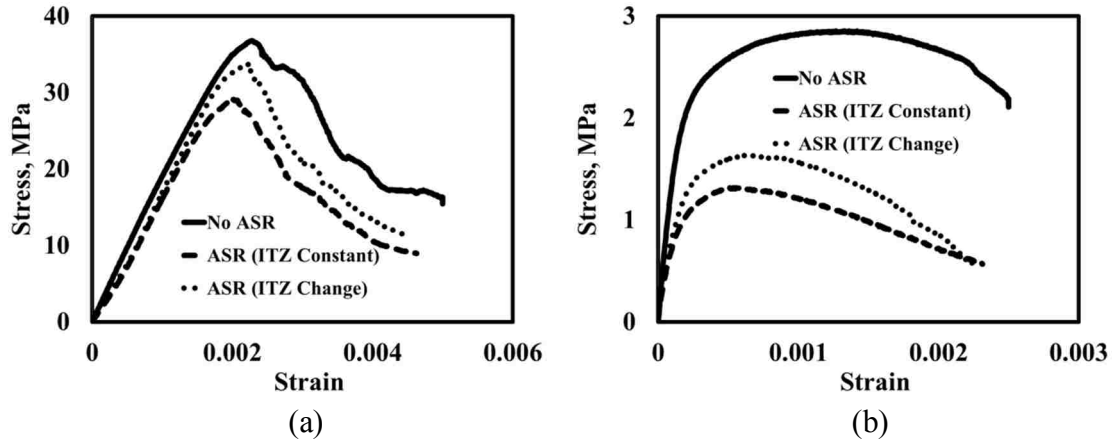


Figure 5.31: Stress-strain curve generated from RVE for concrete mix by Fan et al. (1998); (a) Compression; (b) Tension (ASR expansion ratio 0.21%)

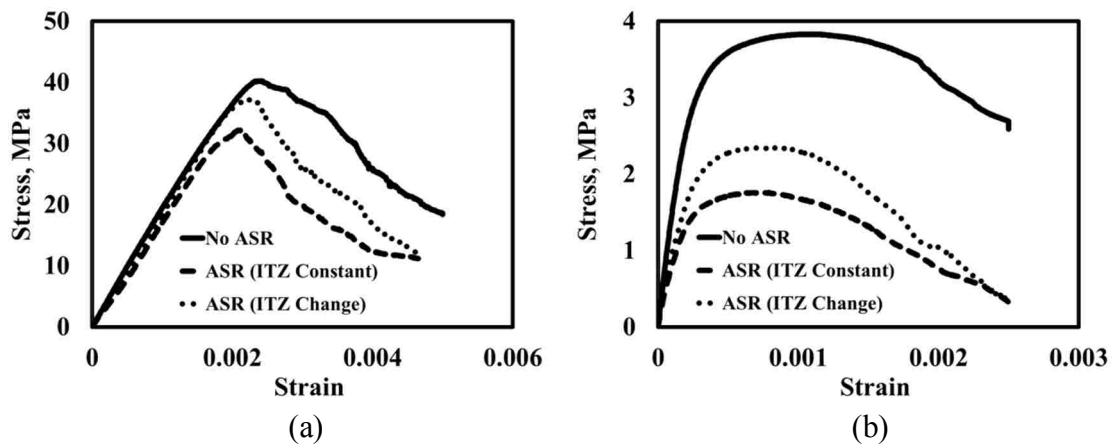


Figure 5.32: Stress-strain curve generated from RVE for concrete mix by Asai et al. (2009); (a) Compression; (b) Tension (ASR expansion ratio 0.21%)

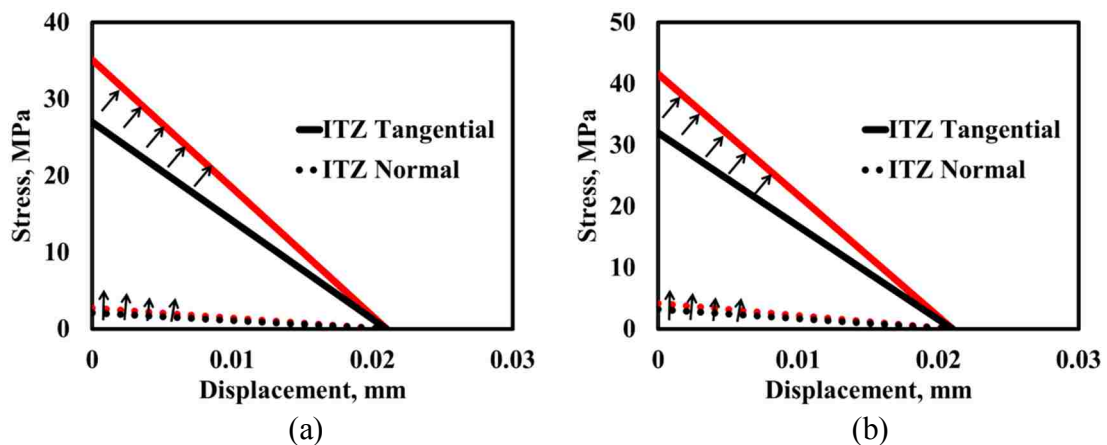


Figure 5.33: Change of ITZ properties used in (a) Concrete mix by Fan et al. (1998); (b) Concrete mix by Asai et al. (2009) (ASR expansion ratio 0.21%)

The simulated results are compared with experimental results in Figure 5.34.

Simulated results are in good agreement with experiment.

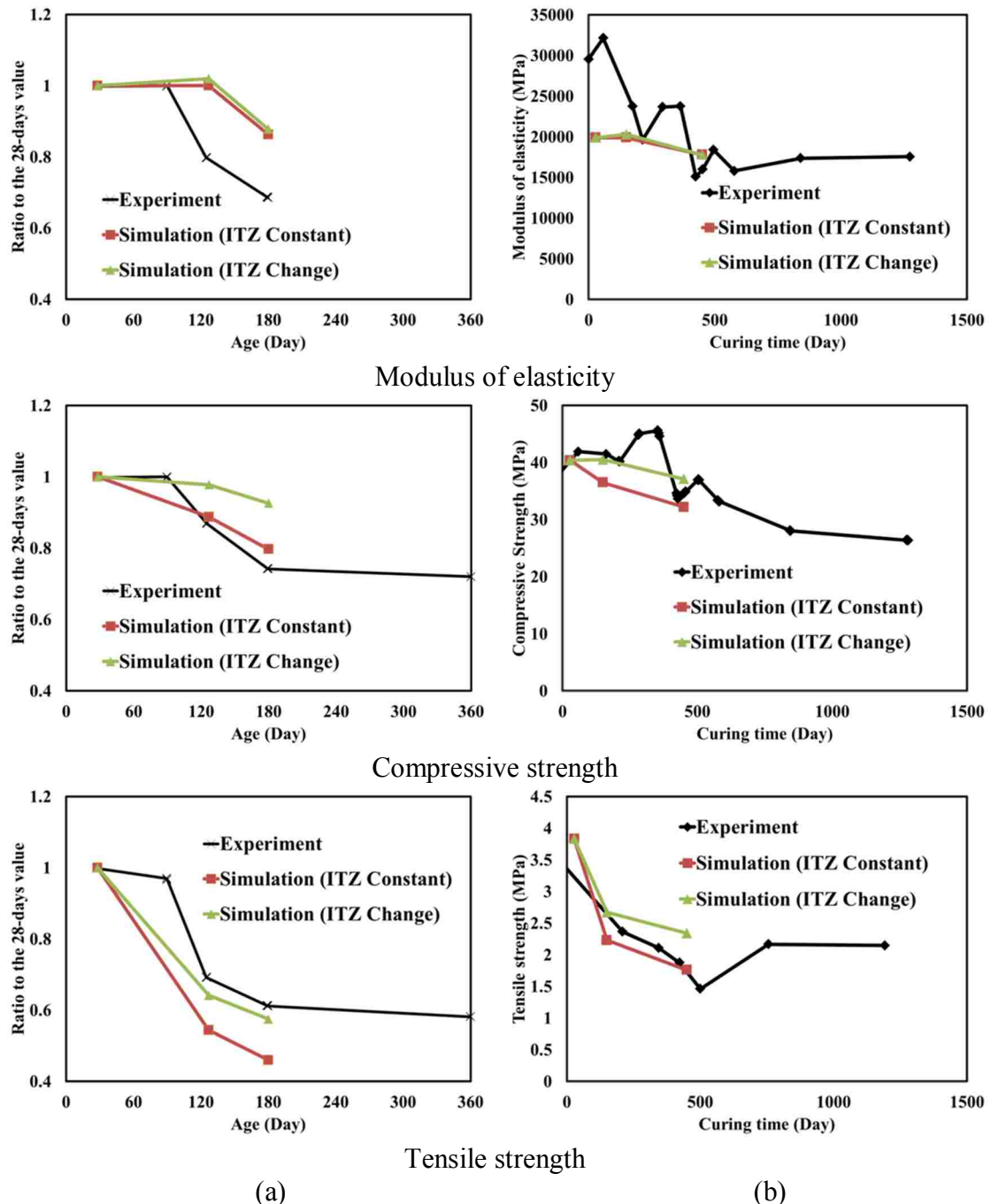


Figure 5.34: Simulated and experimental results (a) Concrete mix by Fan et al. (1998); (b) Concrete mix by Asai et al. (2009)

Actually, the experimental results scatter in a wide range. For example, in Asai et al (2009) experiments, when ASR expansion ratio is 0.21%, the test results of compressive strength range from 20 MPa to 50 MPa while the average value is 39 MPa, and the test results of modulus of elasticity range from 10 GPa to 30 GPa while the average value is 21 GPa. den Uijl & Kaptijn (2002) reported that, for drilled cylinder from structure, the tensile strength range from 0.84 MPa to 1.61 MPa, and cube compressive strength ranges from 50.4 MPa to 60.6 MPa. The scattered test results can be partially attributed to the uncertainty of concrete microstructure. It is important to emphasize that, ASR in concrete is not uniform, which exacerbates the uncertainty of mechanical properties of concrete subjected to ASR.

Cracking pattern of concrete can be changed by ASR expansion, which is demonstrated by the numerical model. As shown in Figures 5.35 & 5.36, because aggregate expansion damages ITZ, the failure modes of concrete subjected to compression or tension are different compared with concrete without ASR. For each simulation with different model parameters, the cracking pattern in RVE varies, as shown in Figures 5.35(b) & (c). Moreover, different ASR expansion ratio can bring out different cracking patterns at failure, as shown in Figure 5.37.

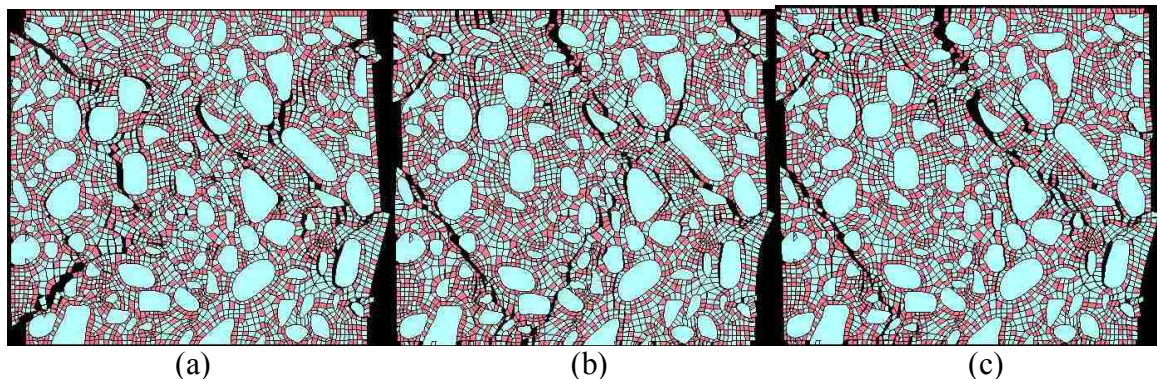


Figure 5.35: Cracking pattern in compression at failure (Scale factor 5.0); (a) without ASR; (b) ASR-ITZ constant; (c) ASR-ITZ change for concrete mix by Fan et al. (1998)

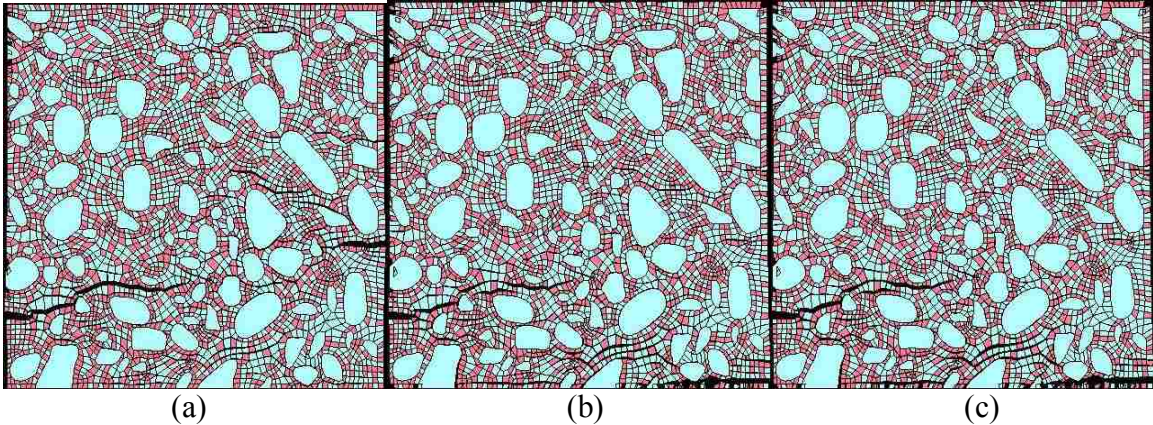


Figure 5.36: Cracking pattern in tension at failure (Scale factor 10.0); (a) without ASR; (b) ASR-ITZ constant; (c) ASR-ITZ change for concrete mix by Fan et al. (1998)

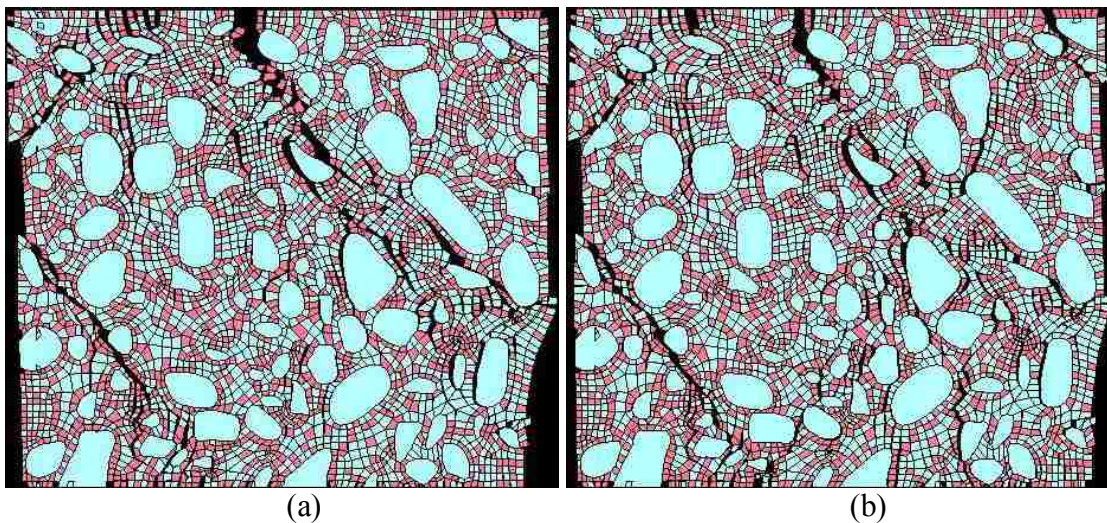


Figure 5.37: Cracking patterns at failure in compression for concrete mix by Fan et al. (1998) (ITZ constant, scale factor 5.0) (a) ASR expansion ratio 0.10%; (b) ASR expansion ratio 0.21%

The proposed homogenization model of concrete, to some extent, captures the deterioration mechanism of concrete due to ASR, that is, swelling of ASR gel will damage ITZ and detach particles in concrete. However, some challenges concerning ASR simulation are remain unresolved, such as stress relaxation during ASR expansion, anisotropy of ASR expansion, effects from prestress and reinforcement, etc.

Nevertheless, the proposed model shall enable predicting serviceability of RC structures subjected to ASR.

5.3.5. Conclusions

In this dissertation, a homogenization approach for modeling of concrete is presented and applied to simulate ASR mechanical consequences in concrete. The simulated results of the proposed microstructural homogenization model are in good agreement with the experimental observations reported in the literature. There is obviously a good potential of homogenization method to model concrete serviceability.

Chapter 6. Conclusions and Future Works

6.1. Conclusions

This dissertation aims to link the mechanical performance of macrostructure with microstructure. In continuum mechanics, scale separation principle is assumed to be satisfied and this assumption tends to get researchers to forget that composite material is an actual structure. Homogenization is used to rescue the information lost due to the continuum assumption. Facing the difficulty to improve homogenization technique per se, an idea is presented here that material can be treated as discrete particles connected by contact and cohesive elements. Concrete is modeled by this concept. The different mechanical behavior of concrete in tension and compression can be realized by consistent parameters.

To investigate concrete from nanoscale, chemical reaction is unavoidable, For cement and concrete, whose microstructure is time-related due to cement hydration, shrinkage, and potential durability reaction such as alkali-silica reaction (ASR). Combining the chemical models of cement hydration and ASR reported by other researchers with the mechanical models proposed in this dissertation, concrete serviceability is studied. Investigating the different methods to establish this modeling environment, the following conclusions can be drawn.

- Homogenization model of cement paste is established with the help of a 3D cement hydration and microstructure development modeling package CEMHYD3D (Bentz 2005) or HYMOSTRUC® (van Breugel 1995a & 1995b). Cement paste is modeled from microstructure by considering cement

type, particle size distribution, hydration and curing conditions. At certain hydration age, compressive strength, modulus of elasticity and stress-strain curve of cement paste can be attained.

- Nanoindentation tests on cement paste with different percentage of nanosilica are carried out to validate the proposed homogenization model of cement paste. The simulated results are in good agreement with experiment and upscaled as inputs for concrete RVE model.
- Concrete serviceability is studied by using a proposed concrete homogenization model. In this model, aggregate is denoted by circles dispersed randomly in cement matrix. ITZ is introduced to connect cement paste and aggregate particles. From RVE, stress-strain curve of concrete is generated to predict the deflection of a beam. Probabilistic analysis is used to describe uncertainty in beam serviceability.
- An enhanced concrete homogenization model is proposed. In this model, concrete RVE is built on the basis of the realistic concrete section image of a cylinder. Concrete is assumed to be composed of discrete particles linked by ITZ, in which contact and cracking mechanisms are included to simulate the particle interaction. While mechanical properties of cement paste are determined by cement paste homogenization model and mechanical properties of aggregate are found in the literature, properties of ITZ are derived by matching the stress-strain curve generated from RVE to a target one. The simulated results are validated by experimental results published by others.

- The enhanced concrete homogenization model is used to estimate uncertainty in concrete deflection. Assuming bond strength of ITZ is independent of the modulus of elasticity of cement paste, variations of the modulus of elasticity of cement paste, variations of tangential and normal debonding strength of ITZ are considered to get the uncertainties in concrete properties, such as compressive strength, tensile strength and modulus of elasticity. These simulated properties of concrete are used to predict the mid-span deflection of a RC beam. The uncertainty predicted from the homogenization model is in good agreement with test results.
- In order to study uncertainties rooted in the random microstructure of concrete, a method named by cell operation to generate concrete RVE sharing the similar topological information with target one is proposed. Realizing that microstructure of material is specified by the intrinsic rule to generate it rather than by low-order correlation functions, this method (re)constructs material by assuming rules to generate microstructure. Low-order correlation functions such as two-point correlation function are used to check results and optimize parameters. This method includes two steps:
 - To generate irregular shape aggregate in concrete RVE. It is believed that information of particle with irregular shape is included in each cell and can be reproduced by operating this cell. This hypothesis is verified by calculating the two-point correlation function, which is a necessary but not sufficient condition to specify image.

- To disperse generated aggregate particles randomly into cement matrix based on volume fraction, aggregate particle size distribution and distances between aggregate particles.

The similarity between reconstructed concrete RVE and realistic concrete image is checked by low-order correlation functions.

- ASR in concrete is simulated by using the enhanced concrete homogenization model. ASR-induced macro expansion ratio is selected as the controlling parameter to bridge the mechanical consequences and chemical reaction of ASR. ASR expansion is achieved by the swelling of reactive aggregate elements. This is simulated by thermal expansion of aggregate particles. Elements expansion damages ITZ and hence the microstructure of concrete. Simulated results demonstrate that the cracking mode is changed by ASR expansion. The predicted mechanical properties of concrete are in good agreement with experimental results.

6.2. Future works

There are works still need to be done in future.

- Homogenization technique. Due to the complicated nonlinear mechanisms adopted in concrete RVE, homogenization technique used here is simple and intuitive, which means there is information lost during the transportation of information from microscale to macroscale. Homogenization technique which can handle complicated nonlinear case with reasonable computational cost needs to be developed.

- Contact and debonding mechanisms and their numerical implementation. In the discrete homogenization model of concrete, contact and debonding mechanisms play the key role in the RVE model. For large deformation (ASR expansion ratio $\geq 0.4\%$), the proposed contact and debonding methods might cause convergence problem. Numerical technique of ITZ needs to be improved.
- Creep and shrinkage shall be considered. Creep can be considered by particles movement in RVE and thereafter stress relaxation. The way to simulate shrinkage is to introduce water elements in RVE; with the drying process, compression stress and shrinkage will be induced. Stress relaxation also needs to be considered to achieve realistic shrinkage modeling.
- Interaction of ASR expansion with confinement from reinforcement and prestress. ASR is simulated by expanding aggregate particles. However, interaction of ASR expansion and confinement from reinforcement and prestress is a challenge. For reinforced concrete, it might be reasonable to include reinforcement in concrete RVE to consider this effect. For large bulk plain concrete, its self-weight shall be considered as prestress in RVE.
- Stress relaxation during ASR expansion shall be considered. In the proposed model of concrete subjected to ASR, stress relaxation is neglected. However, it is believed that stress relaxation will happen. In future, stress relaxation mechanism shall be modeled.
- So far, the chemical mechanism of ASR is not clear. To improve this proposed homogenization modeling of concrete, it is necessary to investigate

material microstructure further and understand the chemical reaction of cement hydration and ASR.

- Strain rate dependent homogenization is also a challenge. For concrete under impact load, strain rate shall be considered. This could be achieved by explicit finite element simulation. The RVE models developed here are based on static loading and elasticity principle. These assumptions will change to model concrete under impact or blast.

REFERENCES

- ACI Committee 318 (2008). Building Code Requirements for Structural Concrete (318-08) and commentary (318R-08). American Concrete Institute, Farmington Hills, USA.
- Ahmed, T., Burley, E., & Rigden, S. (1999). Effect of alkali-silica reaction on bearing capacity of plain and reinforced concrete. ACI Structural Journal, Vol. 96, No. 4, 557-570.
- Aïtcin, P.-C. (1998). High performance concrete. E and FN Spon, London, UK.
- Alfano, G., & Crisfield, M.A. (2001). Finite element interface models for the delamination analysis of laminated composites: Mechanical and computational issues. International Journal for Numerical Methods in Engineering, Vol. 50, 1701-1736.
- Allair, G. (2001). Shape Optimization by the Homogenization Method, Springer.
- Ang, A.H.-S., & Tang, W. H. (2006). Probability Concepts in Engineering: Emphasis on Applications to Civil and Environmental Engineering, Hoboken, NJ,: Willey.
- ANSYS (2007). Anslys Reference Manual (Version 10.0). Available via <http://www.ansys.com/>.
- Asai, H., Maeno, H., Morishita, N., & Nakamura H. (2009). Study on creep of PC beam damaged by ASR. Creep, Shrinkage, and Durability Mechanics of Concrete and Concrete Structures - Tanabe et al. (eds.), Taylor & Francis Group, London, ISBN 978-0-415-48508-1, 1147-1153.
- ASTM C 1260-05, (2005). Standard test method for potential alkali reactivity of aggregate (Mortar-Bar Method). Annual Book of Standards, ASTM International, West Conshohocken, Pennsylvania.
- ASTM C 1293-05, (2005). Standard test method for determination of length change of concrete due to alkali-silica reaction. Annual Book of Standards, ASTM International, West Conshohocken, Pennsylvania.
- Bangert, F., Kuhl, D., & Meschke, G. (2004). Chemo-hygro-mechanical modelling and numerical simulation of concrete deterioration caused by alkali-silica reaction. International Journal for Numerical and Analytical Methods in Geomechanics, Vol. 28, 689-714.
- Barnes, P. (1983). Structure and Performance of Cements, Applied Science Publishers, London, UK and New York.

- Bažant, Z. P., & Oh, B.-H. (1985). Microplane model for progressive fracture of Concrete and Rock. Journal of Engineering Mechanics, Vol. 111, 559-582.
- Bažant, Z. P., & Steffens, A. (2000). Mathematical model for kinetics of alkali-silica reaction in concrete. Cement and Concrete Research, Vol. 30, 419-428.
- Bazant, Z. P., Caner, F. C., Cedolin, L., Cusatis, G. & Di Luzio, G. (2004). Fracturing material models based on micromechanical concepts: Recent advances. Fracture Mechanics of Concrete Structures (Proc., FraMCoS-5, 5th Int. Conf. on Fracture Mech. of Concrete and Concr. Structures, Vail, Colo.), Vol. 1, V.C. Li, K.Y. Leung, Willam, K.J., and Billington, S.L., eds., IA-FraMCoS, 83-90.
- Bear, J. & Bachmat, Y. (1990). Introduction to the modelling of transport phenomena in porous media. Kluwer Academic, Dordrecht, Netherlands.
- Bentz, D. P. (1997). Three-dimensional computer simulation of Portland cement hydration and microstructure development. Journal of the American Ceramic Society, Vol. 80, No. 1, 3-21.
- Bentz, D. P. (2005). CEMHYD3D: A three-dimensional cement hydration and microstructure development modeling Package (Version 3.0). National Institute of Standards and Technology, NISTIR 7232.
- Bentz, D. P., Jensen, O. M., Coats, A. M., & Glasser, F. P. (2000). Influence of silica fume on diffusivity in cement-based materials I. Experimental and computer modelling studies on cement pastes. Cement and Concrete Research, Vol. 30, No. 6, 953-962.
- Berdichevsky, V. L. (2007). Entropy of microstructure. Journal of the Mechanics and Physics of Solids, doi:10.1016/j.jmps.2007.07.004
- Böhlke, T., Jöchen, K., Kraft, O., Löhe, D., & Schulze, V. (2010). Elastic properties of polycrystalline microcomponents. Mechanics of Material, Vol. 42, 11-23.
- Broadhouse., B. J. (1995). The Winfrith concrete model in LS-DYNA3D. Report: SPD/D(95)363. Structural Performance Department, AEA Teleology. Winfrith Technology Centre: U.K.
- Canadian Standard Association, (2000). Canadian Highway Bridge Design Code. CHBDC. CAN/CSA-S6-00, Canada.
- Chang, C. S., Wang, T. K., Sluys, L. J., & van Mier, J. G. M. (2002). Fracture modeling using a micro-structural mechanics approach—I. Theory and formulation. Engineering Fracture Mechanics Vol. 69, 1941-1958.
- Chang, T. S. & Kesler, C. E. (1958). Static and fatigue strength in shear of beams with tensile reinforcement. ACI Journal, Vol. 54, Issue 6, 1033-1057.

- Chen, J., & Bull, S. J. (2006). On the relationship between plastic zone radius and maximum depth during nanoindentation. Surface & Coatings Technology, Vol. 201, 4289-4293.
- Choi, B.-S., Scanlon, A., & Johnson, A. P. (2004). Monte Carlo simulation of immediate and time-dependent deflections of reinforced concrete beams and slabs. ACI Structural Journal, Vol. 101, 633-641.
- Christiansen, K. (1988). Eight-year deformation tests on reinforced concrete beams. Materials and Structures (RILEM), Vol. 21, 172-178.
- Comby-Peyrot, I., Bernard, F., Bouchard, P.-O., Bay, F., & Garcia-Diaz, E. (2009). Development and validation of a 3D computational tool to describe concrete behaviour at mesoscale. Application to the alkali-silica reaction. Computational Materials Science, Vol. 46, 1163-1177.
- Constantinides, G., & Ulm, F.-J. (2003). On the use of nanoindentation for cementitious material. Materials and Structures, Vol. 36, No. 257, 191-196.
- Constantinides, G., & Ulm, F.-J. (2004). The effect of two types of C-S-H on the elasticity of cement-based materials: Results from nanoindentation and micromechanical and modeling. Cement and Concrete Research, Vol. 34, 67-80.
- Constantinides, G., & Ulm, F.-J. (2007). The nanogranular nature of C-S-H. Journal of the Mechanics and Physics of Solids, Vol. 55, 64-90.
- Cusatis, G. & Cedolin, L. (2007). Two-scale study of concrete fracturing behavior. Engineering Fracture Mechanics, Vol. 74, 3-17.
- Cusatis, G., Bazănt, Z. P., & Cedolin, L. (2003a). Confinement-shear lattice model for concrete damage in tension and compression: I. Theory. Journal of engineering Mechanics, Vol. 129, No. 12, 1439-1448.
- Cusatis, G., Bazănt, Z. P., & Cedolin, L. (2003b). Confinement-shear lattice Model for concrete damage in tension and compression: II. Computation and validation. Journal of engineering Mechanics, Vol. 129, No. 12, 1449-1458.
- Cusatis, G., Beghini, A., & Bazănt, Z. P. (2008a). Spectral stiffness microplane model for quasibrittle composite laminates-Part I: Theory. Journal of Applied Mechanics, Vol. 75, 021009-1
- Cusatis, G., Beghini, A., & Bazănt, Z. P. (2008b). Spectral stiffness microplane model for quasibrittle composite laminates— Part II: Calibration and validation. Journal of Applied Mechanics, Vol. 75, 021010-1
- Cusatis, G., Di Luzio, G. & Cedolin, L. (2011). Meso-scale simulation of concrete: blast and penetration effects and AAR degradation. Applied Mechanics and Materials, Vol. 82, 75-80.

- den Uijl, J. A., & Kaptijn, N. (2002). Structural consequences of ASR: An example on shear capacity. Heron, Vol. 47, Issue 2, 125-139.
- Doerner, M. F. & Nix, W. D. (1986). A method for interpreting the data from depth-sensing indentation instruments. Journal of Materials Research, Vol. 1, No. 4, 601-609.
- Dormieux, L., Kondo, D., & Ulm, F.-J. (2006). Microporo mechanics. John Wiley & Sons, Chichester, England.
- Fan, R., Yuan, Z., & Fish, J. (2010). Adaptive two-scale nonlinear homogenization. International Journal for Computational Methods in Engineering Science and Mechanics, Vol. 11, 27-36.
- Feyel, F. (2003). A multilevel finite element method (FE²) to describe the response of highly non-linear structure using generalized continua. Computer Methods in Applied Mechanics and Engineering, Vol. 192, 3233-3244.
- Fischer-Cripps, A. C. (2004). Nanoindentation. Springer.
- Fish J., & Shek, K. L. (2000). Multiscale analysis for composite materials and structures. Composites Science and Technology: An International Journal, Vol. 60, 2547-2556.
- Fish J., Shek K., Pandheeradi, M., & Shephard M. S. (1997). Computational plasticity for composite structures based on mathematical homogenization: Theory and practice. Computer Methods in Applied Mechanics and Engineering, Vol. 148, 53-73.
- Fish, J., & Chen, W. (2001). Higher-order homogenization of initial/boundary-value problem. Journal of Engineering Mechanics, Vol. 127, No. 12, 1223-1230.
- Fling, R. S. (1992). Practical considerations in computing deflection of reinforced concrete. ACI Special Publication, Vol. 133, 69-91.
- Ghali, A., Elbadry, M., & Megally, S. (2000). Two-year deflections of the confederation bridge. Canadian Journal of Civil Engineering, 27 (6), 1139-1149.
- Grimal, E., Sellier, A., Multon, S., Le Pape, Y., & Bourdarot, E. (2010). Concrete modelling for expertise of structures affected by alkali aggregate reaction. Cement and Concrete Research, Vol. 40, 502-507.
- Guedes, J. M., & Kikuchi, N. (1990). Preprocessing and postprocessing for materials based on the homogenization method with adaptive finite element methods. Computer Methods in Applied Mechanics and Engineering, Vol. 83, Issue 2, 143-198.
- Guo, L.-P., Carpinteri, A., Roncella, R., Spagnoli, A., Sun, W., & Vantadori, S. (2009). Fatigue damage of high performance concrete through a 2D mesoscopic lattice model. Computational Materials Science, Vol. 44, 1098-1106.

- Haecker, C.-J., Garboczi, E. J., Bullard, J. W., Bohn, R. B., Sun, Z., Shah, S. P., & Voigt, T. (2005). Modeling the linear elastic properties of Portland cement paste. Cement and Concrete Research, Vol. 35, 1948-1960.
- Häfner, S., Eckardt, S., Luther T., & Könke C. (2006). Mesoscale modelling of concrete: geometry and numerics. Computers and Structures Vol. 84, 450-46.
- Hall, P. L., & Strutt, J. E. (2003). Probabilistic physics-of-failure models for component reliabilities using Monte Carlo simulation and Weibull analysis: A parametric study. Reliability Engineering and System Safety, 80(3), 233-242.
- Hashin, Z. (1983). Analysis of composite material-A survey. Journal of Applied Mechanics, Vol. 50, 481-505.
- Hashin, Z., & Shtrikman, S. (1962). On some variational principles in anisotropic and non-homogeneous elasticity. Journal of the Mechanics and Physics of Solids, Vol. 10, 335-342.
- Hashin, Z., & Shtrikman, S. (1963). A variational approach to the theory of elastic behavior of multiphase materials. Journal of the Mechanics and Physics of Solids, Vol. 11, 127-140.
- Heijnen, W. M. M., & Larbi, J. A. (1999). Preventive measures against concrete damage to ASR in the Netherlands current state-of-affairs. HERON, Vol. 44, No. 4, 285-298.
- Hill, R. (1956). Surveys in mechanics: The G.I. Taylor 70th anniversary volume. Cambridge University Press, 7-31.
- Hill, R. (1963). Elastic properties of reinforced solids: Some theoretical principles. Journal of the Mechanics and Physics of Solids, 11(5), 357-372.
- Hollister, S. J., & Kikuchi, N. (1992). A comparison of homogenization and standard mechanics analyses for periodic porous composites. Computational Mechanics, Vol. 10, Issue 2, 73-95.
- Huang, Y.-J., Shen, J., Sun, Y., & Sun, J.-F. (2010). Indentation size effect of hardness of metallic glasses. Materials and Design, Vol. 31, 1563-1566.
- Ideker, J. H., East, B. L., Folliard, K. J., Thomas, M. D. A., & Fournier, B. (2010). The current state of the accelerated concrete prism test. Cement and Concrete Research, Vol. 40, 550-555.
- Jansson, S. (1992). Homogenized nonlinear constitutive properties and local stress concentrations for composites with periodic internal structure. International Journal of Solids Structures, Vol. 29, No. 17, 2181-2200.

- Jiang, M., Ostoja-Starzewski, M., & Jasiuk, I. (2001). Scale-dependent bounds on effective elastoplastic response of random composites. Journal of the Mechanics and Physics of Solids, 49, 655-673.
- Jiao, Y., Stillinger, F. H., & Torquato, S. (2007). Modeling heterogeneous materials via two-point correlation functions: Basic principles. Physical Review, E 76, 031110.
- Jiao, Y., Stillinger, F. H., & Torquato, S. (2008). Modeling heterogeneous materials via two-point correlation functions. II. Algorithmic details and applications. Physical Review, E 77, 031135.
- Ju, J. W., & Chen, T. M. (1994). Effective elastic moduli of two-phase composites containing randomly dispersed spherical inhomogeneities. Acta Mechanica, Vol. 103, 123-144.
- Kaczmarczyk, L., Pearce, C. J., & Bicanic, N. (2008). Scale transition and enforcement of RVE boundary conditions in second-order computational homogenization. International Journal For Numerical Methods in Engineering, 74, 506-522
- Kalidindi, S. R., & Pathak, S. (2008). Determination of the effective zero-point and the extraction of spherical nanoindentation stress-strain curves. Acta Materials, Vol. 56, 3523-3532.
- Kanit, T., Forest, S., Galliet, I., Mounoury, V., & Jeulin, D. (2003). Determination of the size of the representative volume element for random composites: statistical and numerical approach. International Journal of Solids and Structures, 40, pp. 3647–3679.
- Khisaeva, Z. F., & Ostoja-Starzewskib, M. (2006). On the size of RVE in finite Elasticity of random composites. Journal of Elasticity, Vol. 85, 153-173.
- Kim, J. J., & Reda Taha, M. M. (2009). Robustness-to-uncertainty: An alternative perspective in realizing uncertainty in modeling deflection of reinforced concrete structures. Journal of Structural Engineering (ASCE), 135(8), 998-1001.
- Kim, J. J., Fan, T., & Reda Taha, M. M. (2009). Examining uncertainty in deflection of reinforced concrete beams using concrete homogenization techniques. 1st Computational Design and Engineering (CODE): Seoul, Korea. CD-ROM.
- Kim, S. M., Rashid K., & Abu Al-Rub, R. K. (2011). Meso-scale computational modeling of the plastic-damage response of cementitious composites. Cement and Concrete Research, Vol. 41, 339-358.
- Kouznetsova, V. G., Geers, M. G. D., & Brekelmans, W. A. M. (2004). Multi-scale second-order computational homogenization of multi-phase materials: A nested finite element solution strategy. Computer Methods in Applied Mechanics and Engineering, Vol. 193, 5525-5550.

- Kurukuri, S. (2005). Homogenization of damaged concrete meso-structure using representative volume elements: Implementation and application to Slang. M.S. Thesis, University Weimar, Germany.
- Le Pape, Y., Toulemonde, C., & Sanahuja, J. (2009). Upscaling concrete properties: A rational approach to account for the material complexity and variability. International Journal of Material and Structural Integrity, Vol. 3, No. 2/3, 227-246.
- Le, Q. V., Meftah, F., He, Q. C., & Le Pape, Y. (2007). Creep and relaxation functions of a heterogeneous viscoelastic porous medium using the mori-tanaka homogenization scheme and a discrete microscopic retardation spectrum. Mechanics of Time-Dependent Materials, Vol. 11, 309-331.
- Li, A. Q., Li, R. G., & Fish, J. (2008). Generalized mathematical homogenization: From theory to practice. Computer Methods in Applied Mechanics and Engineering, Vol. 197, 3225-3248.
- Li, D. S., Baniassadi, M., Garmestani, H., Ahzi, S., Reda Taha, M. M., & Ruch, D. (2010). 3D reconstruction of carbon nanotube composite microstructure using correlation functions. Journal of Computational and Theoretical Nanoscience, Vol.7, 1-7.
- Li, G. Q., Zhao, Y., & Pang, S. S. (1999). Four-phase sphere modeling of effective bulk modulus of concrete. Cement and Concrete Research, Vol. 29, 839-845.
- Lin, R. Y., & Sheen, Y. N. (2005). Influence of nanosilica powder on the permeability of high performance concrete. Materials Science, Vol. 19, No. 4, 451-460.
- Logan, D. L. (2007). A first course in the finite element method (4th Editon). Thomson.
- Loov, R. E. (1991). A general stress-strain curve for concrete: Implications for high strength concrete columns. Annual Conference of the Canadian Society for Civil Engineering, Vancouver, B.C.
- LS-DYNA (2007). LS-DYNA Keyword User's Manual (Version 9.71). Livermore Software Technology Corporation (LSTC).
- LS-DYNA (2007). LS-DYNA Theory Manual. Livermore Software Technology Corporation (LSTC).
- Matsushima, M., Yokota, M., & Nakagawa, H. (2009). Study on numerical model of cracking induced alkali silica reaction. Creep, Shrinkage, and Durability Mechanics of Concrete and Concrete Structures - Tanabe et al. (eds.), Taylor & Francis Group, London, ISBN 978-0-415-48508-1, 1045-1050.
- Mehta, K., & Monterio, P. J. M. (2006). Concrete: Microstructure, properties and materials. Third Edition. McGraw-Hill Professional, New York.

- Meyer, C., & Baxter, S. (1998). Use of recycled glass and fly ash for precast concrete. Report NYSERDA 98-18 (4292-IABR-IA-96) to New York State Energy Research and Development Authority, Dept. of Civil Eng. and Eng. Mech., Columbia University.
- Michel, J. C., Moulinec, H., & Suquet, P. M. (1999). Effective properties of composite materials with periodic microstructure: A computational approach. Computer Methods in Applied Mechanics and Engineering, Vol. 172, 109-143.
- Mondal, P., Shah, S. P., & Marks, L. (2007). A reliable technique to determine the local mechanical properties at the nanoscale for cementitious materials. Cement and Concrete Research, Vol. 37, 1440-1444.
- Monette, L. J., Gardner, N. J., & Grattan-Bellew, P. E. (2002). Residual strength of reinforced concrete beams damaged by alkali-silica reaction - examination of damage rating index method. ACI Materials Journal, Vol. 99, No. 1, 42-50.
- Multon, S., & Toutlemonde, F. (2006). Effect of applied stresses on alkali-silica reaction-induced expansions. Cement and Concrete Research, Vol. 36, 912-920.
- Multon, S., Seignol, J.-F., & Toutlemonde, F. (2005). Structural behavior of concrete beams affected by alkali-silica reaction. ACI Material Journal, Vol. 102, No. 2, 67-76.
- Multon, S., Seignol, J.-F., & Toutlemonde, F. (2006). Chemomechanical assessment of beams damaged by alkali-silica reaction. Journal of Materials in Civil Engineering, ASCE, July/August, 500-509.
- Multon, S., Seignol, J.-F., & Toutlemonde, F. (2006). Concrete beams submitted to various moisture environments. Structural Engineering and Mechanics, Vol. 22, No. 1, 71-83.
- Multon, S., Sellier A., & Cyr M. (2009). Chemo-mechanical modelling for prediction of alkali silica reaction (ASR) expansion. Cement and Concrete Research, Vol. 39, 490-500.
- Nemat-Nasser, S., & Taya, M. (1981). On effective moduli of an elastic body containing periodically distributed voids. Quarterly of Applied Mathematics, Vol. 39, 43-59.
- Neville, A. M. (2005). Background to minimising alkali-silica reaction in concrete. The Structural Engineer, Vol. 83, No. 18, 18-20.
- Neville, A. M. (2005). Properties of Concrete, 4th Edition, Pearson Education Limited, England.
- Nijland, T. G., & Siemes, A. J. M. (2002). Alkali-silica reaction in the Netherlands: experiences and current research. HERON, Vol. 47, No. 2, 81-85.
- Nowak, A. S., & Szerszen, M. M. (2003). Calibration of design code for buildings (ACI 318): Part I-Statistical Models for Resistance. ACI Structural Journal, Vol. 100, No. 3, 377-382.

- Oliver, W. C. & Pharr, G. M. (1992). An improved technique for determining hardness and elastic modulus by load and displacement sensing indentation experiments. Journal of Materials Research, Vol. 7, 1564-1583.
- Ostoja-Starzewski, M. (2006). Material spatial randomness: From statistical to representative volume element. Probabilistic Engineering Mechanics, 21, 112-132.
- Ostoja-Starzewski, M. (2007). Microstructural randomness and scaling in mechanics of materials. Chapman & Hall/CRC.
- Paulon, V. A., Volin, D. D., & Monteiro, P. J. M. (2004). Statistical analysis of the effect of mineral admixtures on the strength of the interfacial transition zone. Interface Science, Vol. 12, 399-410.
- Pharr, G. M., Strader, J. H. & Oliver, W. C. (2009). Critical issues in making small-depth mechanical property measurements by nanoindentation with continuous stiffness measurement. Journal of Materials Research, Vol. 24, No. 3, 653-666.
- Poon, B., Rittel, D. & Ravichandran, G. (2008). An analysis of nanoindentation in linearly elastic solids. International Journal of Solids and Structures, Vol. 45, 6018-6033.
- Powers, T. C. & Brownyard, T. L. (1946-1947). Studies of the physical properties of hardened Portland cement paste (nine parts). Journal of the American Concrete Institution, Vol. 43, 971-992.
- Powers, T. C. (1960). Physical properties of cement paste. 4th International Symposium on the Chemistry of Cement. Washington, D.C., Paper V-1, 577-609.
- Qing Y., Zean, Z., Deyu, K., & Rongshen, C. (2007). Influence of nano-SiO₂ addition on properties of hardened cement paste as compared with silica fume. Construction and Building Materials, Vol. 21, 539-545.
- Reda Taha, M. M., & Hassanain, M. A. (2003). Estimating the error in calculated deflections of HPC slabs: a parametric study using the theory of error propagation. Deflection Control for the Future, ACI SP-210, Gardner, N.J., Ed., 65-92.
- Sacco, E. (2009). A nonlinear homogenization procedure for periodic masonry. European Journal of Mechanics A/Solids, Vol. 28, 209-222.
- Scanlon, A. & Pinheiro, L. (1992). Allowable deflections: The other side of the equation. ACI SP-133, 111-120.
- Schackelford, J. F. (2005). Introduction to Materials Science for Engineers. 6th Edition, New York.
- Schlangen, E. & van Mier, J. G. M. (1992). Simple lattice model for numerical simulation of fracture of concrete materials and structures. Materials and Structures, Vol. 25, 534-542.

- Schlangen, E., & Copuroglu, Q. (2007). Concrete damage due to ASR: A new method to determine the properties of the expansive gel. Proceedings Framcos6, Catania, Italy.
- Scrivener, K. L. (2004). The interfacial transition zone (ITZ) between cement paste and aggregate. Interface Science, Vol. 12, 411-421.
- Sellier, A., Bourdarot, E., Multon, S., Cyr, M., & Grimal, E. (2009). Combination of structural monitoring and laboratory tests for assessment of alkali-Aggregate reaction swelling: Application to gate structure dam. ACI Materials Journal, Vol. 106, No. 3, 281-290.
- Sharp, J. H. (2006). Surely we know all about cement – don't we? 48th Mellor Memorial Lecture, Advanced in Applied Ceramics, Vol. 105, No. 4, 162-174.
- Smit, R. J. M., Brekelmans, W. A. M., & Meijer, H. E. H. (1998). Prediction of the mechanical behavior of nonlinear heterogeneous systems by multi-level finite element modeling. Computer Methods in Applied Mechanics and Engineering, Vol. 155, 181-192.
- Stanton, T. H. (1940). Expansion of concrete through reaction between cement and aggregate. Proceedings of American Society of Civil Engineering, Vol. 66, 1781-1811.
- Sumanasooriya, M. S., Bentz, D. P., & Neithalath, N. (2010). Planar image-based reconstruction of pervious concrete pore structure and permeability prediction. ACI Material Journal, Vol. 107, No. 413-421.
- Sun, C. T., & Vaidya, R. S. (1996). Prediction of composite properties from a representative volume element. Composites Science and Technology, Vol. 56, 171-179.
- Suquet, P. M. (1985). Local and global aspects in the mathematical theory of plasticity. Plasticity today: Modelling, methods and applications (Sawczuk, A., & Bianchi, G. Editors), Elsevier, Amsterdam, 279-310.
- Suter, M., & Benipal, G. S. (2010). Constitutive model for aging thermoviscoelasticity of reacting concrete II: Results and discussion. Mechanics of Time-Dependent Materials, Vol. 14, No 3, 2010, 291-305
- Takakura, M., Watanabe, Y., Hosokawa, T., Ishii, T., Takiguchi, K., & Masuda, Y. (2005a). Vibration measurement and simulation analysis on a reinforced concrete structure with alkali-silica reaction. 18th International Conference on Structural Mechanics in Reactor Technology (SMiRT 18), Beijing, China, 2026-2035.
- Takakura, T., Ishikawa, T., Matsumoto, N., Mitsuki, S., Takiguchi, K. & Masuda, Y. (2005b). Investigation on the expansion value of turbine generator foundation affected by alkali-silica reaction. 18th International Conference on Structural Mechanics in Reactor Technology (SMiRT 18), Beijing, China, 2061-2068.
- Takemoto K., & Uchikawa, H. (1980). Hydration of pozzolanic cement. Proceedings of the 7th International Congress on Chemistry of Cement, Paris, Vol. 1, IV-2/1-IV-2/29.

- Taylor, H. F. W. (1997). Cement chemistry, 2nd Edition. Thomas Telford, London, UK.
- Terada, K., & Kikuchi, N. (1995). Nonlinear homogenization method for practical applications. Computational Methods in Micromechanics AMSE (Ghosh, S. and Ostoja-Starzewski, M. Editors), AMD Vol. 212, 1-16.
- Thompson, D. P. & Scanlon, A. (1988). Minimum thickness requirements for control of two-way slab deflections. ACI Structural Journal, Vol. 85, 12-22.
- Torquato, S. (2002). Random heterogeneous materials: Microstructure and macroscopic properties. Springer, New York.
- Ulm, F.-J., Coussy, O., Li, K. F., & Larive, C. (2000). Thermo-chemo-mechanics of ASR expansion of concrete structures. Journal of Engineering Mechanics, March, 233-242.
- van Breugel, K. (1995a). Numerical simulation of hydration and microstructural development in hardening cement-based materials (I): Theory. Cement and Concrete Research, Vol. 25, No. 2, 319-331.
- van Breugel, K. (1995b). Numerical simulation of hydration and microstructural development in hardening cement-based materials (II): Applications. Cement and Concrete Research, Vol. 25, No. 3, 522-530.
- Van Mier, J. G. M., Van Vliet, M. R. A., & Wang, T. K. (2002). Fracture mechanisms in particle composites: statistical aspects in lattice type analysis. Mechanics of Materials, Vol. 34, 705-724.
- Voyiadjis, G. Z. & Peters, R. (2010). Size effects in nanoindentation: an experimental and analytical study. Acta Mech, Vol. 211, 131-153.
- Wang, T. K., Chang, C. S., van Mier, J. G. M., Sluys, L. J., & Bittencourt, T. N. (2001). Fracture modelling of concrete using two different microstructural mechanics approaches, 2001 MECHANICS AND MATERIALS SUMMER CONFERENCE, ASME Materials Division and Applied Mechanics Division, ASCE Engineering Mechanics Division, Society of Engineering Science (SES), 27-29 June, San Diego, California, pp.186.
- Washa, G.W. (1947). Plastic flow of thin reinforced concrete slabs. ACI Journal Proc, Vol. 44, 237-258.
- Wight, J. K., & MacGregor, J. G. (2008). Reinforced concrete: Mechanics and design (5th Edition). Prentice Hall.
- Wittmann, F. H., Roelfstra, P. E., & Sadouki, H. (1984-1985). Simulation and Analysis of Composite Structures. Materials Science and Engineering, Vol. 68, 239-248.
- Wriggers, P., & Mofteh, S. O. (2006). Mesoscale models for concrete: Homogenisation and damage behaviour. Finite Elements in Analysis and Design 42, 623-636.

- Wu, W., Yuan, Z., & Fish, J. (2010). Eigendeformation-based homogenization of concrete. International Journal for Multiscale Computational Engineering, Vol. 8, Issue 1, 1-15.
- Yajun, J., & Cahyadi, J. H. (2004). Simulation of silica fume blended cement hydration. Materials and Structures, Vol. 37, 397-404.
- Yeong, C. L. Y., & Torquato, S. (1998). Reconstructing random media. Physical Review, E 57, 495.
- Yeong, C. L. Y., & Torquato, S. (1998). Reconstructing random media. II. Three-dimensional media from two-dimensional cuts. Physical Review, E 58, 224.
- Yu, W., & Tang, T. (2007). Variational asymptotic method for unit cell homogenization of periodically heterogeneous materials. International Journal of Solids and Structures, vol. 44, 3738-3755.
- Yuan, Z., & Fish, J. (2009). Multiple scale eigendeformation-based reduced order homogenization. Computer Methods in Applied Mechanics and Engineering, Vol. 198, 2016-2038.
- Yvonnet, J., Gonzalez, D., & He, Q. C. (2009). Numerically explicit potentials for the homogenization of nonlinear elastic heterogeneous materials. Computer Methods in Applied Mechanics and Engineering. Vol. 198, 2723-2737.
- Zheng, W., Kwan, A. K. H., & Lee, P. K. K. (2001). Direct tension test of concrete. ACI Material Journal, Vol. 98, 63-71.
- Zhu, W., Hughes, J. J., Bicanic, N., Pearce, C. (2007). Nanoindentation mapping of mechanical properties of cement paste and natural rocks. Materials Characterization, Vol. 58, 1189-1198.
- Zundeleovich, S., Hamada, H. S., & Chiu, A. N. (1974). Variability of deflections of simply supported precast prestressed concrete beams. ACI Special Publication, Vol.43, 547-571.